Spring 5-8-2021

Marinopyrrole Derivatives as Putative Antiparasitic Molecules Promoting Initiation of Programmed Cell Death in Toxoplasma gondii

Matthew C. Martens
University of Nebraska Medical Center

MARINOPYRROLE DERIVATIVES AS PUTATIVE ANTI-PARASITIC MOLECULES PROMOTING INITIATION OF PROGRAMMED CELL DEATH IN *TOXOPLASMA GONDII*

by

Matthew Christian Shelton Martens

A DISSERTATION

Presented to the Faculty of
the University of Nebraska Graduate College
in Partial Fulfillment of the Requirements
for the Degree of Doctor of Philosophy

Interdisciplinary Graduate Program in Biomedical Sciences
(Immunology, Pathology & Infectious Disease)

Under the Supervision of Professor Paul H. Davis

University of Nebraska Medical Center
Omaha, Nebraska

April, 2021

Supervisory Committee:

Marilynn Larson, Ph.D.
William Tapprich, Ph.D.
Caroline Ng, Ph.D.
Paul H. Davis, Ph.D.

ACKNOWLEDGMENTS

It is beyond words to fully convey my gratitude to the many people who have made this educational experience a reality over these past four years, through trials and triumphs. Without their help, I would never have had the humbling privilege to pursue my passion for science and reach this ultimate goal. First, and with the fullest sincerity, I thank my wonderful family for nurturing me and providing unwavering support during this challenging, but rewarding, experience: I would like to especially thank my parents, Mark and Stephanie Martens, for unceasingly providing their insight, love, and continuous assistance; without them, I am confident that I would not be here in this remarkable position. I would also like to thank my brothers, Jacob and Zachary Martens, who have been phenomenal supporters throughout my life.

I would also extend my heartfelt gratitude to Dr. Paul Davis, my mentor through both my undergraduate and graduate education. He has taught me infinitely more than I can express, ranging from microbiology techniques to effective scientific communication. He has challenged me to become a better scientist and critical thinker and has been incredibly supportive for the duration of these degrees. I am incredibly thankful to have found a niche in his laboratory that has allowed me to grow and develop as both a scientist and as a professional in the field, and this has been tantamount to my successes thus far.

It is equally incredible to have had such an outpouring of support from a number of friends and lab-mates over this time. There are more people than I could name here; the following are simply a small number of the many who have made this possible. I would like to thank my “lab dad” and co-worker Austin Sanford for his commiseration and encouragement, and for his substantial *in vivo* work present in Chapter 1; Maggie Bartlett for giving us so much insight and comradery even after graduating; Alex Wallick and Rosalie Warner for their kindness and for their help in and out of lab, particularly in helping run

toxicity and efficacy assays for numerous compounds; Braydon Dreher and Ryan Chapman for their invaluable assistance in running the many, many qRT-PCR and bioinformatics assays that went into this work and beyond; Tom Schulze and Andrew Neville for their help and much-needed conversation; and my longtime friend Jacob Bliss, who has provided continuous support from day one.

A number of key individuals also made this scientific progress a reality: I would particularly like to thank the other members of my Supervisory and Examining Committee—Dr. Marilynn Larson, Dr. Carline Ng, Dr. William Tapprich, and Dr. Rakesh Singh—for reviewing and challenging my scientific work. I would like to extend additional thanks to Dr. Larson for her fundamental role in my training, both in the BSL-3 laboratory and in my rotations, and for her insight on our often-challenging government projects. In addition, I am extremely grateful to Dr. Rongshi Li for his synthesis and description of novel marinopyrrole compounds, for which he was a key collaborator. I wholeheartedly thank Tuire Cechin, as well, for her incredible help and guidance through the Ph.D. program.

Finally, I would like to thank the following University of Nebraska Medical Center cores for their assistance in completing this research and would like to acknowledge them as follows, with the recommended acknowledgements included below:

The UNMC Genomics Core Facility receives partial support from the National Institute for General Medical Science (NIGMS) INBRE - P20GM103427-19, as well as the National Cancer Institute, The Fred & Pamela Buffett Cancer Center Support Grant-P30CA036727, The Center for Root and Rhizobiome Innovation (CRRI) 36-5150-2085-20, and the Nebraska Research Initiative. This publication's contents are the sole responsibility of the authors and do not necessarily represent the official views of the NIH or NIGMS.

I would like to thank Tom Bargar and Nicholas Conoan of the Electron Microscopy Core Facility (EMCF) at the University of Nebraska Medical Center for technical assistance. The EMCF is supported by state funds from the Nebraska Research Initiative (NRI) and the University of Nebraska Foundation, and institutionally by the Office of the Vice Chancellor for Research.

MARINOPYRROLE DERIVATIVES AS PUTATIVE ANTI-PARASITIC MOLECULES PROMOTING INITIATION OF PROGRAMMED CELL DEATH IN *TOXOPLASMA GONDII*

Matthew C. S. Martens, Ph.D.

University of Nebraska Medical Center, 2021

Supervisor: Paul H. Davis, Ph.D.

Toxoplasma gondii is a globally-distributed obligate intracellular parasite and the causative agent of toxoplasmosis in humans, a biphasic disease often culminating in lifelong chronic infection. Though often mild, toxoplasmosis can lead to severe clinical presentation in immunocompromised patients and developing fetuses. Current therapeutic options are severely limited, with a combinatorial pyrimethamine/sulfadiazine regimen acting as the current standard of care for toxoplasmosis; however, both of these compounds can elicit serious adverse reactions in patients, and, additionally, are only effective against the acute stage of infection. To address these limitations, screenings of several analogs derived from the marine natural product marinopyrrole A identified a series of small-molecule inhibitors against *T. gondii* tachyzoites: RL002, RL003, and RL125. The most potent molecule, RL003, showed an *in vitro* IC_{50} of 0.096 µM and corresponding low toxicity to non-tumorigenic immortalized human cell lines, with a selectivity of ≥20X for parasites over any susceptible host cell line. RL003 also potently inhibited encysted bradyzoites *in* vitro, with an IC_{50} of 0.245 µM. Further screening of RL003 demonstrated additional activity against other pathogens, including a number of gram-positive and gram-negative bacteria, such as *Mycobacterium bovis* BCG, *Naegleria fowleri,* and *Acanthamoeba castellanii*. Forward genetic screening of mutagenized compound-resistant *T. gondii* clones suggested a role of parasite-specific cGMP-dependent protein kinase (PKG) as a mediator of RL003 activity, with subsequent observations of impaired invasion, motility, and egress supporting this finding. Identification of apoptosis-like morphological changes by scanning

electron microscopy (SEM) followed by differential expression analysis by both RNA-seq and RT-qPCR provided evidence for downstream upregulation of programmed cell death pathways in compound-treated parasites. Taken together, these data support the role of RL003 as a novel and pathogen-selective antiparasitic compound.

TABLE OF CONTENTS

LIST OF FIGURES

LIST OF TABLES

LIST OF ABBREVIATIONS

Abbreviation	Definition
A260/280	Ratio of absorbance at 260 nm and 280 nm
(O)ADC	(Oleic acid), albumin, dextrose, catalase supplementation
AIDS	Acquired immunodeficiency syndrome
ATCC	American Type Culture Collection
ATP	Adenosine triphosphate
AZM	Azithromycin
BALB/C	Inbred albino mouse strain
BAM	Binary data storage file
BCG	Bacille de Calmette et Guérin (vaccine) strain
BCS	Bovine calf serum
BCYE	Buffered charcoal-yeast extract
BEI	Biological and Emerging Infections Resources Program)
BHI	Brain-heart infusion
BSA	Bovine serum albumin
C57BL/6	Inbred "black 6" mouse strain
CA	Community-acquired
cAMP	Cyclic adenosine monophosphate
CDPK	Calcium-dependent protein kinase
cGMP	Cyclic guanosine monophosphate
cKD	Conditional knockdown
CLM	Clindamycin
cLogP	Logarithmic partition coefficient

CNS	Central nervous system
CRM	Clarithromycin
D10	Parasite and host cell medium with 10% BCS
DHFR	Dihydrofolate reductase
DHFR-TS	Dihydrofolate reductase-thymidylate synthase
DHPS	Dihydropteroate synthase
DMEM	Dulbecco's Modified Eagle Medium
DMSO	Dimethyl sulfoxide
DNA	Deoxyribonucleic acid
dTMP	Deoxythymidine monophosphate
dUMP	Deoxyuridine monophosphate
dUTP	Deoxyuridine triphosphate
DXY	Doxycycline
EDTA	Ethylenediaminetetraacetic acid
EMCF	Electron Microscopy Core Facility
EMS	Ethyl methanesulfonate
FBS	Fetal bovine serum
FC	Fold-change
FDA	Food and Drug Administration
GFP	Green fluorescent protein
GO	Gene ontology
GTP	Guanosine triphosphate
HA	Hospital-acquired
HC-04	Human hepatocyte cell line
HEK-293	Human embryonic kidney cell line

HEPES	4-(2-hydroxyethyl)-1-piperazineethanesulfonic acid
HepG2	Human hepatocellular carcinoma cell line
HFF	Human foreskin fibroblast cell line
IAA	3-indoleacetic acid
IC50	50% maximum inhibitory concentration
Log2FC	Log2(fold-change)
LVS	Live vaccine strain
mAID	mini-Auxin-inducible degron
MIC	Minimum inhibitory concentration
MIC50	50% minimum inhibitory concentration
MIC90	90% minimum inhibitory concentration
mRNA	Messenger ribonucleic acid
MRSA	Methicillin-resistant *S. aureus*
MΦ	Macrophage
NEB	New England Biolabs
NMR	Nuclear magnetic resonance
OD600	Optical density at 600 nm
PBS	Phosphate-buffered saline
PBST	PBS and 0.1% triton-X
PBT	PBS, 3% BSA, and 0.1% triton-X
PCD	Programmed cell death
PCR	Polymerase chain reaction
PI3K	Phosphatidylinositol-3-kinase
PKG	cGMP-dependent protein kinase
PMA	Phorbol 12-myristate 13-acetate

PTD	Solvent for murine infection (PBS, 30% propylene glycol, 5% Tween-80, 62% water/dextrose, 3% DMSO)
PYR	Pyrimethamine
dTom	tdTomato fluorescent protein
RNA	Ribonucleic acid
RPMI-1640	Roswell Park Memorial Institute-1640 Medium
rRNA	Ribosomal RNA
RT-qPCR	Reverse-transcription quantitative PCR
SAG1	Major surface antigen 1
SDZ	Sulfadiazine
SEM	Scanning electron microscopy
SMX	Sulfamethoxazole
SNP	Single nucleotide polymorphism
SNV	Single nucleotide variant
THP-1	Human acute monocytic leukemia (monocyte) cell line
TIR	Transport inhibitor response auxin receptor
TMP	Trimethoprim
TSA	Trypticase soy agar
TSB	Trypticase soy broth
TUNEL	Terminal dUTP nick-end labelling
U2-OS	Human osteosarcoma cell line
UNMC	University of Nebraska Medical Center
UPRT	Uracil phosphoribosyltransferase
VRSA	Vancomycin-resistant *S. aureus*
WT	Wild-type

INTRODUCTION

I. *Toxoplasma gondii*: Introduction to the parasite

Toxoplasma gondii is an obligate intracellular parasite estimated to infect up to one-third of the global population and is the causative agent of toxoplasmosis in humans, a potentially-severe disease with serious public health and economic effects [1; 2]. Infection often occurs following consumption of undercooked meat, produce, or even water containing viable parasite cysts [3], but may also occur through exposure to highly-stable oocysts shed in cat feces as a result of the exclusive sexual reproduction of *T. gondii* in the intestinal epithelium of hosts from the *Felidae* family [4]. While most infections are self-limiting, particularly in the acute, symptomatic phase, immunocompromised individuals and developing fetuses are at substantially higher risk of severe clinical manifestations [1; 5; 6; 7]; in the former population, infection of the central nervous system can lead to toxoplasmic encephalitis [8], while in the latter population, acute infection during pregnancy can lead to serious or fatal birth defects [9; 10]. Even in otherwise-healthy patients, toxoplasmosis progresses to an asymptomatic chronic phase for which no current treatments are available [11], leading to a high rate of infection throughout the human population and potential deleterious effects if immunosuppression occurs later in life [12]. Together, the high public health burden and potentially severe nature of infection supports a continued need for further studies of both the fundamental biology of the *T. gondii* as well as potential antiparasitic therapies.

The *T. gondii* parasite itself is an apicomplexan, eukaryotic organism that requires a homeothermic host for successful replication due to its dependence on scavenged components, including purines [13] and the amino acids tyrosine [14], tryptophan, and arginine [15], from the infected cell. The asexual portion of the parasitic life cycle is responsible for disease in the intermediate hosts, which include a majority of homeothermic animals [16;

17], and is biphasic, being comprised of an acute stage and a chronic stage [18]. In the acute stage, pathogenesis is characterized by mild, flu-like symptoms arising as a consequence of rapid proliferation and dissemination of actively replicating tachyzoites following exposure [19]. Roughly equivalent to metabolically active trophozoites in other biphasic protists [20], tachyzoites are a highly motile and replicative form of the parasite that is able to infect any nucleated cell [17]. The acute stage is followed at 2-3 weeks post-exposure by progression to an asymptomatic chronic stage in immunocompetent individuals [21], characterized by the differentiation of resident tachyzoites into bradyzoites that aggregate to form thick-walled, stable cysts in brain and muscle tissue [21] that are believed to form as a consequence of stressors initiated by the immune response [22]. At this point, the infection is lifelong, as cysts cannot be effectively cleared by the host immune system [22].

Initiation of the acute infection occurs rapidly upon exposure to parasites, most often by consumption of contaminated food or water [3]. Ingested parasites travel through the digestive tract, avoiding damage by acidified host compartments as a consequence of their protective cyst walls [23], and reach the small intestine, at which point they are able to shed their protective covering to infect epithelial cells of the intestinal lining [24]. Following initial invasion of the small intestine epithelium, tachyzoites replicate within and subsequently lyse the infected enterocytes, breaching the basement membrane before entering the blood vessels and traveling through the bloodstream for dissemination to distal tissues [25]. The movement of free parasites through blood and lymph vessels and the infection of white blood cells by tachyzoites facilitate rapid movement of parasites to brain and muscle tissues within days of infection [26]. Recent data suggests that parasite-laden white blood cells, particularly monocytes, may play roles as “trojan horses,” allowing for crossing of the blood-brain barrier and infection of the central nervous system [27; 28; 29], though the observed rupturing of endothelial layers in low-shear cerebral capillaries may

point to a more direct breach of this barrier [30]. At this stage, parasites are able to replicate within brain and muscle tissue prior to initiation of the chronic infection [30].

As host immune responses mount and external stressors build, tachyzoites in brain and muscle tissue begin to differentiate into bradyzoites, a slower-growing form of the parasite that, rather than lysing the host cells, aggregates in the nascent vacuole and forms a thick-walled tissue cyst [21; 31]. Though the precise mechanisms by which bradyzoite differentiation are triggered remain unclear, it is known that alkaline stress [32], nutrient deprivation [33], oxidative stress [34], and temperature shock [35] cause differentiation *in vitro*. *In vivo*, it appears that the presence of a functional immune system effectively allows for preferential maintenance of *T. gondii* bradyzoites due to apparent clearance of systemic tachyzoites, and that immunosuppression allows for uninhibited tachyzoite replication [36]. It is less clear whether specific immune effectors are responsible for this conversion—although, based on the parasitic response to stress and based on the importance of immune response in maintaining chronic rather than acute infection [37], it is evident that the immune system plays a central role in this process. Following differentiation, glycoproteins and polysaccharides begin to assemble beneath the parasitophorous vacuole membrane, forming a cyst wall that protects the encysted bradyzoites from the host immune response [21; 38].

Together, the acute and chronic stages of the *T. gondii* life cycle generate the disease presentation seen in humans and other intermediate hosts, with fundamental parasite processes strongly influencing the progression of toxoplasmosis [1; 39].

II. Clinical presentation of toxoplasmosis and relevance

Toxoplasmosis in in the clinical setting varies in its presentation based on the stage of the infection as well as the health of the patient [1; 39]. While acute toxoplasmosis is generally self-limiting in a majority of infected individuals [1], producing mild illness that

may be completely unnoticed, infection of immunocompromised patients—such as HIV/AIDS patients [40], solid-organ transplant recipients [60], individuals undergoing TNF-α therapy [41], and those undergoing extended treatment with corticosteroids (such as prednisone) [42]—can generate severe clinical manifestations, including toxoplasmic encephalitis [43]. Toxoplasmic encephalitis occurs when tachyzoites present in brain matter lead to abscesses or lesions containing peripheral parasite populations surrounding regions of infiltrating leukocyte populations and lipidated macrophages [44]. The resulting inflammation results in rapid encephalopathy including necrotizing vasculitis and meningitis, which, left untreated, results in serious or fatal damage to the central nervous system [45]. Clinical progression in these cases can occur quickly, with severe symptoms such as seizures, muscle weakness, confusion, and behavioral changes occurring within days of post-reactivation [46; 44].

Other clinical manifestations of *T. gondii* are observed apart from or in conjunction with toxoplasmic encephalitis, including ocular toxoplasmosis and rare instances of toxoplasmic pneumonitis [5]. Intraorbital exposure to *T. gondii* can result in ocular toxoplasmosis, a condition aggravated in immunocompromised individuals but also present in immunocompetent individuals given the immune-privileged nature of the eye [47]. Pathology is characterized by posterior uveitis [48] and necrotizing retinitis that eventually lead to scarring of the retina and, in immunocompromised patients, severe inflammation [47]. Less commonly than ocular infection, several select cases of *Toxoplasma* infection in immunocompromised patients not taking preventative therapies against *Pneumocystis carinii* have been observed to lead to pneumonia as a consequence of parasite proliferation in bronchioalveolar tissues [49; 50; 51].

In recent years, these severe effects arising from infection with *T. gondii* are decreasingly prevalent in immunocompromised populations as a result of prophylactic

trimethoprim/sulfamexothazole combinatorial treatments widely-implemented by healthcare professionals [52]; however, these serious manifestations do still occur. For example, 26-38% of *Toxoplasma*-positive untreated AIDS patients experience severe onset of toxoplasmic encephalitis, representing a potentially-serious threat for immunocompromised groups [53].

In addition to severe pathology in immunocompromised patients, *T. gondii* is a leading cause of serious birth defects worldwide, with an estimated frequency of 1-10/10,000 live births [10]. Infection during gestation leads to crossing of the placenta by tachyzoites and entry into fetal circulation, the consequence of which is movement into cerebral and muscular tissues [54]. While as many as 85% of infections during the third trimester result in subclinical presentation of the newborns, occupation of fetal tissues during first and second trimester infection of the developing fetus leads to serious or fatal congenital defects [9]. Toxoplasmosis in these cases ranges in presentation from hydrocephaly, macrocephaly, cerebral calcification, and microcephaly to less-defined neurological disorders and, in severe cases comprising 3-5% of total infections, spontaneous abortion or stillbirth [9; 55]. Treatment with spiramycin significantly improves the ultimate outcome, although it is still possible for seemingly-mild congenital cases to leas to chorioretinitis and neuromuscular disorders between the ages of 20 and 30 [55].

Compounding matters, patients carrying cysts from an infection occurring earlier in life, even if they showed few symptoms at initial infection, can have recrudescence of acute infection if later they become immunocompromised, posing a continued threat to those infected [56]. Recrudescence in humans has been poorly described, and represents an area of intensive study; however, several animal models have been used to gain some insight into this phenomenon, though the particular mechanisms by which reactivation occurs are still widely speculative. In mice (*Mus musculus*), type II and III parasites present

in brain tissue at 10 days post-infection were found by bioluminescent imaging and immunohistochemistry to be reactivated—defined as actively replicating and expressing luminescent markers—after approximately 14 days of immunosuppression by hydrocortisone [56]. In these mice, foci of reactivation were preferentially distributed across the frontal and parietal cortices and were characterized by high levels of infiltrating leukocytes [56], although the use of highly *Toxoplasma*-sensitive C57BL/6 and BALB/C inbred mouse strains [57] may have led to more severe pathology than may be present in outbred strains. Performing a similar study in rats (*Rattus norvegicus*), which respond less catastrophically to *Toxoplasma* infection and have been observed to mount an immune response more similar to that of humans [58], immunosuppression by a synergistic application of hydrocortisone and dexamethasone led to a significant reactivation of latent brain-dwelling cysts leading to conversion to tachyzoites, with concomitant rapid progression of physiological symptoms of toxoplasmic encephalitis [59]. Similar findings were also observed in assayed muscle tissues from these rats, which showed high reactivation of cysts [59]. Whether this finding is more clinically significant than the CNS neuropathology, however, is less clear, particularly in humans. Surprisingly, multiple case studies demonstrate that, post solid-organ transplant, patients have been observed to experience recrudescence of latent toxoplasmosis through *donor-derived* tissue infection; this has particularly been observed in the lungs and the liver [60]. In these pre-operative *Toxoplasma*-negative patients, presumably-encysted parasites present in the transplanted tissues from the donor reactivated upon application of immunosuppressive therapies, leading to rapid proliferation in these essential organs; however, of note, none of these patients were taking the recommended trimethoprim/sulfamexothazole regimen that is common in immunosuppressed individuals [60], suggesting that infection may have been contained with the appropriate prophylactic. In either case, recrudescence of latent infection in previously-

infected patients and donor-infected transplant recipients can have severe ramifications for susceptible individuals.

In sum, the high prevalence of *Toxoplasma* infection, in combination with severe clinical outcomes in immunocompromised patients and developing infants, demonstrates the substantial patient health and economic burdens levied by this parasite. These concerns underscore the importance of understanding parasite physiology, interaction with the host, and underlying mechanisms leading to pathogenicity in *Toxoplasma gondii*.

III. Current Clinically-Implemented Pharmacological Targets and Small-Molecule Interventions Against *Toxoplasma gondii*

To address the widespread clinical ramifications of toxoplasmosis, a number of therapeutic regimens have been implemented against the acute stage of infection in the interest of preventing serious patient presentation and providing some level of control of parasite burden; a summary of existing clinically relevant therapies is presented in **Table I.1**. These pharmaceuticals have been implemented broadly, with varying degrees of success, and include antifolates, apicoplast protein synthesis inhibitors, and molecules impeding parasite mitochondrial activity (**Table I.1**). However, high-potency, consistently effective treatments are relatively few in number, representing a serious patient health concern given the high prevalence and potentially-severe manifestations of *T. gondii* infection [11; 61]. In addition, compounding matters, no FDA-approved treatments have currently been implemented for treatment of chronic infection [61], suggesting a critical need for effective anti-*Toxoplasma* interventions.

Primary treatment of acute toxoplasmosis is often provided by antifolates—most commonly by combinatorial pyrimethamine and sulfadiazine regimen, both of which target components of the folate pathway [53]. This pathway in *Toxoplasma* is primarily responsible for the

Class	Compound	*T. gondii* Target	Subcellular Location of Target	*In vitro* IC_{50}(μM)	*In vivo* Murine Dose and Survival	Clinical Dosage: Duration (if applicable)
Antifolate	Pyrimethamine	DHFR-TS	Cytoplasm	0.4-0.6	4-10 mg/kg/day: 90%	50-75 mg/day PYR + 4-6 g/day SDZ: 1-3 weeks
	Sulfadiazine	DHPS	Cytoplasm	1.6	375 mg/kg/day: 100%	
	Trimethoprim	DHFR-TS	Cytoplasm	17.2	70 mg/kg/day: 20%	5-10 mg/kg/day TMP + 23-50 mg/kg/day SMX: 4-6 weeks
	Sulfamethoxazole	DHPS	Cytoplasm	365	600 mg/kg/day: 100%	
Tetracycline	Doxycycline	23S rRNA	Apicoplast	14.4	300 mg/kg/day: 100%	400 mg/kg/day DXY + 25 mg/kg/day PYR
Macrolide	Spiramycin	23S rRNA	Apicoplast	17.8	400 mg/kg/day: 0%	3 g/day
	Azithromycin	23S rRNA	Apicoplast	11.5	200 mg/kg/day: 80-100%	500 mg/day AZM + 75 mg/day PYR: 4 weeks
	Clarithromycin	23S rRNA	Apicoplast	401	300 mg/kg/day: 100%	2 g/day CRM + 75 mg/day PYR: 6 weeks
Lincosamide	Clindamycin	23S rRNA	Apicoplast	0.002-0.014	400 mg/kg/day: 61%	50-75 mg/d PYR, up to 4.8 g/d CLM: 1-3 weeks
Quinone	Atovaquone	Cytochrome bc_1 complex	Mitochondria	0.138	5 mg/kg/day: 20%	750 mg/day – 3 g/day: 6+ weeks

Table I.1. Summarized clinically-relevant anti-*Toxoplasma* therapies, their targets, and their efficacies *in vitro* and *in vivo*. The widely-available clinically-approved medications showing activity against acute *T. gondii* infection are summarized above, including the broad antimicrobial class, validated molecular target, location of the target within the parasite, lowest reported *in vitro* IC_{50}, *in vivo* dosages of most successful report along with corresponding survival, and published clinical dosages utilized. Abbreviations: DHFR-TS: dihydrofolate reductase-thymidylate synthase; DHPS: dihydropteroate synthase; PYR: pyrimethamine; SDZ: sulfadiazine; TMP: trimethoprim; SMX: sulfamethoxazole; DXY: doxycycline; AZM: azithromycin; CRM: clarithromycin; CLM: clindamycin; ATV: atovaquone.

crucial *de novo* biosynthesis of thymidine; this is particularly important due to the ability of parasites to salvage purines, but not pyrimidines, from the host [62]. Pyrimethamine targets the parasite bifunctional dihydrofolate reductase/thymidylate synthase (DHFR-TS) enzyme [63; 64] responsible for the conversion of deoxyuridine monophosphate (dUMP) to deoxythymidine monophosphate (dTMP) in conjunction with the reduction of dihydrofolate to tetrahydrofolate [65]; one pitfall, as demonstrated by the unintended hematological consequences of extended pyrimethamine use discussed below, is that the parasite DHFR-TS protein carries substantial homology to the human DHFR protein, allowing for nonspecific host interaction [66]. Sulfadiazine, on the other hand, targets the highly parasite-specific dihydropteroate synthase (DHPS) protein [67; 68], which facilitates the dihydropteroate diphosphate to 7,8-dihydropteroate—an upstream essential process for eventual production of dihydrofolate and dTMP synthesis, though *in vivo* and in the clinic this is insufficient to clear parasite infection [69; 53]. Together, the synergistic effect of pyrimethamine and sulfadiazine on the folate pathway significantly improves the therapeutic applicability of these molecules [70].

Clinical implementation of pyrimethamine and sulfadiazine has been successful, due in part to the high potency and synergy of these compounds in combination. *In vitro* 50% inhibitory concentrations for pyrimethamine have been found to be as low as 0.4 μM [71], with up to 90% *in vivo* survival at 4-10 mg/kg/day [72], while sulfadiazine shows *in vitro* and *in vivo* efficacies of, respectively, 1.6 μM [69; 11] and 375 mg/kg/day (reaching 100% survival) [73]; however, these results are highly variable and strain-dependent, with the higher-virulence type I strains showing a greater capacity to induce rapid death in the hypersensitive murine model [71] compared to the less virulent, cyst-forming type II and III strains [1]. Further, either treatment administered alone resulted in relapse of infection within several days upon completion of treatment [73]. In humans, clinical dosages are

variable due to patient tolerance, particularly with the use of both pyrimethamine and sulfadiazine, but typically falls within a range of 50-75 mg/day of pyrimethamine for an average adult in addition to 4-6 g/day of sulfadiazine for a total of 1-3 weeks [53]. The high dosages of pyrimethamine and sulfadiazine over such an extended period can cause serious hematopoietic shifts, including bone marrow suppression, leukopenia, thrombocytopenia, and megaloblastic anemia [74]. To partially ameliorate these severe effects, folic acid supplements are typically provided in conjunction with this intervention to facilitate an improved outcome and reduced hemotoxicity [75], as inhibition of the folate metabolic pathway by both pyrimethamine and sulfadiazine is not exclusive to parasites and can affect human tissues with high metabolic and/or replicative activity [53]. In humans, the folate pathway a crucial component of both purine (through production of tetrahydrofolate) and pyrimidine biosynthesis (through generation of thymidine) as well as production of the amino acids methionine and serine [76; 77]. Folinic acid supplements are administered to reduce the severity of these effects [75].

Other existing antifolates have also been found to show efficacy against toxoplasmosis in murine models and in humans. Previous clinical suggestions included a combinatorial trimethoprim/sulfamethoxazole treatment, with trimethoprim targeting DHFR-TS and sulfamethoxazole targeting DHPS, similarly to pyrimethamine and sulfadiazine [78]. However, the *in vitro* and *in vivo* potencies of trimethoprim are substantially lower than those of pyrimethamine at 17.2 µM [78] and 70 mg/kg/day (for only 20% survival of acute lethal murine challenge) [79], while the corresponding potencies of sulfamethoxazole are 365 µM *in vitro* [78] and 600 mg/kg/day in mice (though 100% survival was obtained with this dosing) [79]. Clinically, dosages of trimethoprim and sulfamethoxazole are, respectively, 5-10 mg/kg/day and 23-50 mg/kg/day for 4-6 weeks [5; 53; 80]. Immunocompromised patients may already take prophylactic doses of this treatment for prevention of *P.*

carinii pneumonitis, a factor that has been found to contribute to positive clinical outcomes in *Toxoplasma*-seropositive patients [60]. A similar molecule, dapsone, was found at 50 mg/kg/day to facilitate only 10% survival in a murine model; however, synergistic effects were shown when used in combination with epiroprim (another antifolate; 50 mg/kg/day) or pyrimethamine (with 100 mg/kg/day dapsone and 18.5 mg/kg/day pyrimethamine) led to survival of 100% of lethally-infected mice [81]. As with the standard pyrimethamine/sulfadiazine, folinic acid supplements are typically recommended to compensate for strong hematopoietic shifts that can occur at the doses required for parasite clearance [82].

Molecules inhibiting components of the prokaryotic-like plastid organelle, called the apicoplast, represent attractive anti-*Toxoplasma* targets, given that they provide a desirable level of specificity to parasites over host [83; 84]. Multiple antibacterial molecules found to inhibit the apicoplast in some capacity—through such pathways as apicoplast replication, translation of proteins (via the endogenous ribosome), or processing of fatty acids—have been implemented clinically [83]. The tetracycline antibiotic doxycycline is one such molecule: believed to target the 23S rRNA of the large ribosomal subunit in the apicoplast, inhibiting the binding of mRNA to the ribosome and thereby preventing protein synthesis [53; 85], doxycycline was identified *in vitro* to inhibit parasite growth at 14.4 µM [86], and *in vivo* to allow for up to 100% survival in lethally-infected mice at 300 mg/kg/day [86]. Use in the clinic is less common than for the drugs described above, though it has been used previously in prophylactic treatment for malaria [87]. Due to case-specific use of doxycycline against toxoplasmosis, dosing is not yet as broadly standardized as for other drugs; however, treatment consisting of 400 mg/kg/day doxycycline in addition to 25 mg/kg/day pyrimethamine was shown in one patient to improve clinical outcome of toxoplasmic encephalitis by resolution of cerebral lesions [88].

Several other inhibitors of prokaryotic and apicoplast protein synthesis—belonging to the antibacterial macrolide and lincosamide classes—have also been used for either combinatorial treatment with one or more antifolates or as standalone treatments, though, as above, pyrimethamine and sulfadiazine remain the most potent [11]. Macrolides inhibit protein synthesis by interference with the transpeptidation site of the large ribosomal subunit (23S rRNA), particularly in prokaryotic or prokaryotic-like ribosomes (such as those in the apicoplast) [89; 90; 91]. Among the macrolides, spiramycin has been found to be well-tolerated in pregnant individuals with suspected *Toxoplasma* exposure, with dosages of 3 g/day until delivery appearing to have fewer ill effects on both the mother and fetus than pyrimethamine/sulfadiazine [53]. Unfortunately, spiramycin cannot clear fetal infection once established, as it cannot efficiently pass the placental barrier at doses lethal to parasites [92]. Additionally, spiramycin has a much lower potency *in vitro* (17.8 μM) [93] and showed lack of survival in treated mice at 400 mg/kg/day *in vivo* [94]. Other macrolides, such as azithromycin and clarithromycin, have also been used with varying degrees of success, with measured *in vitro* efficacies of 11.5 μM for the former [93], and, in stark contrast, 401 μM for the latter [72; 95]. These potencies correspond to 80-100% survival in type II-strain-infected mice at 200 mg/kg/day for azithromycin [94], and up to 100% survival in similarly infected mice at 300 mg/kg/day for clarithromycin (surprisingly, given the low potency *in vitro*; this may suggest that the compound is modified in some form *in vivo* into a more bioactive molecule) [96]. Clinically, azithromycin at 500 mg/day in combination with pyrimethamine at 75 mg/day appeared to cause enhancement of favorable outcomes for AIDS patients against toxoplasmic encephalitis in a small study conducted [97], while high-dose 2 g/day clarithromycin with 75 mg/day pyrimethamine also appeared to enhance patient outcomes [98]; however, there is little homogeneity in dosing, and optimization is needed to more accurately evaluate this compound, particularly given that, in both studies, high instances of severe adverse effects were reported.

Among the lincosamides, which similarly affect apicoplast protein synthesis by interference with the transpeptidation site of the large ribosomal subunit, clindamycin has been shown to have a high potency against *T. gondii* RH-strain tachyzoites, with an IC_{50} value reported to be as low as 2.4-14.1 nM [99; 100]; however, this value appears to be highly variable across various studies and may be influenced by cell type, parasite archetypal lineage, or culturing conditions. Interestingly, and perhaps contributing to these variations in observed potency, clindamycin causes a “delayed death” phenotype, in which toxicity of the drug is observed after a subsequent passage of parasites; in fact, this phenomenon led to an incorrect assignment of inefficacy for this compound prior to 1992 [99]. *In vivo*, clindamycin was shown to have a much poorer potency, with 400 mg/kg/day allowing for survival in only 61% of lethally-infected mice [101; 102]. Combination with pyrimethamine alone (initial doses of 50-75 mg/d pyrimethamine, up to 4.8 g/day clindamycin) or with trimethoprim/sulfamethoxazole (20 mg/kg/day trimethoprim, 100 mg/kg/day sulfamethoxazole, 1.8 g/day clindamycin) appeared to have a synergistic effect in clinical cases, with patients taking trimethoprim/sulfamethoxazole/clindamycin showing a lower frequency of relapses [103]. Implementation of clindamycin is particularly advantageous for patients exhibiting strong adverse reactions to sulfonamides [104].

Another source of anti-*Toxoplasma* therapies, particularly for patients who respond poorly to standard treatment regimens, are inhibitors of oxidative phosphorylation via the parasitic electron transport chain in the mitochondria. Atovaquone is one such compound; as a hydroxy-1,4-naphtoquinone developed for treatment of malaria [105], but found to show broad antiparasitic activity [106], atovaquone was observed to have high *in vitro* potency at 0.138 µM [107], and, in mice, doses of 5 mg/kg/day facilitated a less-impressive, though significant, 20% survival of acute infection [108]. Synergistic improvements of atovaquone potency have been observed in mice, with co-administration of clindamycin

(50 mg/kg/day atovaquone, 50 mg/kg/day clindamycin) leading to 78% survival in lethal acute infection [101]. Clinically, dosages vary substantially, but typically can be found to reside near 750 mg 1-4 times per day for at least 6 weeks [88], for which little toxicity was found in a clinical study of 7 patients [88], indicating that atovaquone is well-tolerated.

Despite the plethora of antibacterial and antimicrobial agents, few have been clinically implemented—or clinically successful—in clearing *Toxoplasma gondii* infection. A combinatorial pyrimethamine and sulfadiazine treatment remains the current standard of care, [11; 109]. While successful, this treatment regimen demonstrates potentially-serious adverse reactions, including hematological effects and allergic responses arising from high dosages required for presumed clearance [5]. Further, all of the current FDA-approved anti-*Toxoplasma* compounds have only been shown clinically to act against acute toxoplasmosis, leaving a serious gap for individuals housing brain and muscle cysts and leaving the potential for damaging recrudescence to occur later in life [11; 109]. Additionally, the existing alternative treatments show lower potency than pyrimethamine/sulfadiazine and have inconsistent clinical outcomes in addition to poor patient tolerability [104]. Taken together, these factors emphasize a need for improved therapeutic options—both of higher potency and higher specificity for acute infection, and of any efficacy for chronic infection—to more effectively combat *T. gondii*. Through this work, I aim to identify specific and potent molecules that show promise against this infection.

IV. Marinopyrroles: A Novel Class of Marine-Derived Antimicrobial Compounds

Efforts to identify improved therapeutic options for a number of pathogens—notably, pathogens demonstrating resistance to existing pharmaceutical interventions—have led to intensive examinations of numerous organic and synthetic sources. Regarding the former, one well-established realm of study is that of marine natural products, which have thus far provided a plethora of novel antimicrobial and anticancer compounds [110]. A key

contributor to the production of these compounds are the deep-water marine bacteria found in sediment, organic debris, and in symbiosis with other aquatic life forms—more specifically, bacteria belonging to the order *Actinomycetales* (called actinomycetes), which are estimated to have contributed to nearly 70% of the existing marine-derived compounds in clinical use [111]. Of these, a vast majority of products are produced biologically by species belonging to the genus *Streptomyces*, soil-dwelling marine microbes capable of withstanding the low light, temperature, oxygen, and variable salinity of depths exceeding 2000 m [111, 112]. As a consequence of this vastly-different environment, and due to the high competition for limited resources available in these locations, marine *Streptomyces* species produce highly biologically-active metabolites found to exhibit potent antibacterial, antifungal, and anticancer capacities [112], providing a crucial source of novel chemical entities for further treatment of numerous afflictions [110].

Among these novel and bioactive compounds are the marinopyrroles, a novel class of small organic molecules isolated from the marine *Streptomyces* species CNQ-418 [113]. CNQ-418 is an obligate marine sedimentary bacterium first obtained from deep-ocean samples near La Jolla, California, and it was found that lysates from cultures of this bacterium appeared to cause potent inhibition of *Staphylococcus aureus* growth [113]. Subsequent capture and analysis of metabolites revealed two potent antimicrobial molecules in relatively high abundance: marinopyrrole A ([4,5-dichloro-1-[4,5-dichloro-2-(2-hydroxybenzoyl)-1H-pyrrol-3-yl]pyrrol-2-yl](2-hydroxyphenyl)-methanone), also called maritoclax commercially, and marinopyrrole B ([3-[4-bromo-2,3-dichloro-5-(2-hydroxybenzoyl)pyrrol-1-yl]-4,5-dichloro-1H-pyrrol-2-yl]-(2-hydroxyphenyl)methanone) [114]. X-ray crystallography in conjunction with 2D NMR indicated that the structures of these compounds exhibited unique bi-substituted pyrrole structures uncommonly seen in bioactive

molecules [113] (**Figure I.1**). These compounds were also shown to be highly hydrophobic and densely-halogenated, rendering them slightly acidic [113] (**Figure I.1**).

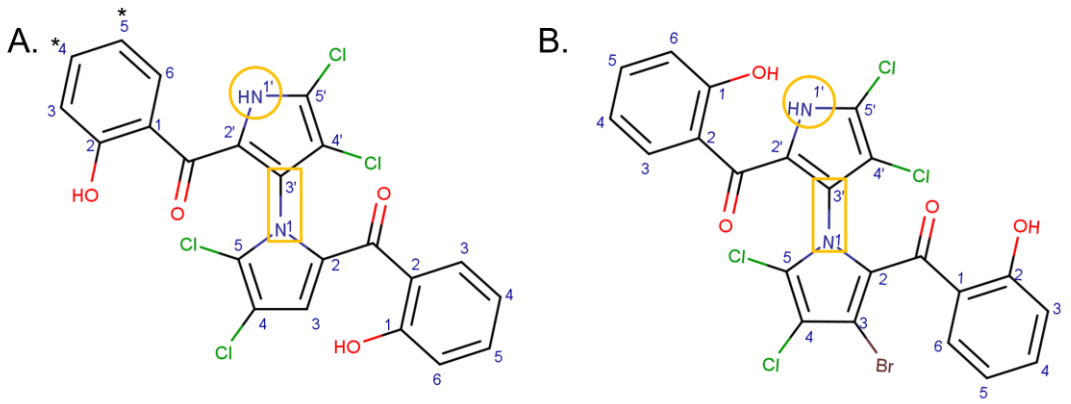

Figure I.1. Structures of (-)marinopyrrole A (A) and (-)marinopyrrole B (B) with sites of modification on (-)marinopyrrole A. From X-ray crystallography in conjunction with 2D NMR, it was possible for Hughes *et al.* [113] to elucidate the structures of marinopyrroles A and B. Subsequent analyses by Hughes [114], Nicolaou [127], Li [128], Cheng [130], and others by modification of the non-halogen polar functional groups (red), halogen groups (green, brown), or the N-H bond (orange circle) supported the central importance of the N-H bond to antimicrobial activity and, further, demonstrated that chlorination or bromination at key aryl positions (*) could generate higher-potency derivatives against *S. aureus* strains. Marvin was used for drawing and displaying chemical structures, Marvin 21.1, 2021, ChemAxon (http://www.chemaxon.com).

Analysis of these structures showed multiple desirable antibacterial properties. Initial screens indicated high bactericidal potency against methicillin-resistant *S. aureus* (MRSA), with 90% minimum inhibitory concentration (MIC_{90}) values of 0.31-0.38 µg/mL and 0.63-1.0 µg/mL for (–)marinopyrrole A (–)marinopyrrole B, respectively [113, 114]. Compared to vancomycin (MIC_{90} 1-2 µg/mL; [115]), gentamicin (MIC_{90} 0.5-1 µg/mL; [116]), and penicillin G (MIC_{90} 6.3-12 µg/mL; [115]), both of these marinopyrroles demonstrated substantially higher potency than either vancomycin or gentamicin and >10X higher potency than penicillin G, prompting rapid interest in examining the antibacterial properties of these molecules, and particularly marinopyrrole A, in detail. A follow-up study examined the efficacy of marinopyrrole A against a series of *Staphylococcus aureus* strains, including hospital-acquired (HA) and community-acquired (CA) MRSA strains, in addition to several vancomycin-resistant *S. aureus* (VRSA) strains [117]. Results demonstrated high

potency (<2 μg/mL) against all examined *S. aureus* strains; for MRSA strains MICs ranged from 0.188-0.375 μg/mL, while for VRSA strains MICs ranged from 0.25-1.5 μg/mL [117], suggesting that marinopyrrole A retains high potency even in the presence of antibiotic resistance. This represents a crucial finding in the continued search for improved antibacterial molecules, particularly given the rapidly-rising rates of antibiotic resistance occurring worldwide.

Further evaluation of the advantageous properties of marinopyrrole A also provided insights into its potential quality as an antibiotic compound. Crucially, toxicity to eukaryotic cell lines HeLa (immortal cervical cancer) and L929 (murine fibroblast) appeared to be quite low, with IC_{50} values for these cell lines exceeding 20-fold those required for inhibition of MRSA [117]. Intriguingly, however, the colorectal cancer cell line HCT-116 did show substantial sensitivity to marinopyrrole A, with an IC_{50} of 4.5 μg/mL, although this value remained >10-fold higher than the MIC for any MRSA strain [114] (and, in addition, may be an artefact of the tumorigenicity of this cell line [31295840], discussed in the paragraph below). In addition, treatment of MRSA cultures with marinopyrrole A followed by subsequent removal led to a significant post-antibiotic effect characterized by dose-dependent defects in growth 4-6 hours post-removal of marinopyrrole A [117]. This compound also showed sub-micromolar antimicrobial activity against multiple gram-positive bacteria, including *S. epidermidis*, *B. anthracis*, *S. pyogenes* as well as activity against the gram-negative bacterium *H. influenzae,* demonstrating a broad antibacterial activity (though highest potency was found against MRSA strains) [117]. Finally, the functional *N, C*-biaryl bond (**Figure I.1.A.**, orange box) is conformationally stable at room temperature, suggesting that the bioactivity of the compound would be retained even without cold storage [114].

Marinopyrrole A showed additional properties as an anticancer molecule acting against several myeloid-derived leukemia and lymphoma cell lines *in vitro*, overcoming the dysregulation of apoptosis common to malignancies [118; 119; 120]. Particularly, the human cell lines lymhoma-60 HL-60 and peripheral T-cell leukemia Jurkat were found to be inhibited by marinopyrrole A at 1.67-2.15 μM and 2.53 μM, respectively [121]. Promotion of apoptosis was found to occur through binding and subsequent induction of proteasomal degradation of the pro-survival apoptosis-associated protein myeloid cell leukemia protein 1 (Mcl-1) [118; 121]. Combination of sub-toxic marinopyrrole A concentrations with the Bcl-2/$Bclx_L$ (B-cell lymphoma-2/B-cell lymphoma extra-large) small-molecule inhibitor ABT-737 appears to provide synergistic stimulation of apoptosis even in cells overexpressing Mcl-1, including myelogenous leukemia K562 and hematopoietic lymphoma-like Raji cells [118; 121]. Critically, in the presence of multidrug resistance in the human leukemia cell line HL-60/VCR, addition of marinopyrrole A caused this cell line to become re-sensitized to ABT-737, suggesting potential use as a combinatorial therapy for treatment-refractory leukemias and lymphomas [118].

However, while marinopyrrole A appears to have several desirable qualities as an antimicrobial, a number of shortcomings have prevented it from gaining more widespread attention and use. Most problematically, the addition of human serum at 20% v/v in media abrogated the activity of marinopyrrole A against MRSA strains, raising the MIC by an excess of 256-fold [117]; this poses a clear issue for use of this compound in clinical practice, given that this may be an indicator of compound binding to serum proteins and subsequent failure of delivery of an effective dose—particularly in the case of systemic infections. However, whether this translates to loss of potency against bacterial infections *in vivo* remains poorly characterized in the existing literature, presumably due to low interest as a consequence of the *in vitro* serum data. In addition, activity against most gram-

negative bacteria was very low, with no observable MIC found for *E. coli* and *K. pneumoniae* [117], representing a limitation to therapeutic application. Finally, the lack of high-specificity mechanistic data for MRSA activity represents an additional hurdle for further study of this compound; this is particularly relevant given the activity of marinopyrrole A against human cancer cell lines [122], as this may suggest some level of cross-reactivity with human protein targets.

Further, marinopyrrole A has several shortcomings as an anticancer molecule. Serum sensitivity has, paradoxically, been poorly characterized in studies of apoptosis induction—though, presumably, the common use of 5-10% serum in tissue cell culture [123; 124] may indicate that serum sensitivity is less pronounced in the anticancer activity of this compound. In *vivo* data is generally lacking; though several studies have been conducted to address the *in vivo* impacts of marinopyrrole A in murine leukemia and lymphoma models [121; 119], more extended effects of this compound on the host have not been established. This is particularly important due to the observation that the 50% lethal dose (LD_{50}) in mice is low relative to the effective dose; the former was seen to be 25 mg/kg, while the latter is 20 mg/kg [119], which may bode poorly for use as a therapeutic option. It is feasible that host toxicity may be a consequence of low target specificity, as more recent data indicates that Mcl-1 does not appear to be an exclusive target of marinopyrrole A [125]: multiple target analyses showed apparent compound binding to actin by acyl-dye transfer [126]. Combined with the established antibacterial activity, this could indicate that this molecule may have multiple targets, providing potential avenues for unintended host damage.

To attempt to overcome these limitations while retaining or improving the desirably-high potency, multiple groups set out to generate numerous analogs derived from the main structure of marinopyrrole A, focusing on both activity against MRSA in addition to multiple

leukemia and lymphoma lines; however, due to the focus on microbial activity in this work, the former will be described here. The first set of semi-synthetic derivatives were generated by Hughes *et al.* in response to improvements in cultivation of CNQ-418 that facilitated identification of several other marinopyrroles (C-F) that had not previously been identified [114]. These derivatives focused on "capping" the polar functional decorating groups on the aryl rings as well as on modifying the N-H bond to evaluate its importance [114] (**Figure I.1.A.**). None of the designed derivatives improved on the activity of the marinopyrroles; in fact, all performed substantially worse against MRSA, with MICs being increased by >20-fold relative to marinopyrrole A in cases of "capping" the decorating groups, and with activity being completely lost upon modification of the N-H bond, suggesting a crucial importance for this functionality in antibacterial activity [114]. Further attempts to generate anti-MRSA derivatives by Nicolaou *et al*. demonstrated a >500-fold loss in potency relative to marinopyrrole A following methylation of phenol groups, indicating a critical role for these constituents in antibacterial activity [127]. Replacement of chlorine halogenated groups with bromine halogenated groups (**Figure I.1.A.,** green groups) failed to improve anti-MRSA activity, though did not intrinsically inactivate the activity in the same manner as capping of the functional groups [127].

As none of the derivatives had yet improved the potency of marinopyrrole A, Li *et al.* began design and synthesis of asymmetric marinopyrrole derivatives, aiming to improve upon the bactericidal activity of marinopyrrole A while overcoming or improving the sensitivity to serum [128]. Asymmetry was hypothesized to result in biologically-distinct mechanisms of action that could lead to superior antimicrobial activity through site-specific hydrogen bonding and restriction of molecule orientation [110]. Supporting this hypothesis, chlorination or fluorination of one phenol group (at positions 4 or 5, respectively; **Figure I.1.A.**, asterisks) in the parental compound led to a 2-4-fold increase in potency against

MRSA in addition to more rapid killing kinetics, providing crucial insight into the role of halogenated functional groups and free hydroxide groups in the anti-MRSA activity of marinopyrroles [110; 128; 129]. Compellingly, these derivatives were also much less inhibited by serum; rather than complete abrogation of activity, MICs were increased by ~100-fold which, while not ideal, still left the MICs at <25 µg/mL (as opposed to >96 µg/mL for marinopyrrole A) [128; 129]. Halogenation at other locations on the phenol groups (i.e., 2, 3, 6; **Figure I.1.A.**), in addition to methylation of halogenated groups and hydroxy groups (**Figure I.1.A.)**, led to reduction in activity and loss of potency in serum [110].

Cheng *et al.* also generated several derivatives following this schema [130]. Most of these derivatives were much less active than marinopyrrole A, with the exception of a remarkably-potent molecule with a trifluoromethyl substitution at position 4 on the phenol group [130]. This molecule showed a promising 2-4-fold increase in potency against MRSA (as well as a substantial 31-fold increase in potency against methicillin-resistant *S. epidermidis*) relative to marinopyrrole A [130]; however, the activity in 20% serum was not reported, which represents a crucial consideration based on the previously-established sensitivities of these compounds to serum.

Though representing marked improvements to the existing marinopyrrole compounds, these derivatives remain in very early stages of development. *In vitro* determination of host toxicity for these compounds has been largely restricted to cancer cell lines, such as HeLa, HL-60, HCT-116, and several others [117; 118; 131]. These lines are representative of only select tissue types and, additionally, are well-known to be cancer cell lines that may not accurately represent healthy tissues given their variable number of chromosomes and intrinsic genetic instability [132; 133; 134]. Because of this, the toxicity of these compounds to the tested human cell lines may be a consequence of the tumorigenicity, altered metabolism, or altered morphology characteristic of human cancers [134;

135] rather than a consequence of broad mammalian toxicity. Similarly, none of these compounds have, at least as reported in literature, been examined in primary or terminally-differentiated primary cell lines, which may pose different results than the immortalized lines typically used in cell culture [136]. These derivatives are also poorly evaluated in any *in vivo* model; while marinopyrrole A has been examined to some limited extent, as discussed above, the newer derivatives have not yet been evaluated for toxicity *in vivo* or, crucially, for their efficacy *in vivo*. Though improved over marinopyrrole A, the continued sensitivity of these derivatives to serum emphasizes a need for further exploration of *in vivo* potency, particularly against MRSA or other bacterial pathogens, in order to evaluate their therapeutic potential [137]. Additionally, further investigation into the mechanisms of action for these molecules would be advantageous for future design and eventual movement into animal or clinical trials [138].

Despite these shortcomings, the overall broad and potent activity against prokaryotic pathogens and human cancer cell lines still presents promise for these compounds, or derivatives of these compounds, as therapeutic interventions. This is particularly important for identification of improved small-molecule drugs acting against antibiotic-resistant gram-positive infections and treatment-refractory cancers [139]. The high potency and unique activity spanning both prokaryotes and eukaryotes may suggest activity against organisms not yet described in the literature. In particular, given the role of potent antibacterial agents described above in addition to the clear capacity to impact eukaryotic cellular functions, these derivatives may well serve as novel antiparasitic molecules. Therefore, given their high *in vitro* potency and given the similarity of key protist organelles to bacterial structures [83-84], these compounds may provide promising efficacious therapies against parasites for which treatments are currently lacking, such as *T. gondii* [61].

With this work, I intend to investigate the potential antiparasitic activity of marinopyrrole derivatives, focusing on *T. gondii*, and aim to evaluate host cell toxicity in order to establish viability of these derivatives as future therapeutic agents. Additionally, I aim to determine whether successful anti-*Toxoplasma* derivatives demonstrate broader antiparasitic and antibacterial activity.

SPECIFIC AIMS

T. gondii is an obligate intracellular parasite demonstrating widespread global infection and a significant threat in immunocompromised individuals [5]. Current treatments are extremely limited and potentially manifest severe adverse effects, emphasizing a need for improved therapeutic options [61]. One class of small organic molecules, marinopyrroles, were isolated from cultures of marine *Streptomyces* species [113]; one compound, “marinopyrrole A,” was found to demonstrate high efficacy against methicillin-resistant *S. aureus* [114], and now *T. gondii* (described in this work).

A series of distinct compounds synthetically derived from this molecule has been generated, providing potential opportunities for antiparasitic investigation. **We hypothesized that, based on the presumed bacterial origin of the apicoplast [83], one or more derivatives will demonstrate at least 10-fold increased potency against acute-stage *in vitro T. gondii* as compared to the standard therapeutic regimen, plus high (>20x) selectivity compared to host cells.**

Further, numerous anti-*Toxoplasma* compounds, such as trimethoprim and spiramycin [11], are used clinically as antibacterial therapies. Early testing of marinopyrrole derivatives suggests that one or more of these compounds may have efficacy against a broad range of bacterial pathogens beyond *S. aureus*; **we therefore hypothesized that one or more anti-*Toxoplasma* marinopyrroles will demonstrate *in vitro* efficacy against at least two bacterial pathogens of less than 5 μM, and that insights into bacterial susceptibility will provide guidance for elucidation of potential compound targets.**

Finally, we aimed to examine possible genetic underpinnings causing anti-*Toxoplasma* toxicity for at least one compound in this series, **hypothesizing that this would**

manifest in forward genetic screens or differential parasite transcriptomics. We intended to test these hypotheses through three Specific Aims:

Specific Aim 1: Screen compounds against *T. gondii* tachyzoites and additional selected pathogens.

A. Evaluation of *in vitro* antiparasitic activity for compounds against *T. gondii* RH (Type I) and PruKU80 (Type II) tachyzoites.

B. Assessment of selected compound against prokaryotic pathogens *Mycobacterium bovis* BCG, *Escherichia coli, Vibrio cholerae, Staphylococcus aureus* USA300 MRSA, *Legionella pneumophila, Streptococcus pneumoniae, Francisella tularensis subsp. holarctica* LVS, *Shigella sonnei, Yersinia pseudotuberculosis, Bacillus anthracis* lacking pXO2, and *Salmonella enterica* serovar Typhi.

C. Assessment of selected compound against eukaryotic parasites *Leishmania donavani* and *Acanthamoeba castellanii*

Specific Aim 2: Evaluate physiological phenotypic effects of compounds on *in vitro*-generated *T. gondii* cysts and key host cell lines.

A. Evaluation of *in vitro* antiparasitic activity for a selected compound against *in vitro*-generated *T. gondii* cysts.

B. *In vitro* evaluation of selected compound cytotoxicity against host cell lines derived from multiple tissue types, including HFF (human foreskin fibroblast), HCO4 (hepatocyte), U2-OS (osteocyte), HEK-293 (embryonic kidney), THP-1 (monocyte), and THP-1-derived macrophages.

C. Identification of general host cell phenotypic impacts through precellular, short-term and long-term apoptosis, and extended viability assays against HFF cells.

Specific Aim 3: Investigate *in vitro* mechanistic properties of a selected compound against *T. gondii*.

A. Identification of the likely drug target for selected compound in *T. gondii* by random chemical mutagenesis and molecular complementation.

B. Identification of global transcriptional changes in resistant and susceptible compound-treated tachyzoites as compared to vehicle controls through RNA-seq.

From this work, we *expected* to identify one or more marinopyrrole derivatives demonstrating anti-*Toxoplasma* activity without substantial concomitant host cell toxicity and to identify putative mechanistic properties of at least one compound. This supports our *long-term goal*: the development of improved therapeutic options for the treatment of infections caused by selected pathogenic parasites and bacteria.

CHAPTER 1: ANALOGS OF MARINOPYRROLE A SHOW ENHANCEMENT TO OBSERVED *IN VITRO* POTENCY AGAINST ACUTE *TOXOPLASMA GONDII* INFECTION

T. gondii is a globally distributed apicomplexan parasite predicted to infect up to one-third of the human population [19; 140; 141]. While most individuals experience mild symptoms, rapid proliferation of the parasite in brain tissue of immunocompromised patients, including HIV/AIDS patients and solid-organ transplant recipients, leads to toxoplasmic encephalitis, which is often fatal [1, 8]. Further, crossing of the placenta by parasites following exposure during pregnancy yields prenatal infection culminating in crippling or fatal birth defects, including macrocephaly and hydrocephaly [142; 143; 144]. Complicating matters, few existing treatments effectively clear acute infection, with a combinatorial pyrimethamine/sulfadiazine treatment regimen being the most common pharmaceutical intervention [61; 145]; however, extended treatment with high-dose pyrimethamine causes suppression of bone marrow, even when compensatory folic acid supplementation is provided [74], while sulfadiazine exhibits a high incidence of allergic reactions in patients [147]. In addition, there are no FDA-approved treatments that effectively clear chronic infection [11], leaving the potential for previously healthy patients who become immunocompromised after initial *Toxoplasma* infection to experience reactivation of latent cysts [1; 147; 148]. Taken together, these findings emphasize a clear need for improvements to existing therapeutic options against this prevalent parasite.

In attempting to alleviate this shortage of treatments against *T. gondii*, marine natural products represent a wealth of potential antiparasitic compounds, capitalizing on the existing competition between organisms to generate potent, complex organic molecules that have already been found to range in activity from antibacterial [128; 149] to anticancer [129; 150]. Previous work has provided compelling evidence identifying marinopyrrole A ([4,5-dichloro-1-[4,5-dichloro-2-(2-hydroxybenzoyl)-1H-pyrrol-3-yl]pyrrol-2-yl]-(2-hydroxyphenyl)methanone), a metabolite of marine *Streptomyces* species CNQ-418, as a potent

bactericidal agent against methicillin-resistant *Staphylococcus aureus* (MRSA) *in vitro* [117], and, at higher concentrations, an inducer of apoptosis in a variety of cancer cell lines both *in vitro* and *in vivo* [149].

For our purposes, antibacterial molecules—including doxycycline [86], trimethoprim [78], and spiramycin [94]—have been shown previously to inhibit *Toxoplasma* proliferation, and so, based on the high potency of marinopyrrole A, we sought to evaluate its potential antiparasitic activity *in vitro* and *in vivo* [61].

In this work, we aim to identify the *in vitro* and *in vivo* efficacy of marinopyrrole A against *T. gondii* tachyzoites, and, further, to evaluate several analogs derived from this compound for any enhancements to potency and/or serum sensitivity *in vitro*. We show through our *in vitro* parasite viability assays that marinopyrrole A is a highly-potent anti-*Toxoplasma* molecule that shows significant loss of this potency in concentrations of serum at or exceeding 20% (as has been noted in previous work for other organisms) [128]. Despite this sensitivity to serum *in vitro*, we found that marinopyrrole A still facilitates enhanced survival in an *in vivo* murine model of lethal *Toxoplasma* infection at 20 mg/kg, suggesting potential applicability for further investigation. Further, we show that several of a series of analogs that we designed and generated from marinopyrrole A, including the compounds RL002, RL003, and RL125, have significantly increased potency *in vitro* without concomitant increase in toxicity to host cells, with all analogs having substantially decreased serum sensitivity. Taken together, these data suggest that marinopyrrole A and its higher potency analogs represent previously undescribed anti-*Toxoplasma* molecules, providing crucial insight into improved therapies against this infection.

Results

Marinopyrrole A is toxic to *T. gondii* RH-dTom tachyzoites *in vitro*.

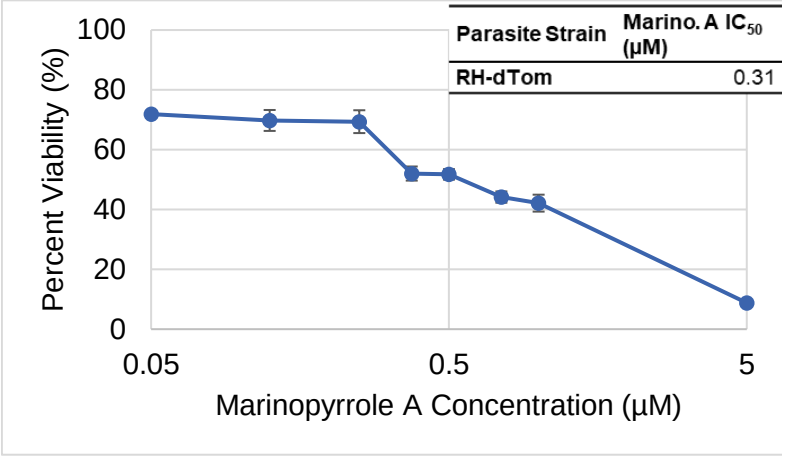

Figure 1.1. Marinopyrrole A demonstrates submicromolar efficacy against *T. gondii* RH-dTom tachyzoites *in vitro*. Determination of marinopyrrole A efficacy was completed by infecting a confluent HFF host monolayers in a 96-well plate with *T. gondii* RH-strain tachyzoites stably expressing the dimerized Tomato protein fluorescent reporter (dTom) at 2,000 parasites/well. Marinopyrrole A was added at increasing concentrations in triplicate across infected wells, with a volume-matched DMSO solvent control included for comparison. Following 5 days of treatment, relative fluorescence of infected wells was quantified and background host fluorescence was removed, after which the 50% inhibitory concentration (IC_{50}) was calculated by comparing each infected well to the corresponding solvent control. Results demonstrated that marinopyrrole A is effective against RH-dTom tachyzoites *in* vitro, with an IC_{50} of 0.31 µM. Error bars represent standard error across triplicate samples.

Based on the broad nature of the antimicrobial effects of marinopyrrole A, and given the historical capacity of antibacterial agents to serve as potent antiparasitic molecules [11; 61], we sought to elucidate the potential anti-*Toxoplasma* activity of marinopyrrole A *in vitro*. To this end, we performed an *in vitro* identification of the 50% inhibitory concentration (IC_{50}) for marinopyrrole A in technical triplicate against type I RH-strain *T. gondii* tachyzoites stably expressing the fluorescent dimerized Tomato protein (RH-dTom) as discussed in our previous work [151]. As shown in **Figure 1.1**, marinopyrrole A demonstrated dose-dependent toxicity and high potency against *T. gondii* parasites, with a sub-micromolar IC_{50} of 0.31 µM (corresponding to an increase in potency of ~2-fold relative to pyrimethamine (**Figure 1.1**)).

The anti-*Toxoplasma* activity of marinopyrrole A is inhibited by the presence of ≥20% bovine calf serum.

Previous characterization of the antimicrobial properties of marinopyrrole A identified strong reduction of anti-MRSA activity when liquid media was supplemented with 20% serum [117]. While we conducted our initial analysis of *in vitro T. gondii* efficacy in the recommended 10% serum for tachyzoite and host cell growth [152], we sought to further identify potential dose-dependent effects of increasing serum concentrations on the anti-*Toxoplasma* activity of marinopyrrole A. We therefore repeated our viability assay to determine the IC_{50} values using the same method as described above, though media in this case was supplemented with 1%, 10%, 20%, 30%, or 50% bovine calf serum (BCS). Dilutions of marinopyrrole A in each serum concentration were completed in technical triplicate. Our data (**Table 1.1**) show a 1.2-fold increase in IC_{50} between 1% BCS and 10% BCS, with the IC_{50} no longer being reached (NR) up to 10 µM in the presence of 20-50% BCS, corresponding to a >38-fold decrease in potency relative to 1% BCS. These findings suggest that, as demonstrated previously in other organisms, serum concentrations at or exceeding 20% inhibit the anti-*T. gondii* activity of marinopyrrole A *in vitro*.

Concentration of Serum (%)	**Marinopyrrole A IC_{50} (µM)**	**Fold Increase in IC_{50} Relative to 1% BCS**
1%	0.26	-
10%	0.31	1.2
20%	NR	>38X
30%	NR	>38X
50%	NR	>38X

Table 1.1. Marinopyrrole A demonstrates a dose-dependent decrease in potency following the addition of serum, culminating in loss of efficacy against RH-dTom tachyzoites at and beyond 20% serum. IC_{50} analyses were conducted in the presence of 1%, 10%, 20%, 30%, or 50% bovine calf serum (BCS) in the base medium. We noted little change in IC_{50} values between 1% and 10% BCS (~1.2-fold increase). Yet marinopyrrole A efficacy against *T. gondii* was completely eliminated the presence of 20% BCS, with the IC_{50} not being reached (NR) up to 10 µM. This corresponded to a >38-fold decrease in potency.

Marinopyrrole A shows efficacy against acute *Toxoplasma* infection in a murine model.

Marinopyrrole A was assessed for its capacity to allow for significant survival in Swiss-Webster mice following a lethal challenge of 5,000 *T. gondii* tachyzoites of the type II ME49 strain (**Figure 1.2)**. Following infection, mice were treated daily with varying dosages of Marinopyrrole A (5, 10 and 20 mg/kg) daily through intraperitoneal injection for 10

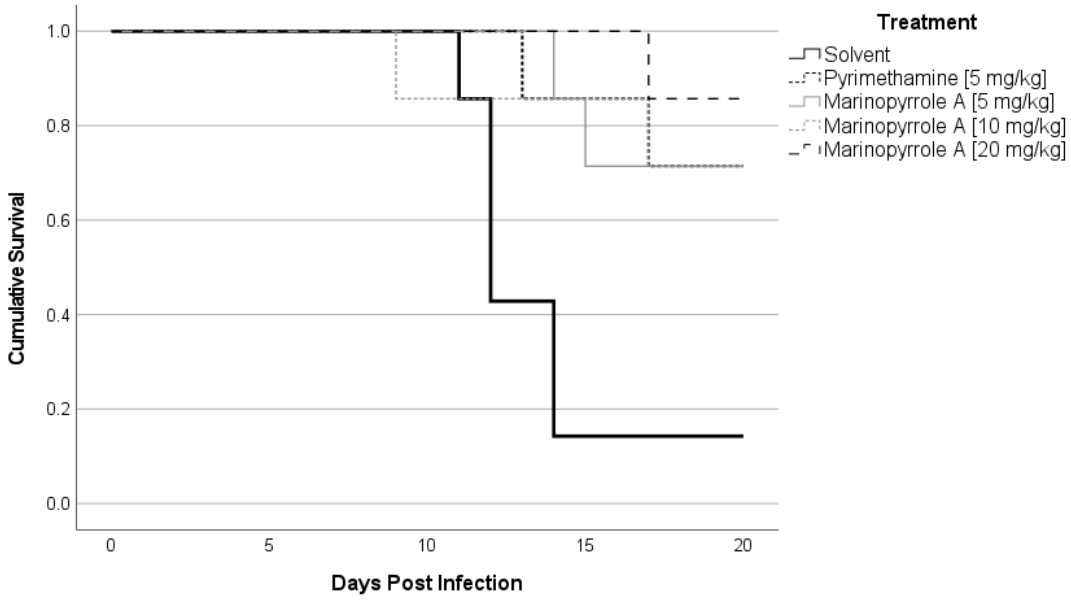

Figure 1.2. Survival of mice lethally infected with *T. gondii* treated with varying marinopyrrole A doses. Swiss-Webster mice were infected with 5,000 ME49 *Toxoplasma gondii* tachyzoites. Following infection, marinopyrrole A treatment began via intraperitoneal injection at 5, 10, or 20 mg/kg given every day for a total of 10 days (n=7 for each dosage). Pyrimethamine was given at 5 mg/kg via intraperitoneal injection once per day for a total of 10 days as a positive control for mouse survival (n=7). Solvent treated by intraperitoneal injection (10 days of treatment) mice were also included as a negative control (n=7). 71.4% of mice survived when treated with either marinopyrrole A at 5 (*p* value=0.01) and 10 mg/kg (*p* value=0.04) while 85.7% of mice survived when treated with 20 mg/kg of marinopyrrole A (*p* value=0.004). 71.4% of pyrimethamine treated mice survived (*p* value=0.02) while only 14.3% of solvent treated mice survived infection. All *p* values are respective to solvent-treated mice.

days post-infection (n=7). Pyrimethamine treated mice were included as a positive control and exhibited 71.4% survival (*p* value=0.02, n=7). Mice treated with only solvent exhibited 14.3% survival (n=7). Marinopyrrole A at both 5 mg/kg (*p*=0.01, n=7) and 10 mg/kg (*p*=0.04, n=7) exhibited 71.4% survival. When marinopyrrole A was increased to 20 mg/kg,

85.7% of mice survived (p=0.004, n=7) (**Figure 1.2**). All p-values shown are respective to solvent treated mice.

Design of marinopyrrole A analogs generated novel compounds RL002, RL003, and RL125.

The analogs RL002, RL003, and RL125 are shown in **Figure 1.3.** A marinopyrrole-based small-molecule library, that we designed and reported recently, showed the clogP values >5. [110; 153; 154]. A majority of these library compounds have poor water solubility. Using a fragment-based approach, a team led by our collaborator, Dr. Rongshi Li, recently designed a natural-product small-molecule library with lower clogP values ranging from 2.0 to 5.0 [155; 156; 157-167]. Their design improved physicochemical and drug-like properties. For example, **RL002** and **RL003** shown in **Figure 1.3** have clogP values of 4.1 and 4.7, respectively. Ligand Efficiency [LE ≅ - ΔG/HAC, defined as the free energy of binding divided by the number of non-hydrogen atoms (HAC)] of **RL002** and **RL003** are 0.54 and 0.56, respectively, doubling that of marinopyrrole A (LE = 0.27).

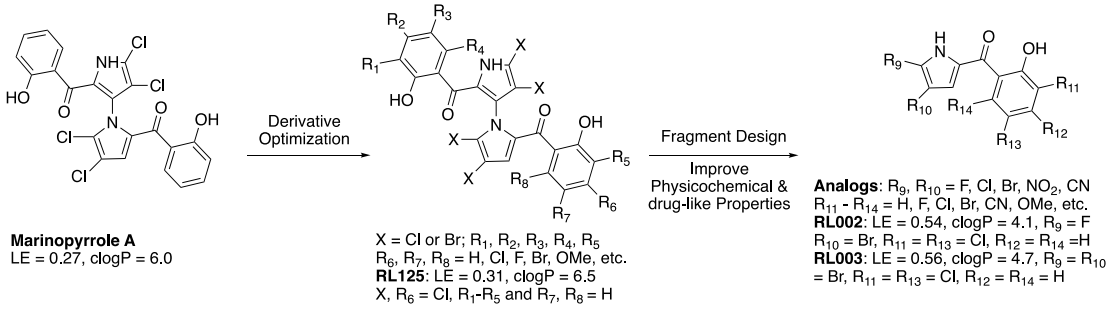

Figure 1.3. Structural diagrams of marinopyrrole A analogs. Marinopyrrole A served as a parent molecule for the generation of derivative **RL125,** which was subsequently used in a fragment-based design process yielding analogs **RL002** and **RL003** as described in the text.

Analogs of marinopyrrole A improve potency against *T. gondii* RH-dTom parasites.

Though retaining overall *in vivo* efficacy, inhibition of marinopyrrole A activity by serum represents a critical and physiologically-inhibitory hurdle. The high potency of this molecule against *T. gondii* at 1-10% serum, prompted our collaborators to generate compounds capitalizing on the advantageous properties of marinopyrrole A while improving

activity in serum. Cheng and others have previously generated a series of drug-like molecules derived from marinopyrrole A [149] (**Figure 1.3**). Given the reduced inhibitory effect of serum for several of these compounds *in vitro* against MRSA [128, 129], we sought to evaluate the potential anti-*T. gondii* activity of compounds RL002, RL003, and RL125 through the use of the tachyzoite viability assay discussed above, with the aim of determining which, if any, showed high potency against RH-dTom tachyzoites.

To determine the efficacy of RL002, RL003, and RL125 against RH-dTom tachyzoites, we conducted another series of viability assays mirroring those conducted against marinopyrrole A, calculating IC_{50}s relative to the solvent control as before. Remarkably, as shown in **Figure 1.4**, all analogs demonstrated dose-dependent sub-micromolar

Compound Identifier	IC_{50} Against RH-dTom Tachyzoites (μM)	Fold Reduction in IC_{50} Relative to Pyrimethamine
Marinopyrrole A	0.31	2.0*
RL002	0.17	3.6*
RL003	0.09	6.8*
RL125	0.16	3.8*
Pyrimethamine	0.61	-

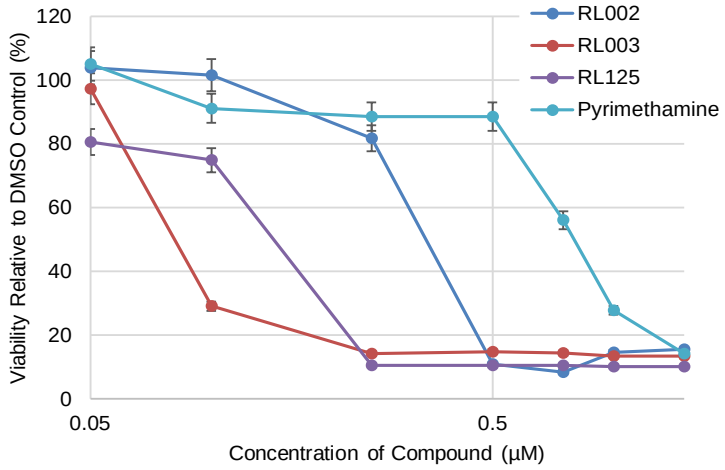

Figure 1.4. *In vitro* antiparasitic activity for marinopyrroles analogs demonstrate substantial dose-dependent efficacy against *T. gondii* RH-dTom tachyzoites with enhanced potency as compared to pyrimethamine. Relative viability compared to the solvent (DMSO) control demonstrated a dose-dependent antiparasitic effect across all derivatives, with pyrimethamine included as a positive control. Derivatives RL002, RL003, and RL125 showed higher potency than the marinopyrrole A parent (included for reference), and RL003 was identified to have the highest potency, with an IC_{50} of 0.092 μM. Assays for each analog were run in technical triplicate and are treated as independent experiments (with the exception of pyrimethamine, which was run on each plate). Error bars represent standard error across technical triplicate samples. *$p < 0.001$ by Student's paired t-test assuming unequal variance.

efficacy against RH-dTom tachyzoites, ranging from 0.092-0.371 μM (corresponding to a statistically-significant 1.6-6.8-fold increase in potency relative to our obtained IC_{50} of 0.60 μM against pyrimethamine). These analogs demonstrated notable 1.9-3.3-fold increases in potency as compared to the marinopyrrole A parent (**Figure 1.4**), suggesting improved anti-*Toxoplasma* activity *in vitro*.

Marinopyrrole A analogs RL002, RL003, and RL125 show reduced sensitivity to serum.

While the observed enhancements to potency represent marked improvements to the advantageous qualities of the marinopyrrole A parent compound, the potential for serum-mediated reduction in activity prompted us to quantify the effects of increasing serum concentrations on the IC_{50} for each analog. To accomplish this, we repeated the serum parasite viability assay described above for marinopyrrole A with analogs RL002, RL003, and RL125. **Table 1.2** shows the results of this analysis: RL002 showed substantial decreases in potency between 1% BCS and 50% BCS, with a ~30-fold increase in IC_{50} corresponding to a value of 5.0 μM at 50% BCS. Though RL125 had a nearly 40-fold increase in IC_{50} compared to the 1% DMSO control, this compound maintained a high-potency efficacy IC_{50} of 0.38 μM at 50% serum. Conversely, RL003 exhibited a 5.91-fold increase in

Concentration of Serum (%)	Marinopyrrole A IC_{50} (μM)	RL002 IC_{50} (μM)	RL003 IC_{50} (μM)	RL125 IC_{50} (μM)
1%	0.26	0.17	0.03	0.01
10%	0.31	0.17	0.09	0.16
20%	NR	3.4	0.10	0.18
30%	NR	4.4	0.14	0.37
50%	NR	5.0	0.15	0.38

Table 1.2. Marinopyrrole A derivatives RL002, RL003, and RL125 demonstrate only modest decreases in potency in the presence of increasing serum concentrations. All marinopyrrole A derivatives exhibited decreased sensitivity in serum compared to marinopyrrole A. These data suggest that marinopyrrole A derivatives RL002, RL003, and RL125 have reduced susceptibility to the serum-mediated loss of potency shown in the parent compound, with RL003 and RL125 maintaining high potency at 50% serum.

IC_{50} between 1% and 50% serum and, further, maintained its sub-micromolar efficacy and overall high potency with an IC_{50} of 0.146 μM. These data suggest that marinopyrrole A derivatives RL002, RL003, and RL125 are less sensitive to serum than the parent compound, with RL003 and RL125 retaining higher potency than pyrimethamine up to 50% serum.

RL003 is a potent inhibitor of *in vitro*-generated *T. gondii* cysts.

Due to its potency against RH-dTom tachyzoites, we aimed to evaluate the efficacy of RL003 against *in vitro*-generated cysts. RH-dTom parasites are not generally considered to form mature cysts in culture due to their high virulence [299], and so we performed our analyses with PruΔ*KU80*-GFP, a type II cyst-forming strain expressing GFP fused to the bradyzoite-specific lactose dehydrogenase (LDH2). To ensure that this strain showed similar susceptibility to RH-dTom, we first completed an IC_{50} analysis that included PruΔ*KU80*-GFP and another type II strain, ME49, for comparison. Parasites were plated as described above prior to treatment with increasing concentrations of RL003 or the positive control pyrimethamine. Volume-matched DMSO solvent controls were also included, and all concentrations were added to triplicate wells. However, neither the PruΔ*KU80*-GFP strain nor the ME49 strain

Parasite Strain	RL003 IC_{50} (μM)	Pyrimethamine IC_{50} (μM)
ME49	0.056	0.60
PruΔ*KU80*-GFP	0.071	0.58

Table 1.3. Type II strains ME49 and PruΔ*KU80*-GFP show susceptibility to RL003 similar to the Type I RH-dTom strain. Differences in archetypal lineage have previously been associated with differences in susceptibility to antiparasitic interventions; therefore, we aimed to determine whether the slower-growing, lower-virulence type II strains ME49 and PruΔ*KU80*-GFP showed similar susceptibility to RL003 compared to RH-dTom. Parasites were plated with RL003 or a volume-matched solvent (DMSO) control in triplicate in 96-well plates as described previously. Quantification of IC_{50} was completed through immunofluorescent staining for the major surface antigen SAG1 and subsequent counting of labeled parasites with an automated microscope. As anticipated, both ME49 and PruΔ*KU80*-GFP had slightly, but not significantly, higher susceptibility to RL003 as compared to RH-dTom, indicating that there is no loss of activity across type I and type II parasite strains. Pyrimethamine was included as a positive control to validate that the method used produced accurate results.

used express fluorescence during the tachyzoite stage; therefore, the quantification procedure was modified by instead performing immunofluorescent staining for the major surface antigen 1 (SAG1) followed by counting of SAG1-positive parasites with an automated microscope. Results of this analysis showed that both PruΔ*KU80*-GFP and ME49 showed similar susceptibility to RH-dTom (IC_{50} = 0.096 µM), with IC_{50} values of 0.071 µM and 0.056 µM, respectively (**Table 1.3**); though these values were lower than that of RH-dTom, this difference was not significant. The pyrimethamine control showed expected IC_{50} values of 0.58 µM and 0.60 µM for PruΔ*KU80*-GFP and ME49, respectively, supporting the validity of the method used (**Table 1.3**). These findings indicated that PruΔ*KU80*-GFP and ME49 tachyzoites do not have significantly altered inhibition by RL003, validating that results obtained from *in vitro* evaluation of chronic infection would not be a consequence of general differences in susceptibility to RL003.

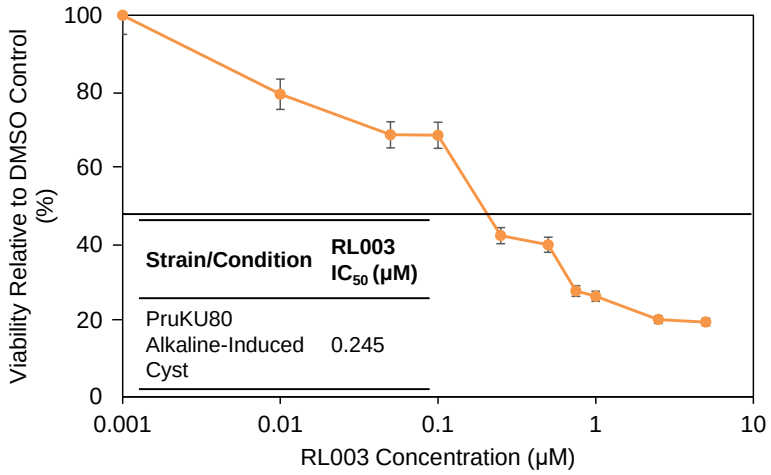

Figure 1.5. RL003 demonstrates submicromolar efficacy against *in vitro*-generated PruKU80 *T. gondii* cysts. Evaluation of the capacity for RL003 to act against tissue cysts of *T. gondii* was conducted *in vitro*. 96-well plates containing PruKU80 parasites constitutively expressing GFP in the bradyzoite stage were treated with alkaline induction media (pH 8.1) for 9 days without added CO_2 in order to induce differentiation into bradyzoites. Upon successful generation of GFP-positive cysts, increasing concentrations of RL003 were added, along with a volume-matched DMSO control. Cysts were counted using an automated microscope and IC_{50} was calculated relative to the solvent control. All concentrations were evaluated in triplicate. Results showed a dose-dependent response of cysts to increasing RL003 concentrations, reaching an IC_{50} of 0.245 µM. This suggests that RL003 is a potent anti-bradyzoite agent able to act against tissue cysts. Error bars represent standard error from the mean.

We proceeded to evaluate the activity of RL003 against encysted bradyzoites of this strain. PruΔ*KU80*-GFP tachyzoites were used to infect HFF cells in 96-well plates

containing D10 media, which is preferential for the replication of this stage, and permitted to invade for 24 hours before differentiation was induced using an alkaline induction media (pH 8.1) described in [186] and in the “Methods” section below. Induction was permitted to occur for 9 days in the absence of added CO_2. The presence of cysts was validated by fluorescent microscopy for GFP and light microscopy. RL003 was then added at increasing concentrations in triplicate to the wells. A volume-matched DMSO control was also included. Plates were incubated for 5 days before counting was performed using an automated microscope, with IC_{50} values calculated as before. Results showed a dose-dependent decrease in GFP-positive cysts upon exposure to increasing concentrations of RL003, reaching a sub-micromolar IC_{50} of 0.245 µM (**Figure 1.5**). This suggests that RL003 is a potent inhibitor of *T. gondii* bradyzoites *in vitro* even when present in cysts.

Analogs of marinopyrrole A show low toxicity to HepG2 and HFF cell lines, demonstrating high selectivity for parasites *in vitro*.

The high potency of the marinopyrrole A analogs provided promising data suggesting antiparasitic activity; however, due to the inherent dependence of *T. gondii* on host cell survival [168] and due to the clinical relevance of excluding compounds that may be disadvantageous to human cells [169], we evaluated the toxicity of each analog to two cell lines: HFF (human foreskin fibroblast) and HepG2 (human hepatocellular

Compound Identifier	IC_{50} Against HFF (µM)	IC_{50} Against HepG2 (µM)
Marinopyrrole A	>50	5.3
RL002	>50	28.0
RL003	>50	49.7
RL125	>50	46.5

Table 1.4. Marinopyrrole A derivatives RL002, RL003, and RL125 show no or limited toxicity to human foreskin fibroblast (HFF) and human hepatocarcinoma (HepG2) cell lines *in vitro*. Confluent HFF or HepG2 monolayers in a 96-well plate were treated in technical triplicate with increasing concentrations of each compound of interest or a volume-matched solvent (DMSO) control for 5 days. Results showed that neither marinopyrrole A nor any of the marinopyrrole derivatives were toxic to the HFF cell line up to 50 µM. Conversely, marinopyrrole A was toxic to HepG2 cells, with an IC_{50} of 5.3 µM; while seemingly low, represents a >50-fold higher IC_{50} than that required for *T. gondii* RH-dTom parasites. The marinopyrrole A analogs had much lower toxicity against HepG2.

carcinoma). To quantify cell viability, we employed the use of a resazurin assay [170] for each cell line in the presence of either increasing compound concentrations or a volume-matched solvent control, with the IC_{50} being calculated relative to the solvent control. We found that RL002, RL003, and RL125 showed no detectable toxicity in HFF cells, reflected by the absence of a quantifiable IC_{50} up to 50 µM shown in **Table 1.4**. Analogs did show some toxicity to HepG2 cells, varying from 28.0-49.7 µM (**Table 1.4**); while initially concerning, these IC_{50} values were much lower than those required for toxicity to parasites, representing ~291-517-fold decreased potencies as compared to the *T. gondii* RH-dTom IC_{50} values and thereby suggesting high selectivity for parasites over the host. Additionally, these analogs had reduced toxicity as compared to marinopyrrole A, which showed an IC_{50} of 5.3 µM against HepG2 cells (**Table 1.4**). Therefore, taken together, these findings addressed preliminary concerns of general host cell toxicity and permitted more focused evaluation of other tissue types.

Expanded screening indicates that RL003 has low toxicity to non-tumorigenic human tissue cell lines, with selectivity >20X for parasites over any susceptible human cells.

With its potent activity against both *T. gondii* tachyzoites and cysts, and with a demonstration of low toxicity against HFF and HepG2 cells, we performed an expanded cell toxicity screen with RL003 to more thoroughly evaluate its effects against lines representative of other tissues. Six additional immortalized cell lines were considered: U2-OS (osteosarcoma), HEK-293 (human embryonic kidney), THP-1 (monocyte), THP-1 MΦ (macrophage), HC-04 (hepatocyte cell line genetically identical to, but functionally distinct from, HepG2), and 17Cl1 (spontaneously-immortalized fibroblasts). Additionally, to evaluate the potential impact of RL003 on a primary cell line, human peripheral blood mononuclear cells (PBMCs) were included for analysis. To perform this evaluation, confluent

monolayers of adherent cells or 1 x 10^5 cells/well of suspension cells (i.e., PMBCs, THP-1, THP-1 MΦ) were treated with increasing concentrations of RL003, incubated for 5 days at 37 ^oC and 5% CO_2, and evaluated for viability through the use of a resazurin assay as described above.

Results showed that HC-04 and THP-1 MΦ lines did not reach an IC_{50} up to 50 µM, indicating >500X decreased potency for host cells over RH-dTom parasites (**Figure 1.6**). THP-1 cells had an IC_{50} of 13.62 µM, which was >100X higher than that of RH-dTom (**Figure 1.6**). In contrast to these lines, the tumorigenic U2-OS, HEK-293, 17Cl1 had lower

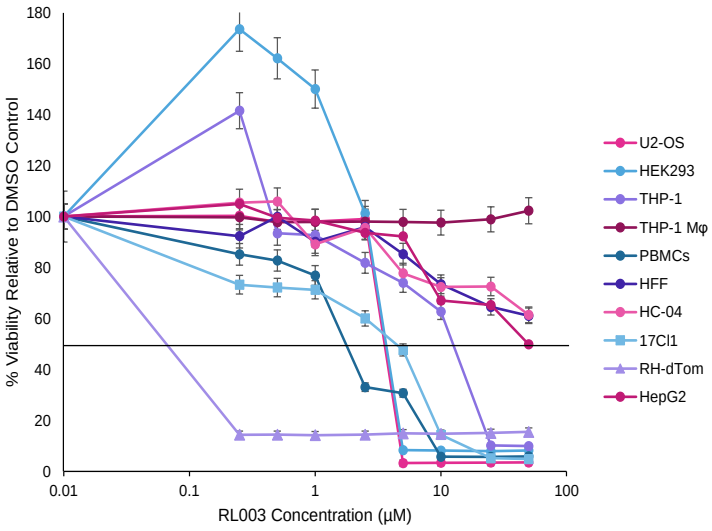

Cell Line Identifier	IC_{50} (µM)	Fold Change Relative to *T. gondii* IC_{50}
U2-OS	3.78	39.4*
HEK-293	3.88	40.4*
THP-1	13.62	141.9*
THP-1 MΦ	NR	>500
Primary PBMCs	1.92	20.0*
HFF	NR	>500
17Cl1	4.52	47.1*
HepG2	49.7	>500
HC-04	NR	>500
T. gondii RH-dTom	0.096	-

Figure 1.6. RL003 shows low toxicity to non-tumorigenic immortalized human cell lines and demonstrates ≥20X selectivity for *T. gondii*. Due to its high potency *in vitro* against *T. gondii* tachyzoites, RL003 was selected for a more widespread evaluation of cytotoxicity against a number of additional cell lines (beyond HFF and HepG2 shown in **Table 1.4**) corresponding to distinct tissue types: U2-OS (osteosarcoma), HEK-293 (human embryonic kidney), THP-1 (monocyte), THP-1 MΦ (macrophage), primary peripheral blood mononuclear cells (PBMCs), HC-04 (another hepatocyte line), and 17Cl1 (another fibroblast line). Cells were evaluated for sensitivity to RL003 as described in **Table 1.4**. Results showed that THP-1 MΦ and HC-04 cells did not reach an IC_{50} up to 50 µM, corresponding to >500X decreases in potency compared to RH-dTom. THP-1 monocytes had an IC_{50} of 13.62 µM, or 141.93X higher than that of RH-dTom. U2-OS, HEK-293, 17Cl1 had lower IC_{50}s of 3.7 µM, 3.88 µM, and 4.52 µM, respectively, though selectivity for RH-dTom was still 39.4-47.1X over these cell lines. Primary PBMCs had an IC_{50} of 1.92 µM, or 20.0X higher than that of parasites. These data provide a comprehensive summary of RL003 activity against common human cell lines and indicate that RL003 has little or no toxicity against non-tumorigenic immortalized cell lines and, further, that this compound shows at least 20X selectivity for parasites over host cells even in cases of cell toxicity. Error bars represent standard error from the mean. *p < 0.001 by Student's paired t-test assuming unequal variance.

IC_{50}s ranging from 3.78-4.52 µM, a substantial increase in toxicity (**Figure 1.6**); however,

comparison to the RH-dTom IC_{50} indicated that, though more toxic, RL003 was still ~39-47X more potent against parasites over these cell lines (**Figure 1.6**). Primary PBMCs showed the highest toxicity against RL003, with an IC_{50} of 1.92 µM; though this represents a ~20X increase in IC_{50} over parasites, such toxicity may warrant further investigation (**Figure 1.6**).

RL003 treatment induces apoptosis in HEK-293, but not HFF, cells with concomitant increase in expression of CAS9 suggesting activation of the intrinsic apoptosis pathway.

The toxicity of RL003 to tumorigenic immortalized cell lines, but not to those of lower tumorigenicity, led us to hypothesize that, given the previous work indicating activity of marinopyrroles against cancer, RL003 may be inducing apoptosis in susceptible cell lines. We evaluated this hypothesis through the use of a terminal dUTP nick-end labelling (TUNEL) assay, which identifies short DNA strand breaks associated with apoptosis [171]. HEK-293 (susceptible) and HFF cells (not susceptible) were treated with 4 µM RL003 or with DMSO for 24 hours. The potent apoptosis inducer BH3I-1, known to potently inhibit the Bcl-2 family of proteins and thereby induce apoptosis, was included as a positive control and added at a concentration of 100 µM for 24 hours [172]. Additionally, due to the low susceptibility in cytotoxicity screenings, HFF was treated for an extended 15 days with either DMSO or RL003 to determine whether any apoptosis-like DNA strand breaks occurred during that time.

Addition of RL003 induced a significant increase in the proportion of TUNEL-positive HEK cells after 24 hours compared to DMSO, with 67.9% of the cells showing TUNEL fluorescence compared to 8.8% of the DMSO control. BH3I-1 showed 90.3% TUNEL-positive cells after 24 hours, as would be expected (**Figure 1.7**). Conversely, HFF had no

significant change in the percentage of TUNEL-positive cells at 24 hours or 15 days compared to the DMSO control, indicating that RL003 was not inducing apoptosis-like DNA strand breaks (**Figure 1.7**). The BH3I-1 control (present only at 24 hours due to the toxicity to HFF at that time) showed 83.9% TUNEL-positive HFF cells, indicating that these results were not a consequence of impaired apoptotic activity in HFF (**Figure 1.7**). Together, these data complement the cell toxicity screening by suggesting that HEK, but not HFF, undergo apoptotic events in response to RL003 treatment.

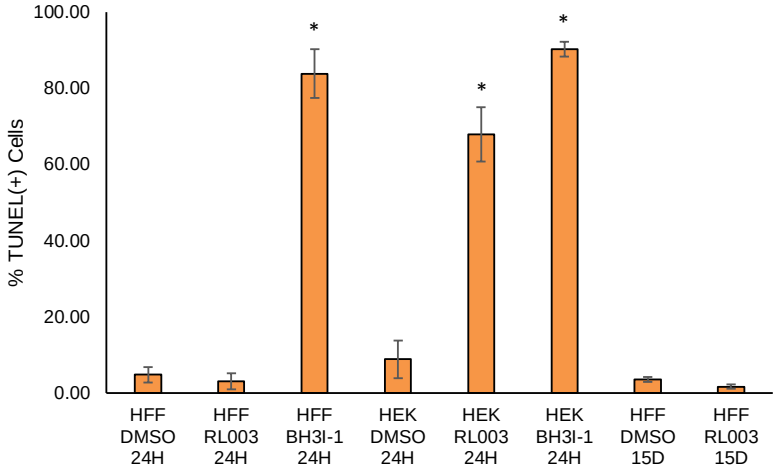

Figure 1.7. RL003 induces apoptosis-like DNA strand breaks in HEK, but not HFF, cells following 24 hours of exposure. To determine whether the cytotoxicity observed in several of the tumorigenic cell lines was a consequence of apoptosis or less controlled mechanisms, an RL003-susceptible cell line (HEK-293, abbreviated HEK) and a non-susceptible cell line (HFF) were treated with 4 µM RL003 or an equivalent volume of the DMSO solvent for 24 hours prior to determination of apoptosis induction with the Apo-BrdU™ TUNEL Assay Kit. As a positive control, the potent apoptosis inducer BH3I-1 was included. TUNEL-positive cells were quantified through counting with the BioTek™ Lionheart automated microscope in triplicate for each sample. Nuclear staining with DAPI was used to quantify total cells to calculate the percentage of TUNEL-positive cells in a given sample. Additionally, to determine whether the effects of apoptosis occur after extended treatment with RL003, an additional sample of HFF was treated with DMSO or RL003 for 15 days and quantified as above. Results showed that RL003-treated HFF had no significant increase in TUNEL-positive cells relative to the corresponding DMSO control, even after 15 days, while 83.9% of BH3I-1-treated HFF cells were TUNEL-positive after 24 hours. Conversely, HEK showed 67.9% TUNEL-positive cells after 24 hours of treatment with RL003, with BH3I-1 showing 90.3% TUNEL-positive cells. Overall, these data suggest that HEK, but not HFF, are induced by RL003 to undergo apoptosis resulting in cytotoxicity. *$p < 0.001$ by Student's Paired *t*-Test with unequal variance.

For further confirmation of this presumptive apoptosis activity, we examined the transcript levels of several apoptosis-associated genes in HEK-293 and HFF cells following RL003 treatment: the executioner caspase CAS3, the intrinsic apoptosis-modulating caspase CAS9, and the apoptosis inhibitor Mcl-1. HFF and HEK-293 were treated with 4

µM RL003 or a volume-matched DMSO for 24 hours as above after which RNA was isolated and RT-qPCR was performed using primers for each gene of interest in addition to the housekeeping genes actin and α-tubulin for comparison of relative fold-change (FC) difference in expression by $2^{-\Delta\Delta Ct}$ [173]. Data collected from this analysis (**Figure 1.8**) showed that, in RL003-treated HEK cells, there was substantial and significant increase

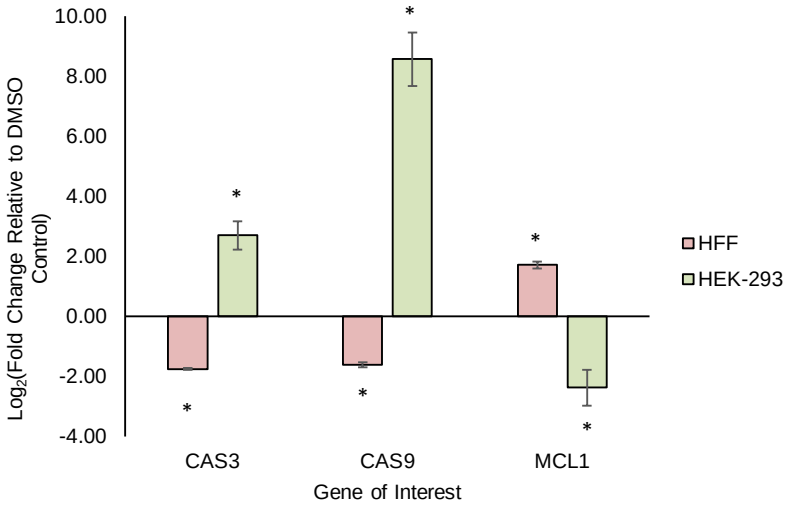

Figure 1.8. RL003 induces upregulation of pro-apoptotic genes CAS9 and CAS3 and downregulation of Mcl-1 in HEK-293 cells but not in HFF cells. To suggest further molecular confirmation of apoptosis activity in HEK-293 cells (abbreviated HEK) after treatment with RL003, and to confirm a lack of apoptosis induction in HFF cells after treatment with RL003, the relative mRNA transcript expression of executioner caspase-3 (CAS3), intrinsic apoptosis marker caspase-9 (CAS9), and the apoptosis inhibitor Mcl-1 (MCL-1) was determined by RT-qPCR. Briefly, confluent cultures of HFF or HEK-293 cells in T25 flasks were treated with 4 µM RL003 (approximately the IC_{50} of HEK-293 cells) or with an equivalent volume of the DMSO solvent for 24 hours before RNA was isolated and RT-qPCR was performed with the Power SYBR™ Green 1-Step RNA-to-Ct kit. For all analyses, f-actin and α-tubulin were included as housekeeping genes for comparison by $2^{-\Delta\Delta Ct}$ analysis of fold change. Results indicated that, following treatment with RL003, HEK-293 cells showed a significant and substantial increase in expression of CAS9 (Log_2FC = 8.57) and a more modest but significant increase in expression of CAS3 (Log_2FC = 2.70). Concomitantly, the expression of MCL-1 was significantly reduced (Log_2FC = -2.37). This pattern was not seen in HFF cells under the same conditions, which showed slight decreases in expression of CAS3 and CAS9 (Log_2FC = -1.74 and -1.61, respectively) and increased expression of MCL-1 (Log_2FC = 1.72). These data suggest that in HEK293, but not in HFF, treatment with RL003 causes strong upregulation of CAS9 and moderate upregulation of CAS3, indicating a likely activation of the intrinsic apoptosis pathway in facilitating the observed cytotoxicity in HEK cells. Error bars represent standard error from the mean. *p < 0.001 by Student's paired t-test with unequal variance.

in CAS9 transcript levels compared to the solvent, with a Log_2FC of 8.57. CAS3 showed a more modest, though significant, increase under RL003 treatment, with a Log_2FC of 2.70; concomitantly, Mcl-1 expression decreased significantly (Log_2FC = -2.37). In

contrast to HEK, HFF cells showed comparatively little change in expression of these genes after treatment with RL003, with slight decreases in CAS3 and CAS9 expression (Log_2FC, respectively, of -1.74 and -1.61) and a slight increase in Mcl-1 expression ($Log_2FC = 1.72$). These data provide further confirmation that HEK, but not HFF, are induced to undergo apoptosis in the presence of RL003; not only so, but the much stronger upregulation of CAS9 implicates a role of the intrinsic apoptosis pathway in mediating this activity.

Discussion

T. gondii infection constitutes a substantial burden to public health, especially for immunocompromised individuals and prenatally-infected infants [143]. Limitations to existing treatments [11] emphasize the importance of developing improved therapeutic interventions against *T. gondii.* The marine microbial product marinopyrrole A has been previously found to show potent antibacterial activity against gram-positive *Staphylococcus* species [117] and to elicit pro-apoptotic stimulation across a variety of cancer cell lines [174], indicating broad antiproliferative properties of this compound across multiple divergent species (both prokaryotic and eukaryotic); therefore, we aimed to address the scarcity of viable *T. gondii* treatments by evaluating the antiparasitic activity of marinopyrrole A *in vitro* and *in vivo*. In this work, we describe the previously-unreported inhibition of *T. gondii* RH-dTom parasites by marinopyrrole A at a significantly higher potency than pyrimethamine, and, further, report less serum-sensitive analogs with even higher potencies up to ~7-fold that of pyrimethamine.

Our *in vitro* analysis of marinopyrrole A efficacy against *T. gondii* tachyzoites shows a remarkably low IC_{50} (0.31 μM), demonstrating critical inhibition of parasite proliferation during the acute-stage lytic cycle. Given our previously-reported *in vitro* IC_{50} of 0.60 μM for pyrimethamine [151], marinopyrrole A presents a substantial and significant

improvement in potency, adding to its existing repertoire of antimicrobial activity [110] (**Figure 1.1**). While previous literature reports some toxicity to human cells via activation of pro-apoptotic cell death pathways in a wide variety of cancer cell lines [174], we demonstrate that toxicity of this compound to the non-cancerous, terminally-differentiated HFF cell line remains undetected. However, marinopyrrole A did show substantial toxicity to HepG2 cells, with an IC_{50} of 5.3 μM (**Table 1.4**); while ostensibly concerning, this value still represents >50X selectivity for parasites over HepG2 cells, supporting our continued analysis of this compound against *Toxoplasma*. Additionally, given that HepG2 cells are a hepatocellular carcinoma line and based on the aforementioned toxicity of marinopyrrole A to cancer cell lines [174], this toxicity against HepG2 is to be expected and, given the continued maintenance of high selectivity, this supports the *in vitro* viability of utilizing this compound in acute *T. gondii* models.

However, despite these promising data, we found that the sub-micromolar efficacy of marinopyrrole A was completely lost by the addition of serum at concentrations greater than or equal to 20% of the media composition, at which point the IC_{50} could no longer be reached at up to ~38-fold higher concentrations of marinopyrrole A than the previously-determined IC_{50} value; that is, up to 10 μM, it was not possible to determine a concentration at which 50% of tachyzoites had been killed (**Table 1.1**). Such strong inhibition by serum is not unprecedented, as Haste and others previously reported abrogation of marinopyrrole A bactericidal activity against methicillin-resistant *S. aureus* in the presence of 20% human serum [117], though, intriguingly, this effect was less pronounced in *in vivo* examinations of anti-cancer properties for neuroblastomas [175]. Nevertheless, loss of anti-*Toxoplasma* activity at 20% serum represents a potential physiological barrier to the translational application of this compound in mammalian models, prompting our interest in progressing to *in vivo* models.

Despite the significant loss of marinopyrrole A potency following the addition of serum, we performed an *in vivo* analysis of anti-*Toxoplasma* activity in a lethal acute murine infection model using outbred Swiss-Webster mice infected with ME49-strain tachyzoites. Surprisingly, we show that dosages at 5 and 10 mg/kg marinopyrrole A facilitated 71.4% survival, as compared to the pyrimethamine control that showed 71.4% survival as well. At 20 mg/kg, marinopyrrole A allowed for an increase in survival at 85.7%, suggesting that the observed *in vitro* serum-mediated loss of potency was abrogated, at least to some extent, *in vivo,* though the means by which this abrogation occurred are not immediately clear (**Figure 1.2**).

The high potency of marinopyrrole A prompted us to investigate several synthesized analogs of this compound—here noted as RL002, RL003, and RL125 (**Figure 1.3**)—for potential improvements to the antiparasitic activity and serum sensitivity of the parent. Our results showed that RL002, RL003, and RL125 exhibit increased parasiticidal activity, with IC_{50} values ranging from 0.092 µM to 0.160 µM—corresponding to significant ~2-7-fold increases in potency relative to pyrimethamine (**Figure 1.4**). These analogs also demonstrate comparatively low toxicity to human cell lines up to 50 µM, with no observed toxicity to HFF cells and HepG2 IC_{50}s 291-517-fold higher than those reached in *T. gondii* (**Table 1.4**). This represents an improvement over the toxicity of the parent to HepG2 cells. In sum, these data demonstrate that, even in a cancer cell line likely to be impacted by a marinopyrrole, these analogs have extremely high (>500-fold) selectivity for *T. gondii* tachyzoites over either human cell line, a desirable trait for a potential therapeutic compound.

Expanded analysis of RL003 susceptibility in host cells indicated several cell lines for which substantial toxicity was observed; these included the immortalized lines U2-OS (IC_{50} = 3.78 µM), HEK-293 (IC_{50} = 3.88 µM), and 17Cl1 (IC_{50} = 4.52 µM). However, it would

be unsupported to indicate that this is an intrinsic consequence of the tissue of origin; both U2-OS and HEK-293 are known to be tumorigenic cell lines [176; 177] and, given the known activity of marinopyrrole A against a number of cancer lines [174], this may be a contributing factor. This possible link is strengthened by the inclusion of a known tumorigenic fibroblast cell line, 17Cl1 [178], that showed >10X higher susceptibility to RL003 as compared to HFF, which are not tumorigenic and for which an IC_{50} was not reached up to 50 µM (**Figure 1.6**). Further, both HepG2 and HC-04, which are cancerous cell lines derived from human hepatocellular carcinoma, are unable to establish tumors in nude mice [179] and, compellingly, showed very low susceptibility to RL003 (**Figure 1.6**); this further suggests that tumorigenicity of a cell line may play a role in its susceptibility to RL003, at least in the case of immortalized cells.

Unexpectedly, the primary cells tested, peripheral blood mononuclear cells (PBMCs), showed the highest susceptibility to RL003 (IC_{50} = 1.92 µM). While initially concerning, this value represents a 20X increase in IC_{50} compared to *T. gondii*, supporting the selectivity of this compound for parasites over even the most susceptible host cell line. In addition, PBMCs are taken directly from donors and may therefore be poorly-acclimated to cell culture, particularly over the 5-day time period needed for evaluation of RL003 activity [180]. We hypothesized that these cells may be hypersensitive to compound insult; supporting this, a comparison of PBMC and HFF sensitivities to pyrimethamine demonstrated that PBMCs were >5X more sensitive to pyrimethamine than HFF, which did not show an IC_{50} up to 10 µM and is typically not expected to show substantial toxicity to host cell lines [61] (**Supplementary Table 1**). This may suggest that the *in vitro* susceptibility of PBMCs is a consequence of heightened sensitivity to compound treatment rather than specific susceptibility to RL003.

A closer examination of the manner in which one susceptible line—HEK-293—was succumbing to RL003 treatment revealed that, rather than general necrosis, this compound appears to follow in the pattern of other marinopyrroles by inducing apoptosis in these cells, though clearly not in cell lines showing low toxicity (**Figure 1.7**). The particularly-strong increase in CAS9 expression ($Log_2FC = 8.57$) in the RT-qPCR analysis (**Figure 1.8**) is suggestive of possible involvement of the mitochondrial-mediated apoptosis pathway. CAS9 is known to be a primary participant in the intrinsic apoptosis pathway, which generally responds to mitochondrial damage or to cascades of signals from the release of cytochrome c [181]. Additionally, the concomitant increase in CAS3 expression, though less pronounced ($Log_2FC = 2.7$), is supportive of a general trend toward apoptosis, given that CAS3 is an executioner caspase acting to fragment DNA and initiate breakdown of cytoskeletal proteins; not only so, but CAS3 is a direct downstream effector of CAS9, given that it is cleaved into its active form by the active CAS9 protein [182]. However, these data are in preliminary stages of development and are indicative only of the expression of transcripts at the 24-hour time point, though these findings do suggest intriguing future studies characterizing RL003-mediated apoptosis.

Critically, we also report a concomitant decrease in sensitivity to serum across all analogs, with each showing an $IC_{50} \leq 5\mu M$ up to 50% serum; this is in stark contrast to marinopyrrole A, which showed dramatic loss of potency (**Table 1.1**). While RL002 demonstrated ~8-fold lower potency than pyrimethamine at 50% serum, RL003 sand RL125 maintained sub-micromolar—and sub-pyrimethamine—IC_{50}s, despite the ~40-fold loss of potency for RL125 from 1-50% BCS (**Table 1.2**). Notably, RL003 showed the lowest loss of potency across serum concentrations at ~5.9-fold, maintaining a ~4-fold lower IC_{50} than pyrimethamine despite this minor reduction in parasiticidal activity (**Table 1.2**). This suggests that, while present, serum sensitivity of these analogs is substantially lower

than that of the parental marinopyrrole A molecule and, importantly, that these analogs maintain high potency up to 50% serum. Particularly, the maintenance of such high potency in RL003 and RL125 even in higher serum concentrations is a desirable trait for continued analysis in future work.

Perhaps most surprisingly, RL003 showed potent inhibition of *in vitro*-generated cysts. Not only was the IC_{50} reached—which itself suggests promise—but the value of 0.245 μM indicated a remarkably high potency (**Figure 1.5**). This is particularly critical for addressing the gaps in treatment options for *T. gondii* infections; given that the cyst stage has no current FDA-approved treatments capable of penetrating the cyst wall and effectively reducing parasite burden [61], this may point to an additional therapeutic application for RL003. Further *in vivo* chronic studies will be needed to more thoroughly evaluate this potential activity in the more complex environment of an animal host.

Taken together, our data point to marinopyrrole A and its analogs as previously-unreported anti-*Toxoplasma* molecules acting against both tachyzoites and cysts, providing a potential avenue for improved therapeutic interventions against both stages this infection. Given the enhanced serum stability of the analogs and our demonstration of their *in vitro* potency, we aim to synthesize sufficient amounts of compound to complete *in vivo* efficacy studies for these and other marinopyrrole A analogs. Additionally, given the apparent preferential toxicity to primarily tumorigenic cell lines, further evaluation of RL003 as a potential anti-cancer compound may be of benefit. Continued analysis of these or related marinopyrrole analogs may provide additional insight into structural components contributing to *in vitro* and *in vivo* potency to parasites as well as sensitivity (or lack thereof) to serum, facilitating continued development of further-improved compounds.

Conclusion

In this work, we showed that marinopyrrole A is a high-potency anti-*Toxoplasma* molecule demonstrating sub-micromolar efficacy against tachyzoites at 1-10% serum concentrations *in vitro*. We also demonstrated a dose-dependent reduction in potency following increasing serum concentrations, with potency being largely lost at serum levels of 20% and above. However, our *in vivo* data demonstrate that, despite this apparent obstacle, marinopyrrole A at 5, 10, and 20 mg/kg facilitated significant enhanced survival in mice as compared to the vehicle control. Improving upon the existing advantageous features of marinopyrrole A, our synthesized analogs RL002, RL003, and RL125 showed low toxicity to non-tumorigenic immortalized cell lines, significantly increased potency against *T. gondii* infection *in vitro*, and reduced sensitivity to serum. Further, RL003 showed potent inhibition of encysted bradyzoites *in vitro*. These analogs, and particularly RL003, therefore represent a series of promising novel anti-*Toxoplasma* compounds for future evaluation *in vivo*, with the ultimate aim of addressing the severe limitations to existing therapeutic options against this infection.

Materials and Methods

Commercial Compounds

Marinopyrrole A, pyrimethamine, phorbol 12-myristate 13-acetate (PMA), and BH3I-1 were obtained from Sigma-Aldrich (St. Louis, MO). These compounds were dissolved in dimethyl sulfoxide (DMSO) prior to completion of relevant assays. RL002, RL003, and RL125 were kindly provided by Dr. Rongshi Li (Department of Pharmaceutical Sciences , University of Nebraska Medical Center). Geneticin (G418 sulfate) was obtained from ThermoFisher Scientific (Waltham, MA).

Cell Lines and Maintenance

HepG2 cells were obtained through CH3 Biosystems® (Buffalo, NY). HFF (ATCC® CRL-4001™), HC-04 (ATCC® PTA-3441™), U2-OS (ATCC® HTB-96™), HEK-293 (ATCC® CRL1573™), and THP-1 (ATCC® TIB-202™) were acquired from ATCC® (Manassas, VA). PBMCs (IQB-PBMC103) were obtained from iQ Biosciences® (Berkeley, CA).

Adherent cell lines were maintained under serial passage at 37 ^{o}C and 5% CO_2 with D10 media: Dulbecco's modified Eagle's medium (DMEM) (Lonza, Walkersville, MD) supplemented with 20% Medium-199 (Corning, Manassas, VA), 10% heat-inactivated bovine calf serum (BCS) (GE Healthcare Life Sciences, Logan, UT), 2 mM L-alanyl-L-glutamine (Corning, Manassas, VA), 100 µg/mL penicillin/streptomycin (Corning, Manassas, VA), and 20 µg/mL gentamicin sulfate (Corning, Manassas, VA). Non-adherent cell lines (i.e., PBMCs, THP-1) were maintained in Roswell Park Memorial Institute-1640 (RPMI-1640) media supplemented as above for D10, with the exclusion of Medium-199.

THP-1 cells were differentiated into macrophages (THP-1 MΦ) by plating $5x10^4$ cells/well in 200 µL/well of a 96-well plate with the addition of 15 µg/mL phorbol 12-myristate 13-acetate (PMA), after which plates were incubated for 48 hours at 37 ^{o}C and 5% CO_2 to allow for differentiation.

Type I *Toxoplasma gondii* RH parasites constitutively expressing an integrated stable fluorescent dimerized Tomato protein (RH-dTom) construct, type II wild-type ME49 parasites, and Pru*ΔKU80* parasites tagged with GFP (Pru*ΔKU80*-GFP) were serially-passaged in HFF cells in D10 media at 37 ^{o}C and 5% CO_2 as reported previously [151] unless otherwise indicated.

Parasite Growth Assays

Determination of the half-maximal inhibitory concentration (IC_{50}) was completed through the procedure outlined in [151; 183]. Briefly, 96-well plates containing confluent HFF monolayers were infected with 2,000 tachyzoites/well of RH-dTom parasites and were subsequently incubated for 12 hours to allow for invasion. Compounds of interest were then added at increasing dilutions (each dilution in technical triplicate) as indicated in the text, with a volume-matched, solvent-only control, and plates were incubated at 37 ^{o}C and 5% CO_2 for 5 days. Fluorescence at 554/581 nm (dTom) was quantified for each well through the use of a BioTek® Synergy™ HT multi-mode plate reader, and IC_{50}s were calculated by determining the compound concentration at which wells exhibited 50% fluorescence relative to the solvent control.

For growth assays in the presence of increasing serum concentrations, heat-inactivated bovine calf serum (BCS) at 1-50%was added to the base media (i.e., D10 without 10% BCS) 48 hours prior to the addition of compound to allow parasites and host cells to acclimate. IC_{50} assays were then completed as above.

Both the PruKU80-GFP and ME49 strains used in these analyses do not stably express fluorescence during the tachyzoite stage; therefore, we quantified parasites by staining for the major surface antigen SAG1 following the general protocol of [184]. Confluent HFF monolayers in 96-well plates were infected with 2,000 parasites/well for 12 hours as before to allow for invasion, after which increasing concentrations of RL003 or a volume-matched DMSO solvent control were added to triplicate wells. After 5 days of incubation at 37 ^{o}C and 5% CO_2, wells were fixed with 4% PFA for 15 minutes, washed with 1X PBS, and blocked with 3% BSA and 0.1% Triton-X in PBS (PBT buffer) for 1 hour at room temperature to permeabilize host cells. Primary murine monoclonal α-SAG1 antibodies (ThermoFisher, Waltham, MA) were added at 1:1,000 dilution in PBT buffer and incubated with the wells for 1 hour at room temperature, after which wells were washed

with 1X PBS to remove residual unbound primary antibodies. Secondary Alexa-488-conjugated goat α-mouse IgG antibodies (ThermoFisher, Waltham, MA) at a 1:1,000 dilution in PBT buffer were then added and plates were incubated away from ambient light for 1 hour at room temperature. SAG1+ parasites, corresponding to viable tachyzoites, were quantified by counting each well in its entirety using the automated BioTek™ Lionheart automated microscope. IC_{50} values were calculated as the RL003 concentration at which wells showed 50% SAG1+ tachyzoites relative to the solvent.

Cyst Viability Assay

PruΔ*KU80* parasites tagged with GFP (PruΔ*KU80*-GFP) on the LDH2 protein, which is expressed exclusively in bradyzoites [185], were used to infect a confluent HFF monolayer at an MOI of 10, and invasion was allowed to proceed for 24 hours. Induction of differentiation was then completed largely as described in [186]: tachyzoite-preferential D10 media was replaced with alkaline induction medium, pH 8.1 (RPMI 1640, 1% heat-inactivated FBS, 50 mM HEPES) and grown without CO_2 at 37 ^{o}C for 9 days, with replacement of media every 2 days and concomitant monitoring of wells for cyst formation. RL003 was then added at increasing concentrations in triplicate across wells, including a volume-matched solvent-only control. After 5 days, GFP-expressing cysts (excitation/emission: 469/525 filter cube) were counted through the use of a BioTek Lionheart automated microscope and compared to the solvent control.

Cell Viability Assays

Calculation of the IC_{50} for HFF and HepG2 host cells was conducted through the use of a resazurin assay as described in [170]. To complete this, confluent monolayers of HFF or HepG2 were treated with various concentrations of each compound of interest, including a volume-matched solvent (DMSO) control, in technical triplicate. Following incubation for 5 days, resazurin salt (MP Biomedicals, Solon, OH) was added at a final

concentration of 10 μM and plates were allowed to incubate at 37 ºC and 5% CO_2 for 4 hours protected from light. Fluorescence was then measured through the use of a Bio-Tek® Synergy™ HT multi-mode plate reader as above, and IC_{50}s were calculated as the concentration at which wells exhibited 50% fluorescence relative to the solvent control.

RNA Isolation and RT-qPCR

RNA isolation from HFF and HEK cells treated with either DMSO or 4 μM RL003 for 24 hours (or 15 days for HFF) was completed using the Qiagen® RNEasy® Plus kit following the manufacturer recommendations. RNA was confirmed for sufficient yields and quality through the use of spectrophotometry (via $A_{260/280}$ ratio). Relative expression was quantified by performing RT-qPCR with the PowerSYBR® Green RNA-to-CT™ 1-Step Kit (ThermoFisher, Waltham, MA), using primers specific to the corresponding gene of interest (**Appendix B**) or to the actin (ACTB) or α-tubulin (TUBA1B) housekeeping genes. Determination of fold change for RL003-treated samples relative to the solvent-treated controls was completed through the $2^{-\Delta\Delta Ct}$ method described in [173]. Each sample was run in technical triplicate and the reported results show the mean (with error bars representing standard error from the mean).

***In vivo* Analysis of Compound Efficacy Against Acute Infection**

Two-month-old female Swiss Webster mice were obtained from Charles River. Mice were infected with 5,000 *T. gondii* ME49 tachyzoites via intraperitoneal injection. Subsequently after infection, Marinopyrrole A treatment began through intraperitoneal injection at 5, 10 and 20 mg/kg (n=7 for each dosage) given once a day for a total of 10 days. Intraperitoneally injected pyrimethamine at 5 mg/kg was included as a positive control (n=7). Solvent treated mice were included as a control for mouse death (n=7). Marinopyrrole A and pyrimethamine were dissolved in PTD solvent [187]: 30% propylene glycol (Sigma-Aldrich), 5% Tween 80 (Sigma-Aldrich), 62% D5W (5% dextrose in water), and

3% DMSO (Sigma-Aldrich) at a final pH of 4-5. Mice were monitored and weighed daily to monitor overall health. Kaplan-Meier survival curves and *p*-value analysis were obtained with IBM SPSS Statistics software. All *in vivo* studies were institutionally approved and carried out under IACUC # 18-075-07.

Statistical Analyses

All statistical tests for variation in IC_{50} values were completed using Student's *t*-test assuming unequal variance, with $p < 0.01$ unless otherwise indicated. All statistical tests for significant increases in mouse survival were completed through IBM SPSS Statistics Software. Kaplan-Meier curves were calculated, and the log-rank test was implemented to determine overall significance of marinopyrrole A treated versus solvent treated mice.

CHAPTER 2: SCREENING OF MARINOPYRROLE DERIVATIVES AGAINST BACTERIAL PATHOGENS AND HUMAN PARASITES *LEISHMANIA DONOVANI*, *ACANTHAMOEBA CASTELLANII*, AND *NAEGLERIA FOWLERI*

The need for improved antimicrobial therapies encompasses a wide variety of both prokaryotic and eukaryotic pathogens. Development of small-molecule inhibitors of pathogen growth has been an intensive area of medicinal chemistry research in recent decades; however, despite the continued progress being made, many pathogenic infections remain difficult to effectively treat with current therapies. Notable amongst these are diarrheal illnesses (especially those associated with *Clostridium dificile* and *Cryptosporidium parvum*), tuberculosis, leishmaniasis, trypanosomiasis, and a variety of amebiases [188-192]. Compounding matters, the global prevalence of antibiotic resistance across such species as *S. aureus* [193], *Streptococcus pneumoniae* [194], *Legionella pneumophila* [195], and *Mycobacterium tuberculosis* [196] is increasing at an alarming rate, causing serious clinical consequences in healthcare facilities where already-susceptible patients are at risk of acquiring an infection for which available antibiotics are ineffective [197].

A number of prokaryotic pathogens remain highly prevalent despite the advent of modern antibacterial agents, due in no small part to the capacity for many of these agents to quickly acquire resistance over several generations [198], particularly in the presence of sublethal dosages [199]. Among the gram-positive bacteria, both *S. aureus* (an opportunistic pathogen typically present as a commensal but capable of causing cutaneous and systemic infections) and *S. pneumoniae* (a causative agent of community-acquired pneumonia) are of particular concern due to their increasing demonstration of multi-drug resistance [200; 201]. Further, *B. anthracis* is a pathogen of serious public health concern due to its high virulence—resulting in skin ulcers or, if inhaled, fatal respiratory infection—and potential economic impact, making it highly concerning for possible use as a

bioweapon [202]; therefore, intentional or unintentional conferral of resistance to antibiotics would be potentially devastating [203].

Gram-negative pathogens also cause millions of infections each year, with substantial economic and public health burden [204]. Infections of the urinary or gastrointestinal tract caused by *Escherichia coli*, *Shigella sonnei*, *Salmonella enterica*, *Yersinia pseudotuberculosis,* and *Vibrio cholerae* represent serious causes of diarrheal and systemic illness, with the presence of multi-drug resistance rendering these typically treatable infections much more dangerous to patients [205]. Other respiratory pathogens, including the potentially serious lung pathogen *Legionella pneumophila* and the potentially-fatal pneumonic infection by *Francisella tularensis*, are of additional concern due to their ease of spread and potential use as biological warfare agents [206; 207]. Related to these, though formally gram-refractory [208], *Mycobacterium tuberculosis* presents as a chronic respiratory infection characterized by the formation of tubercles in lung tissue and persistence of infection [209]; even with the proper antibiotics, treatment is typically recommended for 6 to 9 months following diagnosis [191]. This length of treatment is amenable to patient neglect or incorrect dosage facilitating the alarming rise in multidrug resistance, indicative of an acute global health concern. Together, these concerning cases across gram-positive, gram-negative, and gram-refractory pathogens support the continued search for improved antibacterial interventions, particularly those for which the acquisition of resistance is less likely.

Multiple eukaryotic parasites also represent serious public health concerns, many due to their widespread distribution and numerous annual cases [210-212]. However, infections that have few annual cases are frequently hindered due to lack of available treatment options, particularly for those which result in high likelihood of morbidity or mortality [210-212]. Notable among these are the high-mortality cerebral amebiases caused by

free-living amoebae [213]. *Naegleria fowleri* is one of the most infamous agents leading to high mortality infections; following waterborne activities, accidental inhalation results in movement of these preferentially bacteria-consuming organisms along the olfactory nerve and into the brain, resulting in primary amoebic meningoencephalitis (PAM) [214; 215]. While infections are rare, with only a few cases per year, they are nearly all fatal, with a >95% mortality rate [216]. Similarly, *Acanthamoeba castellanii*, a soil-dwelling organism primarily known for its role as a causative agent of keratitis (inflammation of the cornea resulting from destruction of tissue by amoeba), can cause rare infections of the brain leading to granulomatous amoebic meningoencephalitis (GAM), a condition that is often associated with poor prognosis and substantial mortality [217]. Current treatments are severely limited for both *N. fowleri* and *A. castellanii* with the experimental compound miltefosine showing potential promise as an orally-available medication [216], though no single treatment has yet been shown to effectively eliminate either infection [218; 219].

The neglected tropical disease leishmaniasis is, like the amebic infections described above, capable of causing frequent morbidity and mortality in infected individuals [220]. The most severe form of this disease is visceral leishmaniasis and is most frequently caused by the kinetoplastid parasite *Leishmania donovani* or, in rarer instances, *Leishmania infantum* [221]. Visceral leishmaniasis is a severe systemic infection characterized by sporadic febrile bursts eventually resulting in splenomegaly, hepatomegaly, anemia, and nearly 100% mortality in the absence of treatment [222-224]. Current treatments for this infection are severely limited. The long-standing use of toxic pentavalent antimonials remains widespread outside of the U.S and elicits severe patient responses and illness [222; 225]. More recent advances have identified the FDA-approved intravenous liposomal amphotericin B, a less-toxic alternative that appears to allow for improvements to clinical outcomes after 21 days, although patient side effects remain a substantial issue [226-228].

Miltefosine has recently been approved for treatment of visceral leishmaniasis as an orally administered tablet and seems to show promise [229; 230], but its long-term effects remain unclear [231]. Additionally, drug resistance against both amphotericin B and miltefosine presents a continued concern for treatment-refractory cases of leishmaniasis [232-234].

Combating these infections presents a challenging area of continued research. To this end, marinopyrroles and pyrrolomycins have been generally well-characterized for their capacity to elicit bactericidal activity against a variety of gram-positive pathogens, particularly *S. aureus* and its drug-resistant serovars, such as methicillin-resistant *S. aureus* (MRSA) and vancomycin-resistant *S. aureus* (VRSA) [117]. We have shown that marinopyrrole A as well as several of the pyrrolomycin derivatives are particularly effective against multiple strains of *T. gondii* (**Chapter 1**), suggesting potential activity against eukaryotic parasites. This is supported by the corresponding inhibitory activity against a variety of Mcl-1-dependent eukaryotic cancer cell lines [235]. The potency of these molecules makes them particularly intriguing for their potential antimicrobial activity [235; 130]. Therefore, we hypothesized that, like its parental compound, RL003 would demonstrate potent (<5 μM) antibacterial activity against primarily gram-positive bacterial pathogens, and possibly potent activity against *L. donovani*, *A. castellanii*, and/or *N. fowleri.*

Results

RL003 demonstrates potent inhibition of growth in both gram-positive and gram-negative bacterial pathogens as well as in *Mycobacterium bovis* BCG, suggesting broad antibacterial activity.

Based on the previously-identified potent anti-MRSA activity of marinopyrrole A, we hypothesized that a number of other gram-positive bacteria would show susceptibility to RL003. To broadly test the antibacterial properties of RL003, we determined the 50%

minimum inhibitory concentration (MIC_{50}) for 11 prokaryotic human pathogens spanning gram-positive, gram-negative, and gram-refractory species, as shown in **Figure 2.1**. This was accomplished through comparison of OD_{600} values for compound-treated or solvent-treated overnight cultures of each strain (with the exception of *M. bovis* BCG, for which 2 weeks of growth were allowed), with MIC_{50} values calculated as the compound concentration at which the OD_{600} was 50% that of the solvent control.

Of the species tested, 7 showed dose-dependent susceptibility to RL003, with 6 of these having MIC_{50} values below 1 µM. Following the previously described anti-staphylococcal activity of marinopyrrole A, RL003 showed potent activity against the methicillin-resistant USA300 strain of *S. aureus*, with an MIC_{50} of 0.12 µM (**Figure 2.1**). RL003 also had efficacy against several additional gram-positive organisms: *S. pneumoniae* showed susceptibility similar to *S. aureus*, with an identical MIC_{50}, and *B. anthracis* Ames35 (lacking the pXO2 plasmid to facilitate use outside of a high-containment facility) had an MIC_{50} of 0.95 µM (**Figure 2.1**). While 4 of the 7 gram-negative pathogens tested did not demonstrate susceptibility to RL003 up to 5 µM, *V. cholerae*, and *L. pneumophila* showed substantial susceptibility to RL003 with MIC_{50}s of 0.74 µM and 0.20 µM, respectively (**Figure 2.1**). While not as potent against *Y. pseudotuberculosis*, with an MIC_{50} of 4.49, RL003 did still show activity against this pathogen (**Figure 2.1**). In addition to the gram-positive and gram-negative pathogens, *M. bovis* BCG, RL003 demonstrated potent activity with an MIC_{50} of 0.48 µM after 2 weeks of axenic incubation. Together, these data demonstrate that RL003 is a potent antibacterial molecule whose activity is not exclusively restricted to either gram-positive or gram-negative bacterial species and, further, that this compound shows possible tuberculocidal activity.

Gram Designation	Bacterial Strain	RL003 MIC_{50} (µM)	Ciprofloxacin MIC_{50} (µM)
Negative	*Escherichia coli*	NR	0.055
	Shigella sonnei	NR	0.055
	Salmonella enterica serovar Typhi	NR	0.057
	Francisella tularensis subsp. *holarctica* LVS	NR	6.24
	Yersinia pseudotuberculosis	4.49	0.077
	Vibrio cholerae	0.74	0.072
	Legionella pneumophila	0.20	12.80
Positive	*Bacillus anthracis* Ames35	0.95	0.16
	Staphylococcus aureus MRSA USA300	0.12	16.35
	Streptococcus pneumoniae	0.12	3.37
Neither	*Mycobacterium bovis* BCG	0.48	29.1

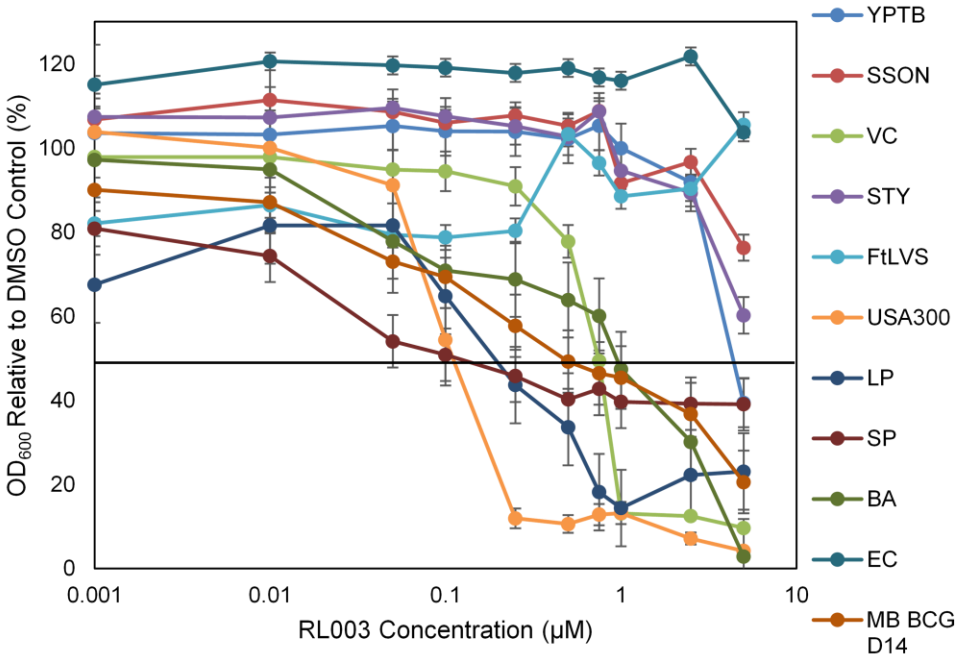

Figure 2.1. RL003 demonstrates broad antibacterial activity. The susceptibilities of 11 bacterial pathogens (representing both gram-negative and gram-positive species) to RL003 or to the positive control ciprofloxacin were evaluated through determination of the 50% minimum inhibitory concentration (MIC_{50}) completed in a high-throughput microplate format and calculated based on OD_{600} values compared to solvent controls. Overall, RL003 showed potent antibacterial activity (<1 µM) against gram-negative pathogens *L. pneumophila* (LP) and *V. cholerae* (VC) as well as against gram-positive pathogens *B.* anthracis (BA), methicillin-resistant *S. aureus* USA300 (USA300), and *S. pneumoniae* (SP). Similarly-potent activity (0.48 µM) was observed against *M. bovis* BCG after 14 days of treatment (MB BCG D14). MIC_{50} values were not reached for *E. coli* (EC), *S. sonnei* (SSON), *S. enterica* serovar Typhi (STY), and *F. tularensis* subsp. *holarctica* LVS (FtLVS) up to 5 µM RL003 despite reaching MIC_{50} values for the positive control. These data suggest that the activity of RL003 is not exclusively dependent on gram properties. Error bars represent standard error from the mean. NR = not reached up to 5 µM.

RL003 shows potent antiparasitic activity against axenic cultures of *Acanthamoeba castellanii* and *Naegleria fowleri in vitro*, but not against *Leishmania donovani* amastigotes.

The broad antibacterial activity shown by RL003, in conjunction with the previously-identified anti-*Toxoplasma* activity shown in **Table 1.4**, led us to hypothesize that RL003 may show efficacy against the intracellular pathogen *L. donovani* in addition to the pathogenic free-living amoebae *A. castellanii* and *N. fowleri*. Parasites were cultured axenically prior to treatment with increasing concentrations of RL003 or with the appropriate solvent control, after which a resazurin assay was conducted for evaluation of toxicity (as a consequence of loss of oxidative phosphorylation activity [170]) by calculation of the IC_{50} as described previously. For a positive control, the experimental antiparasitic molecule miltefosine was included, given that there are no FDA-approved treatments effectively or specifically clearing *N. fowleri* or *A. castellanii* infection and given the limited use of this compound in treatment of visceral leishmaniasis from *L. donovani*.

Organism	RL003 IC_{50} (µM)	Miltefosine IC_{50} (µM)
L. donovani promastigotes	NR	4.68
A. castellanii trophozoites	0.045	8.98
N. fowleri trophozoites	0.175	49.4

Table 2.1. RL003 demonstrates efficacy against axenic cultures of eukaryotic parasites *Acanthamoeba castellanii* and *Naegleria fowleri*, but not against *Leishmania donovani*. The previous activity of marinopyrrole A against both prokaryotic and eukaryotic cells suggested the potential for antiparasitic activity against a variety of extracellular eukaryotes. To test this activity, three distinct parasites for which current treatments are lacking—*L. donovani*, *A. castellanii*, and *N. fowleri*—were examined for their axenic susceptibility to RL003 using the resazurin assay described in the text. For a positive control, the experimental antiparasitic compound miltefosine was included for all species. Results showed that axenic *L. donovani* promastigotes were not susceptible to RL003 up to 5 µM, with the IC_{50} not being reached; miltefosine showed an expected IC_{50} of 4.68 µM, supporting that this was not an error in procedure. Conversely, both *A. castellanii* and *N. fowleri* were potently inhibited by RL003, with IC_{50} values of 0.045 µM and 0.175 µM, respectively, representing a ~200X and a ~280-fold increase relative to the corresponding miltefosine controls. These data suggest that RL003 is a potent antiparasitic molecule acting against *A. castellanii* and *N. fowleri*, potentially indicating use as a novel small molecule inhibitor of these organisms. NR = not reached up to 5 µM.

The results shown in **Table 2.1** demonstrate the potent amoebicidal activity of RL003 against axenic trophozoites, though the same effect was not observed against *L. donovani* promastigotes. The IC_{50} against *A. castellanii* was 0.045 μM, a ~200X increase in potency compared to miltefosine (IC_{50} = 8.98 μM) (**Table 2.1**); this increase in potency was more pronounced against *N. fowleri*, for which the IC_{50} of RL003 was 0.175 μM, representing a ~280X increase in potency relative to miltefosine (IC_{50} = 49.4 μM) (**Table 2.1**). In contrast to the activity against amoebae, RL003 did not demonstrate an identifiable IC_{50} value against *L. donovani* axenic promastigotes up to 5 μM, while miltefosine showed an IC_{50} of 4.68 μM. These data suggest that RL003 is a potent amoebicidal compound against *A. castellanii* and *N. fowleri* trophozoites *in vitro*, but that activity is markedly lower than that of miltefosine against axenic *L. donovani* promastigotes.

Discussion

The recent and concerning rise of antibiotic resistance represents a substantial public health concern given the speed at which resistance arises relative to the discovery and validation of new antimicrobial compounds. Identifying new and potent antibacterial molecules therefore represents an area of intensive research. To this end, the marine-derived product marinopyrrole A has shown promise as a potent inhibitor of drug-resistant *S. aureus* (MRSA, VRSA) with high selectivity for bacteria over healthy human cells. However, activity of this compound is largely restricted to gram-positive bacteria and, additionally, the sensitivity of this activity to the presence of human serum restricts clinical applicability. The marinopyrrole A derivative RL003 is a pyrrolomycin housing the ostensibly-crucial N-H bond (**Figure I.1.**) observed to be essential for anti-MRSA activity [110] with comparatively low serum sensitivity. With its clear efficacy against *T. gondii* (**Table 1.4.**) and given the established anti-staphylococcal activity of the parental compound, we hypothesized that RL003 would show potent antibacterial activity of against additional pathogens.

Determination of the MIC_{50} values for 11 clinically-relevant pathogen strains (**Figure 2.1**) indicated that RL003, in contrast to marinopyrrole A, exhibits broad dose-dependent antibacterial activity against both gram-positive and gram-negative bacteria representing diverse bacterial lifestyles. While *Y. pseudotuberculosis* had an MIC_{50} nearing the 5 µM upper limit of observation (**Figure 2.1**), all other susceptible strains—*B. anthracis*, *V. cholerae*, *L. pneumophila*, *S. aureus* USA300 (a methicillin-resistant clinical isolate), and *S. pneumoniae*—showed MIC_{50} values <1 µM, with the latter three organisms showing MIC_{50} values of 0.12-0.20 µM (**Figure 2.1**). Comparatively, the MIC_{50} values for the positive control ciprofloxacin (a broadly-active fluoroquinolone in wide clinical use) were 3.4-16.4 µM, corresponding to a 28X increase in potency against *S. pneumoniae*, a 137X increase in potency against *S. aureus*, and a 64X increase in potency against *L. pneumophila* (**Figure 2.1**). Importantly, the MIC_{50} values for ciprofloxacin fell within the expected ranges reported in literature, providing support for the accuracy of our data [236-239]. This high potency is promising and seems to suggest that gram-designation alone is insufficient to predict RL003 activity; however, further testing is necessary to further assess the potential therapeutic applicability of this compound.

Further, the gram-refractory and health-relevant *M. tuberculosis* surrogate *M. bovis* BCG showed unexpectedly-high susceptibility to RL003 *in vitro*, with an MIC_{50} <0.5 µM (**Figure 2.1**). The positive control, ciprofloxacin, showed nearly 60X lower potency (MIC_{50} ~29 µM) and appeared to align with expected literature values [240], providing validation for the accuracy of our findings as above. Given the rising incidence of drug-resistant tuberculosis, paired with the extended treatment regimens typically required for effective clearance of the disease [191], this presents particular promise for the role of RL003 as a potential tuberculocidal compound. If, as has been shown for other pyrrolomycins [295], RL003 poses a substantial barrier to resistance due to its targeted processes, this may

serve as a crucial step toward addressing multidrug-resistant tuberculosis. However, evaluation of RL003 in a xenic coculture model of *M. bovis* in the presence of macrophages would prove useful in assessing the clinical applicability of these findings. Additionally, it would be advantageous to repeat this experiment with a fully-virulent *M. tuberculosis* strain, as the efficacy against *M. bovis* BCG may not represent the activity against a fully-virulent strain.

While no efficacy up to 5 µM could be observed against *L. donovani* promastigotes, the potent amoebicidal activity of RL003 is of particular note, with both *A. castellanii* and *N. fowleri* showing sub-micromolar IC_{50} values corresponding to significant and dramatically-increased potencies of ~200X to ~280X compared to the corresponding miltefosine controls (**Table 2.1)**. Mortality in cases of either form of amoebic meningoencephalitis exceeds 90%, stemming largely from failure to diagnose this rare occurrence in addition to the shortage of viable treatments capable of clearing amoebae in a timely manner [214; 217]. The experimental antiparasitic molecule miltefosine has recently been used with limited success against *N. fowleri* in a clinical case as a treatment of last resort and in selected cases of *A. castellanii* infection [214; 241]; however, as shown in **Table 2.1**, the efficacy against *N. fowleri* is nearly 50 µM, presenting a potential issue for therapeutic success. The need for higher potency compounds is, therefore, crucial for improving the poor prognosis of amoebic meningoencephalitis, and RL003 appears to show promise to this end. However, whether this potent activity translates to clinical applicability remains to be seen; RL003 will need to be verified for its activity *in vivo* in order to more thoroughly assess this possibility.

RL003 presents an intriguing antimicrobial pattern of activity; it is uncommon for broad antibacterial molecules to show substantial efficacy against either *A. castellanii* or *N. fowleri*, particularly at such potent levels across both species [214; 241]. The macrolide

antibiotic azithromycin [242], used in the treatment of infections with a variety of bacterial species including *Legionella spp.* and *Mycobacterium spp.* [243], has shown an ability to inhibit *N. fowleri* growth at 13.4 μM *in vitro* [214]; however, this effect was not observed in *A. castellanii*, which had little observable inhibition of trophozoites [244]. Additionally, the potency of this molecule is clearly far lower than that of RL003, which suggests that a shared mechanism is less likely in light of our data. The potent anti-tuberculosis drug rifampicin, which acts through inhibition of RNA polymerase and subsequent disruption of transcription in *M. tuberculosis* [245], has been shown to have strong antibacterial effects across gram-positive cocci, including *Staphylococcus spp.* and *Streptococcus spp*., and *L. pneumophila*, with much lower activity against other gram-negative species [246]. This pattern does seem to resemble that of RL003, and, further, rifampin has been used in combination with other compounds for successfully-treated cases of cerebral amebiases [214]; however, *in vitro*, these anecdotal findings are not supported, with an MIC against *N. fowleri* not being reached even at >40 μM [247]. The remarkable potency of RL003 across both amoebae species and the gram-positive, gram-negative, and gram-refractory prokaryotic pathogens may, therefore, represent either a unique shared mechanism or divergent mechanisms arising from multiple potential targets. These interesting possibilities warrant further evaluation in future work.

Conclusions

Overall, our broad examinations of the antibacterial and antiparasitic activity of RL003 support that this compound is a high potency anti-amoebic and antibacterial molecule *in vitro*. Acting against multiple bacteria regardless of gram designation, and inhibiting the *M. tuberculosis* surrogate *M. bovis*, RL003 shows promise as a possible small-molecule inhibitor to help address the concerning global rise in antimicrobial resistance. Not only so, but the extremely low *in vitro* IC_{50} values against the high-mortality *N. fowleri*—

for which no routinely-successful treatment is currently available, leading to a poor prognosis—and *A. castellanii* may indicate usefulness as a potent amoebicidal agent. Though further examination of this molecule, particularly *in vivo*, is critical, these initial data support further development of this compound against prokaryotic and eukaryotic pathogens.

Methods

Pathogen Lines and Maintenance

The following parasite strains were obtained from BEI Resources, NIAID, NIH: *Naegleria fowleri,* Strain CDC:V636*,* NR-46509; and *Leishmania donovani* 1S2D (+luc) (MHOM/SD/62/1S-CL2D), NR-50182. Additionally, the following bacterial pathogens were obtained from BEI resources: *Francisella tularensis* subsp*. holarctica* CDC Live Vaccine Strain, NR-646; *Bacillus anthracis* Ames35, NR-10355; *Streptococcus pneumoniae* TCH8431, HM-145; *Escherichia coli* K-12, Strain DC10B, NR-49804; *Yersinia pseudotuberculosis*, Strain IP2666, NR-4371; *Salmonella enterica* subsp. *enterica*, Strain Ty2 (Serovar Typhi), NR-514; *Vibrio cholerae*, Strain 395, NR-9906; *Shigella sonnei,* Strain WRAIR I Virulent, NR-519. *Staphylococcus aureus*, Strain USA300-0114, NR-46070, was acquired from the Network on Antimicrobial Resistance in *Staphylococcus aureus* (NARSA) for distribution by BEI Resources, NIAID, NIH. Finally, *Acanthamoeba castellanii* (Douglas) Page (ATCC® 30011™), *Mycobacterium bovis* Karlson and Lessel (ATCC® 3574™), and *Legionella pneumophila* subsp. *pneumophila* Philadelphia-1 (ATCC® 33152™) were acquired from ATCC.

Bacterial lines were maintained by growth on agar plates of the corresponding media recommended for growth by BEI Resources of ATCC. For *E. coli*, *S. sonnei*, *S. aureus*, *V. cholerae*, *B. anthracis*, *Y. pseudotuberculosis*, *S. enterica*, tryptic soy agar (TSA) was used, with the corresponding tryptic soy broth (TSB) used for overnight cultures as needed [248]. The more fastidious pathogens *S. pneumoniae* and *F. tularensis* subsp. *holarctica*

LVS were passaged on chocolate agar plates with 5% CO_2, with brain-heart infusion broth (BHI) used for liquid cultures [249; 250]. *L. pneumonia* was cultured with buffered charcoal-yeast extract (BCYE) agar due to the intrinsic requirement for cysteine and iron to effectively grow [251]. *M. bovis* was grown on Middlebrook 7H10 agar plates or in 7H9 Middlebrook broth as needed with 5% CO_2 [252]. All bacteria were grown at 37 ^oC.

Parasite culture was also carried out based on BEI Resources and/or ATCC recommendations. *L. donovani* axenic promastigotes were maintained by serial passage in a slightly-modified version of Optimized Medium 2736 (Medium-199 with 10% FBS, 1X RPMI vitamin mix, 12 mM $NaHCO_3$, 7.6 mM hemin, 50 U/mL penicillin, 50 µg/ml gentamycin, 1 mM glutamine, 100 µM adenosine, 10 µM folic acid) [253] at 25 ^oC away from light (to protect the hemin). *N. .fowleri* was cultured anaerobically at 35 ^oC with modified PYNFH medium containing 1% peptone, 1% yeast extract, 0.1% yeast nucleic acid, 0.0015% folic acid, 0.0001% hemin, 10% heat-inactivated FBS, and 2% Gomori phosphate buffer (KH_2PO_4/Na_2HPO_4) (ATCC® 327-X) [254]. *A. castellanii*, conversely, was cultured at 27 ^oC in the recommended ATCC® 712 PYG medium (2% proteose peptone, 0.1% yeast extract, 0.4 mM $CaCl_2$, 4 mM $MgSO_4$ x $7H_2O$, 2.5 mM Na_2HPO_4 x $7H_2O$, 2.5 mM KH_2PO_4, 0.1% sodium citrate, 0.05 mM $Fe(NH_4)_2(SO_4)_2$ x 6H2O, 100 mM glucose pH adjusted to 6.5) [241].

Parasite IC_{50} Analyses

Resazurin assays were completed essentially as described in **Chapter 1**, with slight modification. Briefly, $1x10^5$ promastigotes of *L. donovani* or $1x10^5$ trophozoites of each amoeba species were plated in 100 µL of their respective media in a 96-well plate and allowed to acclimate or adhere for 24 hours. RL003 was then added at increasing concentrations (0-5 µM) in technical triplicate for each organism, including solvent controls for each. Miltefosine was included as a positive control (in triplicate) for all parasite species

[255]. Incubation was allowed to proceed for 5 days, and resazurin was then added at 0.15 mg/mL, and plates were incubated at 35 ^{o}C for amoebae or 27 ^{o}C for *L. donovani* for 4 hours away from light [151]. Plates were read on a BioTek Synergy fluorescent plate reader at 530/585 nm excitation/emission [151] and the IC_{50} for each organism was calculated as the concentration of RL003 at which fluorescence (corresponding to metabolic viability) was 50% that of the solvent control.

Bacterial MIC_{50} Analyses

Overnight cultures of bacteria grown under appropriate conditions for optimal growth were resuspended in cation-adjusted Mueller-Hinton broth (with the exception of *L. pneumophila*, for which charcoal-yeast extract broth was used, *F. tularensis* subsp. *holarctica* LVS, for which brain heart infusion (BHI) broth was used, and *M. bovis* BCG, for which Middlebrook 7H9 broth with ADC supplementation and 40 mM sodium pyruvate was used) to $2x10^6$ CFUs/mL. Broth cultures were placed in a 96-well plate at $2x10^5$ CFUs/well and increasing concentrations of or the ciprofloxacin positive control were added, including solvent-only (DMSO for RL003, 0.1N HCl for ciprofloxacin) controls for each antibiotic. Non-*Mycobacterium* plates were grown overnight with shaking at 250 rpm and 37 ^{o}C, with 5% CO_2 supplied for *F. tularensis* subsp. *holarctica* LVS and *S. pneumoniae*. *M. bovis* BCG was allowed to grow in the presence of antibiotics at 37 ^{o}C for 2 weeks. All strains were tested in triplicate to ensure reproducibility. At the end of the allotted incubation times, inhibition of growth was measured by determination of the optical density at 600 nm (OD_{600}) for each tested concentration, with the 50% minimum inhibitory concentration (MIC_{50}) being calculated as the compound concentration at which the OD_{600} was 50% that of the solvent-treated control.

CHAPTER 3: A SINGLE NUCLEOTIDE VARIANT OF cGMP-DEPENDENT PROTEIN KINASE (PKG) IS SUFFICIENT TO CONFER RESISTANCE TO MARINOPYRROLE A DERIVATIVE RL003

Experimental therapeutics acting against *Toxoplasma gondii* have successfully been shown to target a number of essential parasite processes, from pyrimidine biosynthesis [63] and purine scavenging [213] to apicoplast translation [83], fatty acid synthesis [256], and essential kinases for signaling [257] (**Table I.1.**). However, in practice, compounds targeting genes associated with many of these pathways have demonstrated substantial limitations. With low enough specificity to result in potentially severe adverse effects, particularly in the case of antifolates (despite their widespread implementation in clinical cases of toxoplasmosis) [53], lack of sufficient potency and specificity represent drawbacks for many of these compounds [66]. Though new experimental molecules can demonstrate enhanced specificity *in vitro*, the issue of potency, as well as host tolerability, emphasize the need for further development of pharmaceuticals to combat toxoplasmosis with minimal off-target effects in humans.

Our laboratory has previously demonstrated that the novel experimental marinopyrrole A derivative RL003 shows significant antiparasitic activity *in vitro*, as discussed in **Chapters 1-2**, indicating potential promise as a therapeutic molecule. To date, no other groups have examined marinopyrroles or pyrrolomycins against *T. gondii*; as a consequence, the mechanism of action, or even underlying genetic components facilitating resistance, are currently unknown. Given the high potency and specificity of RL003 against these parasites, elucidation of a mechanism of action or routes of resistance would prove extremely useful in pursuing future development of this compound, from *in vivo* trials and onward. Further, insights into the molecular basis for this selectivity and/or potency will provide additional guidance for the development of improved small-molecule therapies against *T. gondii*.

We hypothesized that mechanistic insights into the activity of RL003 would be evident in either forward genetic screening or transcriptomic analyses. Therefore, to determine the potential genetic underpinnings responsible for resistance to RL003—and, by extension, to gain insight into processes affecting compound activity in parasites—we performed a forward genetic screen with positive selection for RL003-resistant parasite populations and identified potential resistance-conferring mutations with whole-genome sequencing. We show that a single C524R mutation in the *T. gondii*-specific cGMP-dependent protein kinase (PKG) is sufficient to confer >2.5X resistance to RL003, supported by phenotypic evidence showing defects in PKG-dependent processes after RL003 treatment of wild-type parasites. Intriguingly, we also show from RNA-seq and RT-qPCR data that primitive programmed cell death pathways in the parasite appear to be strongly upregulated in response to RL003 treatment, indicating that inhibitory activity may be a consequence of programmed cell death rather than nonspecific necrotic damage. These findings may also suggest a previously-unreported link between PKG and programmed cell death in *T. gondii*. In sum, our results point to RL003 as a compound affected by a highly specific parasite protein and support its further development as an anti-*Toxoplasma* molecule.

Results

Precellular and preparasitic assays indicate likely mediation of RL003 activity through parasite processes.

To determine whether the antiparasitic activity of RL003 is mediated through host cells or through direct effects on the tachyzoites themselves, we first performed preparasitic and precellular assays with RL003 as described in [258]. Extracellular parasites (for the preparasitic assay) or uninfected host cells (for the precellular assay) were exposed to RL003 at the 90% inhibitory concentration (IC_{90})—which, for RL003, is 0.2 μM. Viability

of pretreated parasites infecting untreated host cells (preparasitic) or of untreated parasites infecting pretreated host cells (precellular) was determined by relative fluorescence compared to volume-matched solvent controls after 24 hours of growth. Results of this analysis (**Figure 3.1**) indicated that extracellular parasites exposed to RL003 and used to infect host cells exhibited a significant (>40%) reduction in growth after 24 hours relative

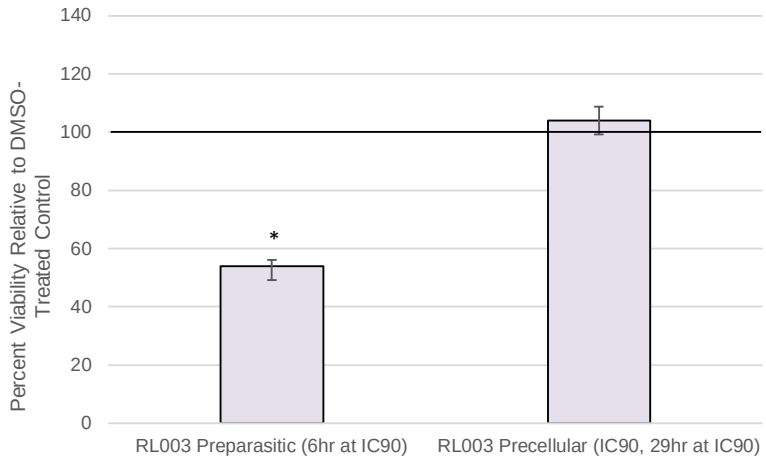

Figure 3.1. RL003 toxicity is likely mediated through parasite processes rather than through host cell modulation as determined by precellular and preparasitic assays. To determine whether the observed anti-*Toxoplasma* activity of RL003 is mediated by parasitic processes or by modification of the host cell (or by a combination of the two) survival of parasites following either pretreatment with compound or infection of host cells previously treated with compound was evaluated. For preparasitic treatment, fluorescent RH-dTom parasites were treated with RL003 at the IC_{90} or with a volume-matched DMSO solvent control for 1 replicative cycle, after which compound was removed and these parasites were used to infect host cells in triplicate wells of a 96-well optical-bottom plate. Viable (dTom-positive) tachyzoites were counted with an automated microscope the number of viable parasites was compared to the DMSO control. In the precellular assay, HFF host cells in optical-bottom 96-well plates were treated with RL003 at the parasite IC_{90} for 1 complete cell cycle prior to removal of compound and infection with *untreated* parasites, with quantification occurring as above. Results demonstrated that pretreated parasites, had a significant ($p < 0.001$) >40% loss in viability relative to the DMSO control at 24 hours post-infection, while pretreated host cells did not show a decrease in parasite viability relative to the DMSO control. This suggests that RL003-mediated toxicity is a consequence of interaction with parasite processes. *$p < 0.001$ by paired *t*-test assuming unequal variance. Error bars represent standard error from the mean.

to parasites treated with DMSO under the same conditions. Pretreatment of host cells did not cause reduction in parasite growth, with no significant change in viability after 24 hours relative to the DMSO-pretreated cells. In conjunction, these complementary data both support a primary role of parasite components, rather than host cell processes, in the activity of RL003.

Random chemical mutagenesis generates significantly- and specifically-resistant clonal isolates harboring key mutations in several essential parasite genes.

Having determined that the means of antiparasitic activity was primarily facilitated by direct activity on tachyzoites, we next aimed to elucidate the possible target of, or potential gene products conferring resistance to, RL003. As successfully implemented in previous work [259], we performed a random chemical mutagenesis on confluent RH-dTom tachyzoites in 2 T25 flasks, denoted α and β, to generate RL003-resistant tachyzoites, combining exposure to the mutagen ethyl methanesulfonate with subsequent selective pressure with RL003 to acquire a series of RL003-resistant clones by serial dilution. In total, we isolated 14 clonal populations, as shown in **Table 3.1**, and determined the 50% inhibitory concentration (IC_{50}) of each clone against RL003 as discussed previously. Most of these isolates were not resistant to RL003 relative to the wild-type control, suggesting a role of

α-Isolates			β-Isolates		
Clone	IC_{50} (μM)	IC_{50} Relative to WT Control	Clone	IC_{50} (μM)	IC_{50} Relative to WT Control
E11	0.096	1.14	E11	0.085	1.01
E12	0.127	1.50*	E12	0.081	0.96
F11	0.098	1.16	F10	0.092	1.09
F12	0.095	1.12	F11	0.223	2.64*
G11	0.095	1.13	F12	0.092	1.08
G12	0.095	1.12	G10	0.083	0.98
H12	0.084	0.99	H11	0.294	3.47*
WT RH	0.085	-	WT RH	0.085	-

Table 3.1. Random chemical mutagenesis of wild-type RH-dTom parasites generates RL003-resistant clonal isolates. Having confirmed a role of parasite processes in the toxicity of RL003, subsequent analysis of more specific processes affecting parasite resistance to RL003 was completed. To facilitate this, mutations were induced by random chemical mutagenesis of two flasks (α and β) of wild-type RH-dTom tachyzoites. RL003-resistant populations were selected by gradually increasing RL003 pressure over several passages until reaching a concentration at which a non-mutagenized flask of RH-dTom failed to recover. From these surviving parasite populations, clonal isolates were obtained by limiting dilution, yielding 14 total isolates (7 from each flask) that were then evaluated for their susceptibility to RL003 using the IC_{50} analysis as described previously. Results demonstrated that, while capable of surviving under RL003 selection, most clonal isolates were not resistant to RL003 (suggesting persistence); however, 3 isolates—3α-E12, 3β-F11, and 3β-H11—showed significant resistance of >1.5X higher IC_{50}s relative to the WT control. Particularly 3β-F11 and 3β-H11 showed IC_{50} values >2X and >3X that of the WT, suggesting significant resistance to RL003 in these isolates. *$p < 0.001$ by Student's paired *t*-test with unequal variance from technical triplicate evaluation.

persistence in survival of the selection process; however, 3 isolates—3α-E12 (“E12”), 3β-F11 (“F11”), and 3β-H11 (“H11”)—were significantly resistant to RL003 (**Table 3.1**), demonstrating IC_{50} values 1.50X, 2.64X, and 3.47X those of the wild-type RH-dTom parasites. This suggested likely resistance to RL003, and so we used these isolates for subsequent analyses.

Due to the potential for nonspecific parasite fitness advantage or broad antiparasitic resistance to facilitate the observed increase in IC_{50} for these clones, we proceeded to evaluate the resistance of each isolate to a panel of antimicrobial agents as well as overall parasite fitness as measured by changes in doubling time. To determine whether H11, F11, or E12 had nonspecific resistance to a variety of antiparasitic compounds, we determined the IC_{50} values for each H11, F11, and E12, as well as the wild-type RH-dTom, against pyrimethamine, clindamycin, atovaquone, and doxycycline. Neither F11 nor H11 showed any significant resistance to the tested compounds compared to the WT control, despite significant resistance to RL003; rather, both strains showed equivalent susceptibility to atovaquone and clindamycin and significantly heightened sensitivity to doxycycline (0.72X and 0.78X IC_{50} compared to WT, respectively) and pyrimethamine (0.50X and 0.83X IC_{50} compared to WT, respectively) (**Table 3.2**). E12, conversely, showed lower resistance to RL003 (1.50X IC_{50} relative to WT) and no significantly altered susceptibility to pyrimethamine, atovaquone, and clindamycin (**Table 3.2**). Intriguingly, E12 did show a significant 2.29X higher IC_{50} to doxycycline relative to the WT, indicating likely resistance to this compound; this resistance was higher than the resistance to RL003 (**Table 3.2**). In sum, these data indicated that H11 and F11 did not have broad antiparasitic resistance to the tested compounds, supporting a more specific resistance to RL003 and suggesting that these would act as better strains for further analysis of RL003 resistance.

Parasite fitness was then examined by determination of doubling time in untreated tachyzoites from H11 and F11; E12 was excluded due to its nonspecific compound resistance. We plated 2,000 tachyzoites/well of F11, H11, or wild-type RH-dTom into wells of confluent HFF in a 96-well plate (in triplicate) and monitored fluorescence as above at 24-hour intervals over 5 days to determine the doubling time of each strain. **Table 3.3** showed the results of this analysis: RH-dTom wild-type parasites showed an expected doubling time of 7.33 hours, while F11 had a similar doubling time of 10.77 hours (1.47X higher than WT; not significant). H11, the strain showing the highest resistance to RL003, also had the longest doubling time at 23.55 hours, representing a significant 3.22X increase relative to the WT (**Table 3.3**). The failure of F11 or H11 to show any decrease in doubling time suggests that the apparent resistance to RL003 is not simply an artefact of increased proliferative ability.

	IC_{50} Relative to WT RH-dTom *T. gondii*				
Clonal Isolate	**RL003**	**Pyrimethamine**	**Atovaquone**	**Clindamycin**	**Doxycycline**
F11	2.63*	0.72*	1.14	1.07	0.50*
H11	3.46*	0.78*	1.14	1.05	0.83*
E12	1.50*	1.02	1.12	1.33	2.29*

Key
Hypersensitive
Resistant

Table 3.2. Clonal resistance to RL003 is not inherently a consequence of broad antiparasitic resistance. Random mutations, such as those generated by EMS mutagenesis, may produce resistance-conferring mutations that affect general parasite susceptibility to compounds, such as by modification of a transporter; in these cases, resistance would not be unique to the compound of interest and would, therefore, be less likely to provide specific insight into the mechanisms guiding specific antiparasitic activity. With this under consideration, clonal isolates demonstrating resistance to RL003, here denoted E12, H11, and F11, were tested against known anti-*Toxoplasma* molecules pyrimethamine, atovaquone, clindamycin, and doxycycline *in vitro* using the IC_{50} analysis described previously, with each compound being run in technical triplicate. IC_{50} values were compared to the wild-type RH-dTom control. Results demonstrated that F11 and H11, which show the highest resistance to RL003, were not resistant to any of the other compounds tested. Both strains showed significantly higher sensitivity to pyrimethamine and doxycycline as compared to the WT control, which may be a consequence of their decreased overall fitness (**Table 3.3**). E12, which was less resistant to RL003, showed largely-similar IC_{50} values for the antiparasitic compounds relative to the WT control, with the exception of doxycycline; intriguingly, E12 was more resistant to doxycycline than to RL003, with >2X increase in IC_{50} relative to the wild-type, indicating potential multi-drug resistance in this strain. Overall, these results demonstrate that the highest-resistance strains are specifically resistant to RL003, indicating that the observed increase in IC_{50} was not a result of broad antiparasitic resistance. *$p < 0.001$ by Student's Paired *t*-Test with unequal variance.

Having identified both general fitness by doubling time and potential multi-compound resistance, we next sought to identify single nucleotide variants (SNVs) present in resistant clones but absent from the parental RH-dTom strain, hypothesizing that one or more of these mutations would be responsible for the observed resistance to RL003. To accomplish this, we performed whole-genome sequencing of our RH-dTom wild-type strain in addition to the RL003-resistant isolates F11, H11, and E12 using paired-end Illumina short reads and identified high-priority mutations using our in-house bioinformatics pipeline (see "Methods"). The highlighted results of this in-depth analysis are presented in **Table 3.4**, identifying four candidate genes selected for further examination. Of particular interest, two genes, cGMP-dependent protein kinase family member protein kinase G (PKG) and calcium-dependent protein kinase (CDPK) were notable due to their essentiality [257], their induced nonsynonymous changes to the amino acid sequence, and, in the case of PKG, the appearance of the mutation across all 3 resistant strains. CDPK, though only present in one clonal isolate, was examined further due to its relation to PKG as a downstream effector, particularly as its presence was restricted to the most resistant strain (H11) (**Table 3.4**). Based on these results, we aimed to proceed with analysis of PKG and CDPK first.

Strain	Doubling Time (h)	Doubling Time Relative to WT
F11	10.77	1.47
H11	23.55	3.22*
WT	7.32	-

Table 3.3. Clonal isolates resistant to RL003 do not show general fitness advantage relative to wild-type parasites. Given that possible overall fitness advantage, represented by more rapid replication under identical conditions, may be responsible for observed variation in resistance to RL003, the doubling times of the two highest-resistant clonal isolates, F11 and H11, were quantified by measurement of fluorescence for 96-well plates housing tachyzoite-infected HFF cells over 5 days. Doubling time was calculated as the time point at which fluorescence had doubled relative to the initial reading. Results showed that the WT strain showed a doubling time of ~7 hours, corresponding to the expected 6-8 hours observed in literature for RH-strain parasites; however, mutant F11 strain had a doubling time of nearly 11 hours, while the most resistant strain, H11, had a doubling time of nearly 24 hours, corresponding to ~1.5X (non-significant) and 3.2X (significant) increases in doubling time for the resistant mutants. This suggests that H11 and F11 do not show a general fitness advantage under identical conditions; particularly, H11 nearly tripled the doubling time, indicating a reduction in proliferation over this time period. These findings support that the observed resistance to RL003 is not a result of general fitness advantage. *$p < 0.001$ by Student's Paired t-Test with unequal variance.

Chromosome	Position	Gene ID	Predicted Protein Product	Mutation	Present in 3B-F11?	Present in 3B-H11?	Present in 3A-E12?
TGGT1_chrXII	2490908	TGGT1_245752	WD domain, G-beta repeat-containing protein	Splice region variant	TRUE	TRUE	FALSE
TGGT1_chrXI	1962311	TGGT1_311360	cGMP-dependent protein kinase family member PKG	C524R	TRUE	TRUE	TRUE
TGGT1_chrVI	1220922	TGGT1_240390	calcium-dependent protein kinase	T683A	FALSE	TRUE	FALSE
TGGT1_chrVIII	1421120	TGGT1_231440	LsmAD domain-containing protein	Splice acceptor variant; Loss of function	FALSE	TRUE	FALSE

Table 3.4. Whole-genome sequencing analysis of RL003-resistant parasite populations identifies nonsynonymous single nucleotide variants. In order to identify possible mutations conferring resistance to RL003, clonal isolates H11, F11, and E12, as well as the parental RH-dTom strain, were subjected to whole-genome sequencing followed by bioinformatic analysis to identify single nucleotide variants (SNVs) present in these populations. Results identified numerous mutations of potential interest; these were prioritized for subsequent analysis based on a variety of factors described in the text, including the number of resistant isolates having the mutation and the predicted essentiality of the genes. The four highest-priority candidates are shown above and include an intronic variant in the WD-domain G-beta repeat-containing protein, present in both of the most resistant strains, the cGMP-dependent protein kinase (PKG) C524R mutation present in all 3 resistant strains, a calcium-dependent protein kinase (downstream effector of PKG) present in the most resistant strain (H11), and a high-impact splice acceptor variation in the LsmAD-domain containing protein present in H11. These SNVs represented the most-likely effectors of parasite resistance to RL003 and so were examined in subsequent steps.

Molecular complementation of single nucleotide variants identifies episomal expression of a PKG^{C524R} nonsynonymous mutation as sufficient for conferring >2.5X resistance to RL003.

The presence of multiple high-priority mutations in our clonal strains, though obviously critical to our analysis, was not sufficient to suggest which, if any, were responsible for the observed resistance to RL003. In an effort to identify the mutation(s) causing this resistance, we performed molecular complementation of mutations into wild-type RH-dTom tachyzoites, aiming to confer resistance through a single nucleotide change, thereby confirming whether the mutation(s) of interest identified from the chemical mutagenesis were conferring resistance to RL003. For each gene to be examined, we performed cloning of the mutant allele or the corresponding wild-type allele by Gibson assembly into the

Transfected Gene	RL003 IC_{50} (μM)	Fold Change Relative to Vector
PKG^{C524R}	0.247	2.55*
$CDPK^{T683A}$	0.146	1.51*
PKG^{WT}	0.122	1.26
$CDPK^{WT}$	0.119	1.23
M2/M3 Vector	0.097	N/A

Table 3.5. Genetic complementation of wild-type T. gondii parasites identifies essential gene PKG as a mediator of RL003 resistance. With multiple candidate mutations identified, it was next critical to identify which, if any, of these particular mutations were responsible for acquired resistance to RL003. Candidate mutations of interest were each cloned into the pyrimethamine selection cassette vector, as were unmutated alleles for each gene to allow for confirmation of observed effects resulting from mutations themselves as opposed to simple overexpression of the gene of interest. Plasmids were transfected into wild-type RH-dTom parasites followed by 7 days of selection with 1 μM pyrimethamine. The IC_{50} of each validated strain was determined against RL003 as described previously, calculated relative to a volume-matched solvent control and subsequently compared to the wild-type vector strain. Results of this analysis revealed that parasites transfected with the SNV-containing variant of PKG (PKG^{C524R}) had a 2.55X higher IC_{50} than the vector control, a value not recapitulated by parasites transfected with the wild-type PKG allele, indicating that this mutation alone was sufficient to confer >2.5X resistance to RL003. Parasites transfected with CDPK expressing the SNV identified ($CDPK^{T683A}$) showed a statistically-significant, though less pronounced, 1.51X higher IC_{50} than the vector control, a value only slightly higher than that of parasites transfected with wild-type CDPK. However, given that CDPK is known to be a downstream effector of PKG, and given that most resistant mutant isolate, H11, was the only strain in which this mutation was identified, this comparatively-minor increase in IC_{50} may be partially responsible for the variation of IC_{50}s between F11 and H11 in **Table 3.4**. *$p < 0.001$ by Student's Paired *t*-test with unequal variance.

M2M3 pyrimethamine resistance cassette. After confirming that the appropriate mutations were present or absent, as needed, by Sanger sequencing (with additional sequencing of the parental RH-dTom wild-type strain to ensure that the mutation was not present), we confirmed specific expression of each gene of interest by RT-qPCR to ensure that the parasites were expressing the constructs as intended (**Supplementary Table 2**). At this point, we ran IC_{50}s of each mutant-transfected or wild-type-transfected strain against RL003 as completed previously and compared these to the vector (M2M3) control for determination of resistance.

Results of examining susceptibility of each of four transfected strains—one expressing an episomal copy of the C524R-mutated PKG gene (PKG^{C524R}), one expressing an episomal copy of the wild-type PKG gene

(PKG^{WT}), one expressing an episomal copy of CDPK carrying the T683A mutation ($CDPK^{T683A}$), and one expressing an episomal copy of the wild-type CDPK gene ($CDPK^{WT}$)—in addition to the vector control showed that the episomal expression of wild-type alleles for PKG and CDPK had no significant increase in IC_{50} relative to the control (**Table 3.5**). Conversely, episomal expression of the PKG^{C524R} mutant allele was sufficient to cause a 2.55X higher IC_{50} than the vector control, while similar expression of the $CDPK^{T683A}$ mutant allele yielded a less notable, but still significant, 1.51X higher IC_{50} than the vector control. However, $CDPK^{T683A}$ was present only in the most resistant isolate (H11), indicating that another mutation is likely responsible for resistance in these strains. Therefore, based on its presence in all clonal isolates from random chemical mutagenesis (**Table 3.5**), in addition to the approximate recapitulation of the RL003 resistance observed in these strains (**Table 3.5**) these data support that a PKG^{C524R} nonsynonymous mutation is sufficient to confer >2.5X resistance to RL003.

RNA-seq analysis of wild-type and RL003-resistant strains indicates differential expression of signaling, cell communication, and oxidation-reduction processes following treatment with RL003, supporting the purported importance of PKG.

To further illuminate our genomic and phenotypic findings, and thereby provide additional support for the potential role of PKG in RL003 activity, we performed RNA-seq analysis to identify global transcriptional changes occurring following treatment of wild-

type, F11, or H11-strain RH-dTom parasites with RL003 at the IC_{90} for 8 hours or 24 hours,

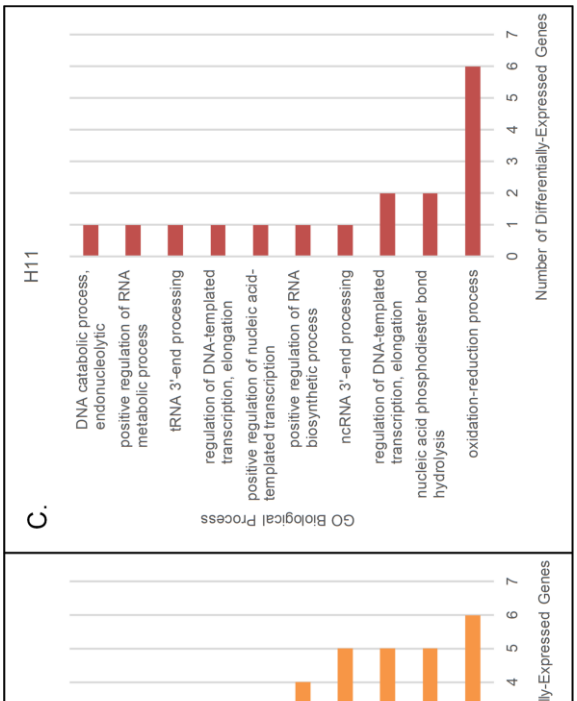

Figure 3.2. Treatment with RL003 causes differential expression of signaling, transport, and cell communication processes in *T. gondii* wild-type tachyzoites and F11 mutant-strain tachyzoites, with fewer significant alterations in H11 mutant-strain tachyzoites. To complement the genetic analysis conducted, we aimed to examine differential expression of tachyzoite transcripts for each of three strains—RH-dTom wild-type, F11, and H11—following treatment with RL003. To accomplish this, confluent flasks of each strain were treated with RL003 at the IC_{90} or with DMSO for 8 and 24 hours, after which RNA was isolated, confirmed for high quality, and submitted to the University of Nebraska Medical Center Genomics Core for library preparation and sequencing. Reads were aligned to the reference GT1 annotated transcriptome and transcript abundance was quantified using Salmon. Differentially-expressed genes for each RL003-treated sample relative to its corresponding DMSO control were identified using DESeq2, filtering for *p*-values <0.05 and |fold-change| exceeding 2.5. remaining genes were annotated with GO Biological Process terms and counted to obtain the top 10 processes most highly impacted for each strain: the RH-dTom wild-type (WT) (**A.**), the RL003-resistant F11 strain (**B.**), and the RL003-resistant H11 strain (**C.**). Compilation of these data showed substantial differential expression of genes involved in cell communication (n=9), transport (n=8), signaling (n=8), signal transduction (n=8), and oxidation-reduction (n=6) processes in WT parasites treated with RL003; similarly, the less-resistant F11 strain (**Table 3.1**) had differential expression of genes involved in oxidation-reduction (n=6), signaling (n=5), signal transduction (n=5), and cell communication (n=5), suggesting a likely-important role in signaling pathways in activity of and/or resistance to RL003. Conversely, in the highest-resistant strain, H11, comparatively little change in expression relative to the DMSO control was seen, intriguingly, with oxidation-reduction (n=6), nucleic acid phosphodiester bond hydrolysis (n=2), and regulation of various nucleotide processes (n=1-2) comprising a majority of these changes. Combined with our genomic data, these findings support a role of oxidation-reduction, nucleic acid metabolism, signaling, and transport processes in the activity of RL003 in addition to a likely role for these processes in resistance to RL003.

comparing all changes to volume-matched solvent (DMSO) treatment of the corresponding strain at the same time points. Results of these analyses are summarized in **Figure 3.2** as well as **Table 3.6**-**3.7**. Overall, treatment of the wild-type parasites with RL003 led to significant ($p < 0.05$) differential expression of numerous genes spanning a number of related biological processes (**Figure 3.2.A.**). In alignment with altered PKG function, the GO processes of cell communication, signaling, and transport had the highest number of differentially-expressed genes compared to the DMSO-treated controls (**Figure 3.2.A.**). The RL003-resistant mutants H11 and F11 showed reduced transcriptional changes, perhaps reflecting their resistance to RL003 (**Figure 3.2.C.**). In sum, these findings point to a number of differentially expressed processes induced by treatment with RL003, with the recurring presence of signaling, vesicular transport/localization (which is crucial to parasite gliding motility, as described in the "Discussion" section), and cell communication (**Figure 3.2.A. and 3.2.B.**) reinforcing a likely important role for these processes in the activity of RL003; given the key regulatory role of PKG in a variety of signaling processes, particularly related to secretion of micronemes for motility and invasion [263], these transcriptional changes strengthen the hypothesis that PKG may be involved in the interaction of RL003 with *T. gondii*, whether by aiding in resistance or by mediating its activity.

To enhance the specificity of our analysis, we more closely examined the predicted functions of the top 5 highly upregulated and downregulated genes for each sample at each time point. These results, summarized in **Tables 3.6 and 3.7,** further support the importance of oxidation-reduction, cell signaling, transport, and nucleic acid-based processes in parasite physiological events following RL003 treatment. Generally, proteins dependent on nucleotide and cyclic nucleotide hydrolysis activity appear to represent common themes in both up- and downregulated genes; these likely coincide with processes of signaling, given the role of cyclic nucleotides like cGMP and cAMP in signal transduction

[260]. Many of the earlier changes occurring at 8 hours post-treatment appear to be more related to signaling components (**Tables 3.6 and 3.7**), while later time points revolve more around oxidation-reduction, alterations in phosphorylation states, and ribosomal function, particularly in wild-type parasites. Though requiring greater depth to draw more concrete conclusions, the functions of these genes support the more global data emphasized above and are in alignment with effects of perturbed signaling pathways that may be expected from PKG activity changes. However, though supportive, these data alone are not sufficient to validate a role of PKG in the activity of RL003.

Conditional knockdown of PKG leads to >500X resistance to RL003 in knockdown, but not complement, strains, supporting a role of PKG in resistance to RL003.

To further validate the potential importance of PKG in either resistance to or activity of RL003 against *T. gondii*, we aimed to evaluate RL003 potency against parasites with reduced PKG activity; however, PKG is essential in *T. gondii* [261], and so cannot be knocked out while maintaining viability [262]. To partially circumvent this issue, we acquired a series of PKG conditional knockdown strains (a generous gift from Dr. Kevin Brown, University of Oklahoma) containing on the endogenous PKG gene a 3' mini-auxin-inducible degron (mAID) tag in a parasite background expressing the auxin receptor transport inhibitor response 1 (TIR1). In these strains, the addition of 3-indoleacetic acid (IAA) results in activation of the mAID tag at the C-terminus of the translated PKG protein, leading to targeting for proteasomal degradation as long as IAA pressure is maintained [263]. This is reversible and PKG expression is restored following removal of IAA, allowing for examination of PKG-

Condition	gene_id	gene_description	Log2FC	Product Description	Computed GO Functions
WT RL003 8H	TGGT1_411100	phenylalanine hydroxylase	3.99	BH4_AAA_HYDROXYL_2 domain-containing protein	iron ion binding;monooxygenase activity;oxidoreductase activity,
	TGGT1_209820	syntaxin protein	3.80	Syntaxin protein	protein binding
	TGGT1_235390	PAN domain-containing protein	3.66	PAN domain-containing protein	hydrolase activity;protein binding
	TGGT1_295015	patched family protein	3.32	Patched family protein	hedgehog receptor activity
	TGGT1_215670	cAMP-dependent protein kinase	3.28	Protein kinase domain-containing protein	AMP-activated protein kinase activity;ATP binding;cAMP-dependent protein kinase activity;protein kinase activity
WT RL003 24H	TGGT1_295720	putative sulfite oxidase	4.27	Cytochrome b5 heme-binding domain-containing protein	electron transfer activity;heme binding
	TGGT1_254380	putative ribosomal protein L11	4.27	Putative ribosomal protein L11	structural constituent of ribosome
	TGGT1_272285	tetratricopeptide repeat-containing protein	3.96	Tetratricopeptide repeat-containing protein	protein binding
	TGGT1_231400A	tubulin/FtsZ family, GTPase domain-containing protein	3.74	Tubulin domain-containing protein	GTP binding;GTPase activity
	TGGT1_320190	SAG-related sequence SRS16B	3.73	SAG-related sequence SRS16B	null
H11 RL003 8H	TGGT1_320150	elongation factor Tu GTP binding domain-containing protein	4.83	Tr-type G domain-containing protein	GTP binding;GTPase activity;translation elongation factor activity
	TGGT1_220420	3'5'-cyclic nucleotide phosphodiesterase domain-containing protein	4.70	Phosphodiesterase	3',5'-cyclic-nucleotide phosphodiesterase activity;metal ion binding;phosphoric diester hydrolase activity
	TGGT1_309330	SAG-related sequence SRS55F	4.31	SAG-related sequence SRS55F	null
	TGGT1_253120	putative mandelonitrile lyase	4.25	Putative mandelonitrile lyase	flavin adenine dinucleotide binding;mandelonitrile lyase activity;oxidoreductase activity, acting on CH-OH group of donors
	TGGT1_210787	Erv1 / Alr family protein	4.03	Sulfhydryl oxidase	flavin-linked sulfhydryl oxidase activity;thiol oxidase activity
H11 RL003 24H	TGGT1_322000	myosin-light-chain kinase	4.03	Protein kinase domain-containing protein	ATP binding;myosin light chain kinase activity;protein kinase activity
	TGGT1_409860	SAG-related sequence protein SRS48Q	3.65	SAG-related sequence protein SRS48Q	null
	TGGT1_295750	IgA-specific serine endopeptidase	3.63	IgA-specific serine endopeptidase	hydrolase activity
	TGGT1_412080	tRNA-Arg	3.49	tRNA-Arg	null
	TGGT1_321580	putative membrane protein	3.41	Putative membrane protein	null
F11 RL003 8H	TGGT1_279000	SAG-related sequence SRS59J	3.63	SAG-related sequence SRS59J	null
	TGGT1_285690	notch (dsl) domain-containing protein	3.55	Notch (Dsl) domain-containing protein	null
	TGGT1_244406	cysteine dioxygenase type I protein	3.54	Cysteine dioxygenase	cysteine dioxygenase activity;iron ion binding;oxidoreductase activity,
	TGGT1_261018	kelch repeat-containing protein	3.44	Kelch repeat-containing protein	protein binding
	TGGT1_360460	SAG-related sequence protein SRS40D	3.35	SAG-related sequence protein SRS40D	null
F11 RL003 24H	TGGT1_307460	Toxoplasma gondii family B protein	4.60	Toxoplasma gondii family B protein	null
	TGGT1_295600	SAG-related sequence SRS10	4.01	SAG domain-containing protein	null
	TGGT1_259965	RING-type domain-containing protein	3.85	RING-type domain-containing protein	null
	TGGT1_272360	EF hand family protein	3.42	EF hand family protein	null
	TGGT1_300621B	ribosomal protein L2	2.61	Ribosomal_L2_C domain-containing protein	RNA binding;structural constituent of ribosome;transferase activity

Table 3.6. Top5 upregulated genes in RL003-treated WT RH-dTom, F11, and H11 mutants. To further elucidate the specific pathways components most strongly upregulated in wild-type RH-dTom, F11, or H11, significantly differentially-expressed genes (p<0.05)from the RNA-seq analysis described in **Figure 3.5** were sorted by Log_2(Fold Change) in the expression of the gene following RL003 treatment relative to the DMSO controls at 8 hours and 24 hours. Gene products predicted to be hypothetical proteins which had no significant alignment to known proteins were removed from the analysis to facilitate clarity. The 5 highest-upregulated genes for each strain at each time point were then identified and annotated for predicted Gene Ontology (GO) biological processes with the built-in GO analysis tool of ToxoDB. Results are shown above and indicated a number of cyclic nucleotide binding and activity-related proteins as well as protein-binding and signaling-associated proteins.

Condition	gene_id	gene_description	Log2FC	Product Description	Computed GO Functions
WT RL003 8H	TGGT1_255710	ULK kinase	-3.87	Protein kinase domain-containing protein	ATP binding;calmodulin-dependent protein kinase activity;phosphotransferase activity
	TGGT1_253480	putative topoisomerase VIA	-3.93	Putative topoisomerase VIA	ATP binding;DNA binding;DNA topoisomerase type II (double strand cut, ATP-hydrolyzing) activity
	TGGT1_266130	peroxiredoxin PRX2	-4.26	Glutathione peroxidase	glutathione peroxidase activity;peroxiredoxin activity
	TGGT1_283530	small rab-related GTPase	-4.28	Small rab-related GTPase	GTP binding;GTPase activity
	TGGT1_300621B	ribosomal protein L2	-5.59	Ribosomal_L2_C domain-containing protein	RNA binding;structural constituent of ribosome;transferase activity
WT RL003 24H	TGGT1_201850	WD domain, G-beta repeat-containing protein	-4.32	WD_REPEATS_REGION domain-containing protein	histone acetyltransferase activity;protein binding
	TGGT1_302000	putative chaperone clp	-4.52	Putative chaperone clp	null
	TGGT1_412100	tRNA-Arg	-4.64	tRNA-Arg	null
	TGGT1_231900	acyl-CoA dehydrogenase domain-containing protein	-4.64	Acyl-CoA dehydrogenase domain-containing protein	acyl-CoA dehydrogenase activity…
	TGGT1_300621B	ribosomal protein L2	-6.30	Ribosomal_L2_C domain-containing protein	RNA binding;structural constituent of ribosome;transferase activity
H11 RL003 8H	TGGT1_216280	adenylate and guanylate cyclase catalytic domain-containing protein	-3.92	Guanylate cyclase domain-containing protein	phosphorus-oxygen lyase activity
	TGGT1_247660	thioredoxin domain-containing protein	-3.92	Thioredoxin domain-containing protein	null
	TGGT1_260460	putative oxidoreductase	-4.04	Putative oxidoreductase	oxidoreductase activity;protochlorophyllide reductase activity
	TGGT1_200230	microneme protein MIC17C	-4.64	Microneme protein MIC17C	protein binding
	TGGT1_266785	zinc finger (CCCH type) motif-containing protein	-5.01	Zinc finger (CCCH type) motif-containing protein	ATP binding;metal ion binding;protein kinase activity
H11 RL003 24H	TGGT1_282230	sulfate adenylyltransferase/adenylylsulfate kinase	-3.09	Sulfate adenylyltransferase/adenylylsulfate kinase	ATP binding;adenylylsulfate kinase activity;sulfate adenylyltransferase (ATP) activity
	TGGT1_229170	formate/nitrite transporter protein	-3.12	Formate/nitrite transporter protein	transmembrane transporter activity;transporter activity
	TGGT1_257945	3'5'-cyclic nucleotide phosphodiesterase domain-containing protein	-3.65	Phosphodiesterase	3',5'-cyclic-nucleotide phosphodiesterase activity
	TGGT1_207650	OTU family cysteine protease	-4.06	OTU domain-containing protein	peptidase activity
	TGGT1_231060	subtilisin SUB9	-4.51	Peptidase_S8 domain-containing protein	serine-type endopeptidase activity
F11 RL003 8H	TGGT1_210260	NAD-dependent glycerol-3-phosphate dehydrogenase	-3.22	Glycerol-3-phosphate dehydrogenase [NAD(+)]	NAD binding;glycerol-3-phosphate dehydrogenase [NAD+] activity;oxidoreductase activity
	TGGT1_282230	sulfate adenylyltransferase/adenylylsulfate kinase	-3.24	Sulfate adenylyltransferase/adenylylsulfate kinase	ATP binding;adenylylsulfate kinase activity;sulfate adenylyltransferase (ATP) activity
	TGGT1_255710	ULK kinase	-3.49	Protein kinase domain-containing protein	ATP binding;calmodulin-dependent protein kinase activity;phosphotransferase activity
	TGGT1_409870	SAG-related sequence protein SRS48K	-3.65	SAG-related sequence protein SRS48K	null
	TGGT1_279000	AGC kinase	-3.74	Protein kinase domain-containing protein	AMP-activated protein kinase activity;ATP binding;cAMP-dependent protein kinase activity;calcium-dependent protein kinase C activity;protein kinase activity
F11 RL003 24H	TGGT1_409870	SAG-related sequence protein SRS48K	-3.43	SAG-related sequence protein SRS48K	null
	TGGT1_223830	fasciclin domain-containing protein	-3.43	FAS1 domain-containing protein	null
	TGGT1_240325	Toxoplasma gondii family E protein	-3.67	Toxoplasma gondii family E protein	null
	TGGT1_294570	rhodanese family domain-containing protein	-3.79	Rhodanese domain-containing protein	null
	TGGT1_240390	calcium-dependent protein kinase	-3.82	Calcium-dependent protein kinase	ATP binding;calcium ion binding;myosin light chain kinase activity;protein kinase activity

Table 3.7. Top5 downregulated genes in RL003-treated WT RH-dTom, F11, and H11 mutants. Analysis of the 5 most strongly-downregulated genes was completed as described in **Table 3.6**, with the modification that the 5 significantly (p<0.05) differentially-expressed genes for each strain and condition with the *lowest* (i.e., most negative) Log_2FC were considered for analysis. Results suggested strong downregulation of a number of cyclic nucleotide-dependent processes, oxidation-reduction processes, and nucleotide binding.

dependent processes. For our purposes, strains examined included PKG-mAID-3HA, used for the IAA-induced conditional PKG knockdown, as well as the corresponding complement PKG-mAID-3HA/PKG^{6Ty} containing a 6-Ty tagged PKG allele present at the uracil phosphoribosyltransferase (*UPRT*) locus, allowing for continued expression of PKG when the endogenous gene is knocked down. With these strains, we performed IC_{50} analyses with RL003 as before, though included for these analyses sample sets of each strain containing IAA in order to trigger the conditional knockdown and corresponding complement. Because these strains do not natively fluoresce as does RH-dTom, the parasites were stained for SAG1 as above and counted with a BioTek Lionheart automated microscope to determine growth and identify the IC_{50} values.

The IC_{50} values shown in **Figure 3.3** demonstrate an increase in the IC_{50} of RL003 following induction of the conditional knockout in the absence of compensatory complementation. Parasites with unchanged PKG levels (PKG-mAID-3HA -IAA), acting as a baseline control for “wild-type” parasites of the PKG-mAID background, showed an IC_{50} of 3 nM (**Figure 3.3**); the corresponding uninduced complement strain having 2 expressed copies of PKG (PKG-mAID-3HA/PKG^{6Ty} -IAA) showed an IC_{50} at 8 nM, or 2.7X that of the PKG-mAID-3HA strain (**Figure 3.3**). Reduction of PKG levels (PKG-mAID-3HA +IAA) increased the IC_{50} to 1.64 µM, representing a significant and substantial 550X increase relative to the uninduced strain of the same genetic background (**Figure 3.3**). In contrast, expression of a single copy of PKG in the complement strain (PKG-mAID-3HA/PKG^{6Ty} +IAA) led to an IC_{50} of 1 nM against RL003; this more closely resembled the value of the “wild-type” surrogate (PKG-mAID-3HA -IAA) but demonstrated a statistically significant reduction to 0.33X the IC_{50} of this strain (**Figure 3.3**), likely due to variation in expression for the non-endogenous PKG construct. Therefore, given that the loss of PKG rendered

parasites dramatically less sensitive to RL003, these data provide strong evidence supporting a role of PKG in resistance to this compound.

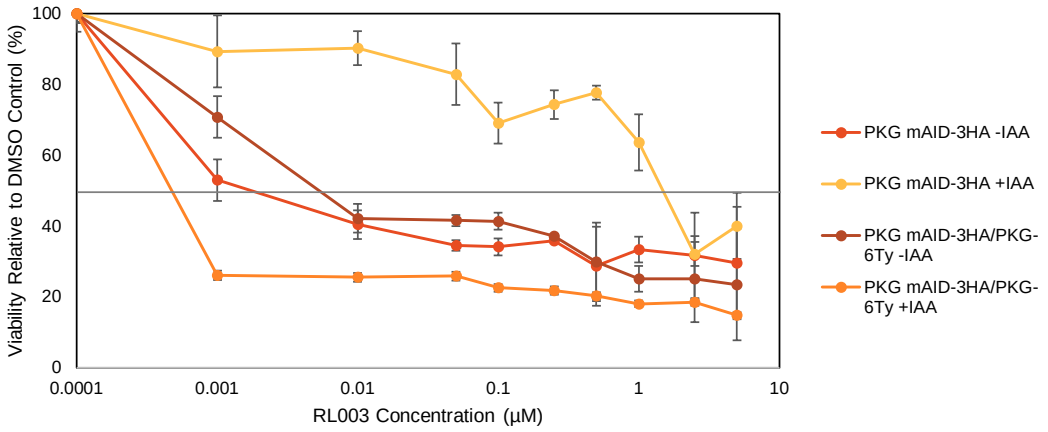

Strain	IAA (+/-)	IC_{50} (µM)	IC_{50} Relative to "WT"	IC_{50} Relative to RH-dTom WT
PKG mAID-3HA ("WT")	**-**	0.003	-	0.03*
PKG mAID-3HA	**+**	1.65	550*	17.18*
PKG mAID-3HA/PKG^{6Ty}	**-**	0.008	2.7*	0.08*
PKG mAID-3HA/PKG^{6Ty}	**+**	0.001	0.33*	0.01*

Figure 3.3. Conditional knockdown of PKG results in high resistance to RL003 that is abrogated by complementation at an alternate locus. With resistance to RL003 arising in response to single nucleotide variation in PKG gene, further evaluation arising from previous work would suggest performing a knockout of the gene to identify changes to parasite susceptibility to the compound. The essentiality of PKG, while advantageous for targeting in antiparasitic molecules, prevents complete knockout with maintenance of viability; however, to compensate for this, Brown *et al.* have generated a transgenic RH tachyzoite line housing on the endogenous PKG gene a 3' auxin-inducible degron tagged with 3X hemagglutinin (mAID-3HA) to allow for conditional knockdown upon the addition of 3-indoleacetic acid (IAA) [263]. Additionally, a 6Ty-tagged complement strain—PKG mAID-3HA/PKG-6Ty—expressing PKG even when the endogenous gene is knocked down was generated for disambiguation of results. These strains were therefore chosen for evaluation of RL003 activity. Parasites were plated in 96-well plates as above for IC_{50} analysis, with each strain being evaluated in triplicate in both the presence (+IAA) or absence (-IAA) of 500 µM IAA, after which compound dilutions for each condition were completed as described (including a solvent-only control). Due to their lack of a stable fluorescent marker, tachyzoites were stained for expression of SAG1 for the invasion and motility assays, and IC_{50} values were calculated relative to the DMSO control. Quantification of IC_{50} values showed that the "wild-type" strain of the same genetic background—represented by the PKG-mAID strain *without* induction of the conditional knockdown by IAA (PKG-mAID-3HA –IAA)—had an IC_{50} of 3 nM, with the uninduced complement (PKG-mAID-3HA/PKG^{6Ty} -IAA) more than doubling this IC_{50} at 8 nM. Addition of IAA to induce conditional knockdown of the PKG gene in the PKG-mAID-3HA strain dramatically and significantly increased the IC_{50} by over 500X to reach 1.64 µM, while addition of IAA to the complement strain (PKG-mAID-3HA/PKG^{6Ty} +IAA) generated an IC_{50} of 1 nM, which more closely approximated that of the "wild-type" uninduced strain (PKG-mAID-3HA –IAA). These data strongly support an important role of PKG in resistance to RL003, and potentially in its mechanism of action. *p<0.001 by two-tailed Student's t-test assuming unequal variance. Error bars represent standard error from the mean.

Phenotypic evidence showing defects in parasite gliding motility, invasion, and egress supports the likely importance of PKG in the activity of RL003.

With both the genomic and transcriptional data appearing to favor a role for PKG in the activity of RL003, we aimed to further characterize phenotypic events following RL003 exposure in wild-type parasites. PKG is known to impact a number of essential parasite processes, ranging from adhesion to the host cell surface by gliding motility to successful invasion through the moving junction and eventual egress upon exposure to the proper stimuli through tight regulation of cGMP signal transduction. Therefore, we hypothesized that, if PKG is involved in either the mechanism of action of or acquisition of resistance to RL003, then one or more of these processes would show significant deficiency following exposure to the compound. To test this, we performed 2-D motility, invasion, and egress assays adapted from methods published previously, treating wild-type RH-dTom parasites with either RL003 at the 90% parasite inhibitory concentration (IC_{90}, 0.200 µM) or with the solvent (DMSO) for 1, 3, or 5 days before performing the appropriate procedures, each in triplicate for every condition.

Comparison of RL003-treated parasites relative to the DMSO (solvent) controls by differential intracellular and extracellular parasite staining showed a significant defect in the invasion of compound-treated parasites, with <10% of surviving parasites completing successful invasion at day 1, ~20% completing successful invasion at day 3, and ~40% completing successful invasion at day 5 (**Figure 3.4.A.**). Similarly, quantification of parasites showing SAG1-staining trails on poly-L-lysine-coated coverslips, representing gliding motility, showed a mild reduction in motility in RL003-treated parasites relative to the DMSO-treated controls on days 1 and 3, with 84% and 88% of treated parasites having SAG1-positive trails (**Figure 3.4.B.**). However, a much stronger deficiency in motility could be seen by day 5, at which point <10% of surviving parasites were shown to have these

characteristic trails (**Figure 3.4.B.**). Together, the motility and invasion assays indicate a possible impact of RL003 on PKG-mediated processes.

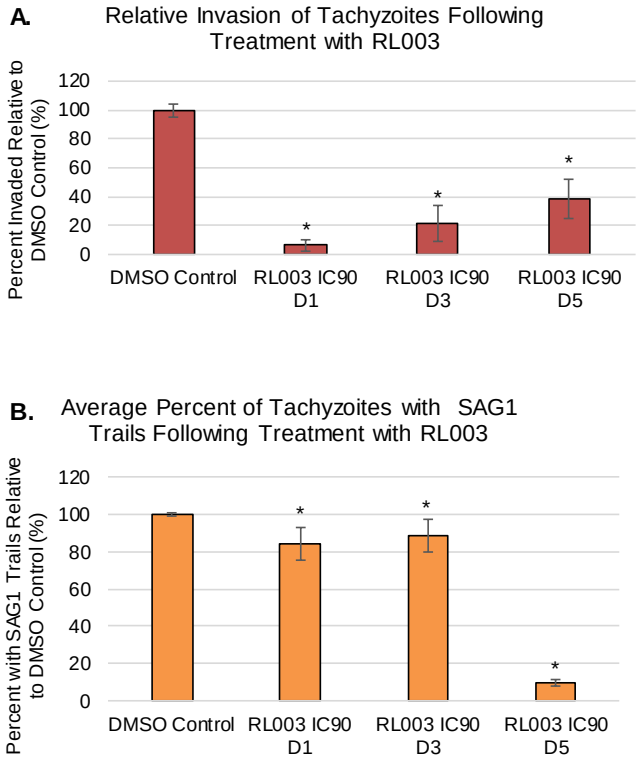

Figure 3.4. Invasion and motility assays support the role of PKG in RL003-mediated parasite toxicity. Effects of RL003 treatment on invasion and motility, both downstream processes impacted by PKG activity, were evaluated in wild-type parasites. To quantify invasion, tachyzoites were treated with RL003 at the IC_{90} or with the solvent (DMSO) 1, 3, or 5 days. Isolated parasites were differentially stained for intracellular/extracellular localization using a murine monoclonal antibody against the surface marker SAG1 in conjunction with secondary goat anti-mouse IgG antibodies conjugated to Alexa-488 to stain extracellular parasites prior to permeabilization and subsequent addition of goat anti-mouse IgG conjugated to Alexa-594 antibodies to stain intracellular parasites. Quantification was completed in triplicate using an automated microscope. Percent invasion was calculated as the number of Alexa-488+ parasites/the total number of parasites (Alexa 488+ and Alexa 594+). Analysis of these data relative to the DMSO (solvent) controls demonstrated that invasion was strongly and significantly reduced in surviving parasites following RL003 treatment, with <10% successful invasion at D1, ~20% successful invasion at D3, and ~40% successful invasion at D5. This is necessary, but not sufficient, to indicate a possible impact of RL003 on PKG-mediated processes.

To determine whether defects in invasion were related to loss of motility, a motility assay was performed, with tachyzoites being treated with either DMSO or RL003 for 1, 3, or 5 days as above. Parasites were allowed to glide on poly-L-lysine-coated coverslips for 1 hour at 37 ^{o}C. Trails containing SAG1, representing deposition by moving parasites, were stained using the SAG1 primary antibody and Alexa-488 secondary antibody as above and imaged with an automated microscope. The percentage of total counted parasites having associated trails for each time point was compared to the DMSO control. Results on D1 and D3 were less pronounced than those of invasion, with 80-85% of parasites having trails; however, by D5, <10% of surviving parasites showed trails, suggesting a significant defect in invasion. This again supports, but does not prove, some level of PKG involvement in RL003 activity. *p < 0.001 by Student's t-test assuming unequal variance. Error bars represent standard error from the mean from technical triplicate values.

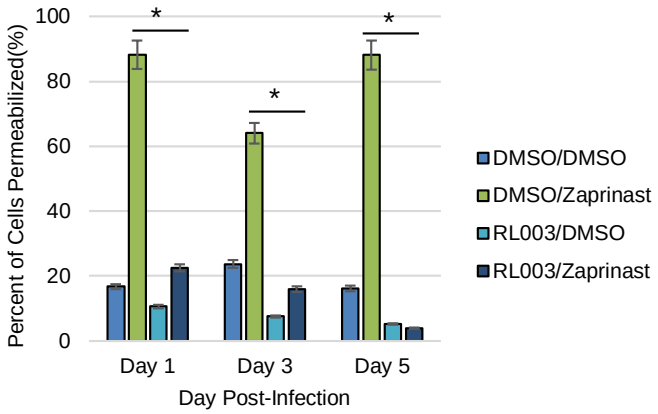

Figure 3.5. Inhibition of egress following compound treatment supports the role of PKG in RL003-mediated parasite toxicity. To further support the suspected impact of RL003 on PKG, another downstream process was examined: egress, which is known to be inhibited or altered in its timing if PKG is strongly downregulated. To determine whether treatment with RL003 affects egress, potentially through PKG, RH-dTom tachyzoites in 96-well plates were treated with RL003 at the IC_{90} or with DMSO (as a solvent control) for 1, 3, or 5 days. To each treatment group, either zaprinast (DMSO/Zaprinast, RL003/Zaprinast), a potent inducer of egress, or a volume-matched DMSO control (DMSO/DMSO, RL003/DMSO) was added. Host cell nuclei, representing permeabilized cells associated with egress, were then quantified using the CellTox-Green nuclear DNA dye followed by counting with an automated microscope. The total number of cells present in the well was subsequently calculated by similar quantification following the addition of 0.1% Triton-X to fully permeabilize all host cells. The relative success of egress was measured as the percentage of cells permeabilized prior to the addition of Triton-X, ostensibly by movement of parasites out of their resident vacuoles. From this method, we found that parasites treated with RL003 had significant reduction in egress relative to the DMSO control, being reduced to ~20% at D1 and D3, compared to ~85% and ~65% on these respective days for the DMSO-treated wells. By D5, egress was reduced to <5% in RL003-treated parasites, which was not significantly different than the DMSO control, suggesting defect in egress. Overall, these findings suggest that treatment with RL003 causes significant reduction in zaprinast-induced egress *in vitro*, providing additional support for a role of PKG in RL003 activity. *$p < 0.001$ by Student's paired t-test with unequal variance. Error bars represent standard error from the mean.

Complementarily, egress of RL003-treated tachyzoites quantified by relative numbers of parasite-infected host cells permeabilized following stimulation with zaprinast, an inducer of egress in *T. gondii* [288], or DMSO, a negative solvent control for egress, showed a marked decrease compared to the DMSO-treated parasite control (**Figure 3.5**). As anticipated, DMSO mock-treated parasites exposed to zaprinast (DMSO/Zaprinast) led to permeabilization of 88% of host cells on days 1 and 5, and 64% of host cells on day 3, with the corresponding solvent control (DMSO/DMSO) having ≤10% permeabilization at all time points (**Figure 3.5**). However, upon treatment with RL003 at the IC_{90}, tachyzoites exhibited a significant decrease in zaprinast-induced egress represented by host cell permeabilization (RL003/Zaprinast), with 23% and 16% permeabilization at day 1 and day 3, respectively. This effect was more pronounced at day 5, with <5% of RL003-treated parasites showing egress; notably, at this stage, permeabilization of zaprinast-treated

samples was not significantly different than the DMSO egress control (RL003/DMSO) (**Figure 3.5**). Together, in agreement with the invasion and motility data, the clear defect in egress satisfies an additional condition to implicate PKG in the physiological alterations of parasites treated with RL003.

RT-qPCR reveals significant upregulation of primitive parasite programmed cell death-associated genes in wild-type parasites, but not in parasites carrying the PKG^{C524R} or PKG^{WT} transfected alleles.

While PKG appeared to be implicated in resistance to RL003, the means by which death of parasites would occur—whether or not PKG represents a target of the compound—had not yet been made clear; however, the differential expression of key signaling pathways suggested that this may occur through a form of systematic, programmed cell death rather than through necrosis, as these pathways have been implicated in mammalian cancer cells to be related to apoptosis. To explore this possibility, and to supplement our RNA-seq data, we examined a number of genes shown previously to be associated with programmed cell death in *T. gondii* [264], including the autophagy-associated protein (TGGT1_221360), programmed cell death proteins 1 (TGGT1_294420) and 2 (TGGT1_305490), DNA endonuclease (TGGT1_208710), phagocytosis-associated protein (TGGT1_253000), and metacaspase (TGGT1_206490), as well as a predicted FASI-like inhibitor of apoptosis (TGGT1_249770). Due to the previous observation that higher upregulation of these genes was seen at 48 hours post-addition of compound [264], we isolated RNA (as was described for RNA-seq) from confluent parasites treated with RL003 at the IC_{90} or with DMSO for 48 hours and performed one-step RT-qPCR using primers suggested by [264]. All samples were completed in triplicate, and, additionally, three housekeeping genes—histone 2B (TGGT1_209910), ribosomal protein L33 (TGGT1_308930), and DEAD-DEAH-box helicase (TGGT1_256900)—were used for

appropriate normalization to allow for calculation of fold-change (FC) by the $2^{-\Delta\Delta Ct}$ method relative to the DMSO-treated samples.

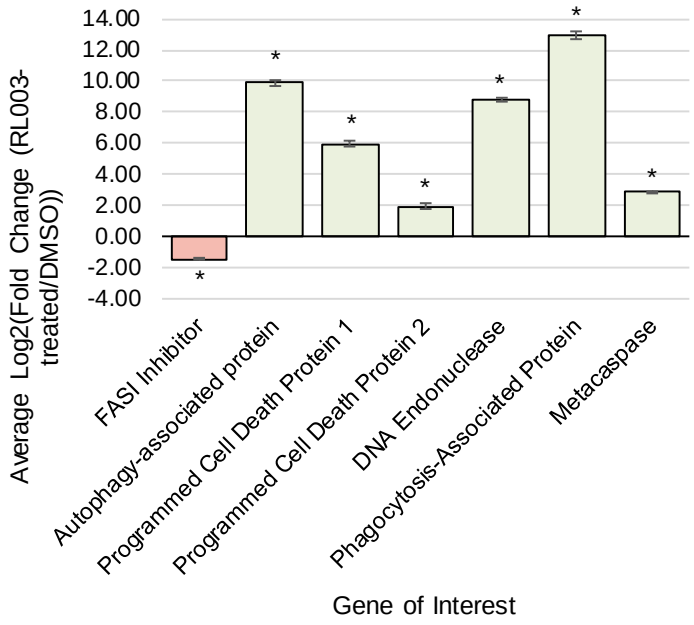

Figure 3.6. RL003-treated tachyzoites demonstrate upregulation of primitive apoptosis-like programmed cell death (PCD)-associated genes. Phenotypic data from TUNEL assays and SEM appeared to provide evidence for apoptosis-like programmed cell death following treatment with RL003 at the IC_{90}. While *T. gondii* has a poorly-defined programmed cell death pathway, carrying hallmarks of primitive apoptosis, autophagy, and phagocytosis, a number of genes have been associated with apoptosis-like cell death following stimulation by chemotherapeutic agents [23468121]; therefore, we hypothesized that *T. gondii* treated at the IC_{50} of RL003 over 48 hours would show upregulation of some of these genes in qRT-PCR. Seven total genes known to be associated with apoptosis-like cell death in tachyzoites were evaluated, each in triplicate with 100 ng of each sample—RL003-treated and DMSO-treated—and, additionally, 3 housekeeping genes—histone 2B, ribosomal protein L33, and DEAD-DEAH-box helicase—were used for normalization of expression. Non-template controls for each gene were used to ensure no cross-contamination of reagents. Relative expression of each gene of interest under RL003 treatment was calculated using the delta-delta Ct method relative to the DMSO-treated samples. Quantification demonstrated that all genes of interest appeared to have some level of differential expression relative to the DMSO sample, with the phagocytosis-associated protein ($Log_2FC = 12.95$), autophagy-associated protein ($Log_2FC = 9.88$), and DNA endonuclease ($Log_2FC = 8.79$) showing strong and significant upregulation. Concomitantly, the single identified *T. gondii* metacaspase was also significantly upregulated ($Log_2FC = 2.83$), as would be anticipated in programmed cell death. These changes in expression support a likely initiation of primitive parasitic cell death pathways by RL003. *$p < 0.001$ by Student's Paired t-Test with Unequal Variance. Error bars represent standard error from the mean.

The results of this quantification (**Figure 3.6**) showed differential expression of all 7 selected genes relative to the DMSO control, with 6 of the 7 genes showing statistically-significant ($p < 0.001$) upregulation and 1 of the 7 genes (the putative FASI inhibitor) showing statistically-significant downregulation in expression ($p < 0.001$) (**Figure 3.6**). Of these,

3 showed >10X (Log2FC > 3.32) increase in expression in RL003-treated samples compared to DMSO: phagocytosis-associated protein (Log_2FC = 12.95), autophagy-associated protein (Log_2FC = 9.88), and DNA endonuclease (Log_2FC = 8.79) (**Figure 3.6**). Though not as strongly upregulated as these genes, the *T. gondii* metacaspase was also significantly upregulated (Log_2FC = 2.83). To evaluate the specificity of this response to RL003, and to rule out the possibility that these changes in expression are common to multiple anti-*Toxoplasma* compounds, a similar analysis was repeated with antiparasitic compounds miltefosine (a positive control that is known to induce programmed cell death in *T. gondii* [264]), atovaquone, and pyrimethamine. Results showed that neither atovaquone nor pyrimethamine recapitulated the changes in expression seen with RL003 treatment, while miltefosine had significant increases in the autophagy-related, phagocytosis-related, and DNA endonuclease proteins that more closely resembled the pattern of RL003 (**Supplementary Figure 2**). This suggests that the strong upregulation of genes seen in RL003 treatment is not shared among all anti-*Toxoplasma* compounds. Taken together, these data point to the initiation of a primitive form of programmed cell death arising from treatment of *T. gondii* with RL003, rather than necrosis culminating exclusively from broad cellular damage.

We hypothesized that, if programmed cell death was responsible for the RL003-mediated antiparasitic effects seen *in vitro*, the transfected mutant strain shown to be the most resistant to RL003—PKG^{C524R} (here called “PKG SNV” for clarity)—should show less pronounced increases in expression of these pro-programmed cell death genes. We therefore repeated our RT-qPCR analysis, this time using “PKG SNV episomal” as well as the corresponding wild-type PKG-transfected strain (“PKG WT episomal”) in examination of these 7 genes at 48 hours post-RL003 treatment or post-DMSO treatment. Like the RH-dTom wild-type strain, analysis by the $2^{-\Delta\Delta Ct}$ method showed that PKG SNV episomal

mutants had significant alterations in their expression of these key genes; however, these changes in transcriptional expression were markedly different from those in the wild-type RH-dTom and PKG WT episomal strains (**Figure 3.7**). Regarding the latter, episomal expression of the PKG WT allele did not appear to result in many significant changes in expression relative to the DMSO control for 4 of the 6 examined genes, indicating potential dysregulation of this pathway (**Figure 3.7**). The phagocytosis-associated protein was upregulated significantly ($Log_2FC = 2.78$) upon treatment with RL003, while the autophagy-associated protein was downregulated (Log2FC = -1.91) (**Figure 3.7**); in the WT RH-dTom strain, these proteins had Log_2FC values of, respectively, 12.95 and 9.88, showing a stark contrast in these strains (**Figure 3.7**). Conversely, the PKG SNV strain had different transcriptional changes than either of the other strains: in this case, the phagocytosis-associated protein showed substantial downregulation ($Log_2FC = -9.17$) following treatment with RL003, a near-complete reversal of the upregulation seen in the RH-dTom WT strain. Further, the autophagy-associated protein ($Log_2FC = -2.96$), programmed cell death protein 1 ($Log_2FC = -2.72$), and DNA endonuclease ($Log_2FC = -2.49$) all showed significant downregulation in the PKG SNV episomal strain (**Figure 3.7**), signifying that, rather than increasing expression of the programmed-cell-death-associated genes, nearly all had marked downregulation, coinciding with the comparative lack of parasite death shown in the IC_{50} analyses. Together, these data may indicate that RL003 treatment does not induce programmed cell death through the 7 selected genes in the PKG-carrying clone—and induces only a few of these genes in the PKG WT strain—despite showing strong induction of expression in RH-dTom wild-type parasites.

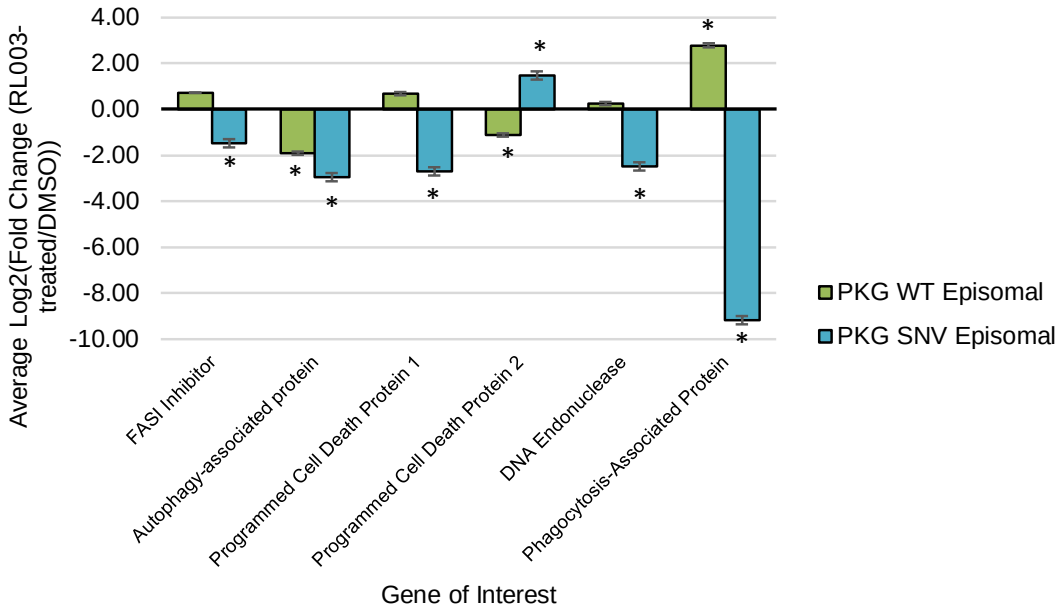

Figure 3.7. Mutants expressing episomal copies of wild-type or SNV-bearing PKG demonstrate downregulation of PCD-associated genes. The resistance of episomal PKG mutants, particularly the mutant housing the C524R nonsynonymous SNV, combined with the observed activation of programmed cell death-associated genes in wild-type RH-dTom, led us to hypothesize that these same genes are likely less upregulated, if upregulated at all, in the mutant strains as compared to the WT control. To test this hypothesis, the qRT-PCR described in **Figure 3.6** was repeated as described using the PKG SNV and PKG WT strains, both treated with RL003 at the IC_{90} for 48 hours or treated with DMSO for 48 hours. From the delta-delta Ct analysis, the RL003-treated PKG mutants showed altered expression of these PCD-associated genes compared to the RL003-treated RH-dTom WT. The WT PKG episomal strain showed no significant variation from the DMSO-treated controls across most of the PCD-associated genes; however, the phagocytosis-associated protein was still upregulated significantly ($Log_2FC = 2.78$), though not to the magnitude of the RH-dTom WT ($Log_2FC = 12.95$), while the autophagy-associated protein was significantly, though not highly, downregulated (Log2FC = -1.91), in contrast to the strong upregulation in the RH-dTom WT ($Log_2FC = 9.88$). In the PKG SNV strain, the phagocytosis-associated protein was strongly and significantly downregulated ($Log_2FC = -9.17$) in RL003-treated parasites, with additional significant downregulation of autophagy-associated protein ($Log_2FC = -2.96$), programmed cell death protein 1 ($Log_2FC = -2.72$), and DNA endonuclease ($Log_2FC = -2.49$). These findings demonstrate that genes associated with PCD that are highly upregulated in RL003-treated wild-type RH-dTom parasites are largely unchanged relative to the DMSO-treated control in PKG WT mutants and are significantly downregulated in the RL003-resistant PKG SNV strain, suggesting that RL003 treatment does not induce PCD in the PKG SNV strain and induces only partial components of the PCD pathway in the PKG WT strain. *$p < 0.001$ by Student's paired *t*-test assuming unequal variance. Error bars represent standard error from the mean. WT = wild-type; PCD = programmed cell death; SNV = single nucleotide variant.

Qualitative analysis by SEM provided insights supporting the occurrence of programmed cell death through distinct apoptosis-like blebbing of tachyzoite membranes following treatment with RL003.

With the combination of phenotypic and transcript-level data pointing to possible triggering of the *T. gondii* programmed cell death pathway, we aimed to qualitatively examine superstructures at the tachyzoite surface through the use of scanning electron microscopy (SEM), hypothesizing that apoptosis-like parasite death would result in morphological changes, such as membrane blebbing and cell shrinkage. We therefore treated tachyzoites in T25 flasks with DMSO or with RL003 at the IC_{90} for 48 hours, isolated them from host cells, and submitted samples to the Electron Microscopy Core Facility (EMCF) at the University of Nebraska Medical Center for imaging. Representative images for both DMSO-treated and RL003-treated parasites are shown in **Figure 3.8**; phenotypic changes are evident in the RL003-treated tachyzoites, which show blebbing of the membrane and formation of vesicle-like structures (arrows, **Figure 3.8.C.-D.**) that were not present in the DMSO-treated parasites. These

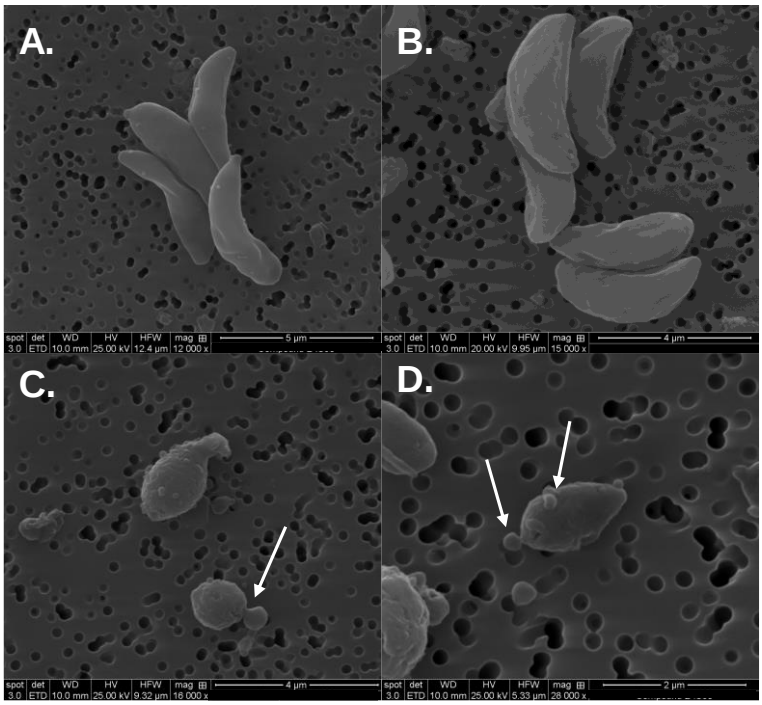

Figure 3.8. Scanning electron microscopy (SEM) of RL003-treated tachyzoites shows phenotypic changes resembling those of mammalian programmed cell death. Evaluation of broad surface-level morphological changes to *T. gondii* was completed through the use of SEM. Tachyzoites treated with either RL003 at the IC_{90} (**C., D.**) or with a volume-matched quantity of DMSO (**A., B.**) for 48 hours were submitted to the Electron Microscopy Core Facility (EMCF) at the University of Nebraska Medical Center for imaging. Results demonstrated notable phenotypic changes of tachyzoite cell surfaces following RL003 treatment that were not seen in the DMSO control; namely, the formation of membrane blebs and vesicle-like structures (arrows) emerging from the membrane, which resembled those of mammalian programmed cell death pathways, particularly apoptosis and autophagy. These qualitative data may suggest a role of programmed cell death in the anti-*Toxoplasma* activity of RL003.

morphological variations are indicative of regulated disposal of cell components rather than nonspecific damage to the cell and support our hypothesis.

Discussion

The high potency of pyrrolomycin derivative RL003, in combination with its specificity to parasite processes, positively supports the potential therapeutic applicability of this molecule; however, given that there is little precedent for evaluation of pyrrolomycin—or marinopyrrole—mechanisms of antimicrobial activity in *T. gondii*, we performed a series of molecular and phenotypic analyses to evaluate potential compound target(s) and/or gene product(s) facilitating resistance to the compound. Compilation of data from whole-genome sequencing of RL003-resistant clonal isolates and subsequent molecular complementation implicated a predicted C524R mutation in the parasite-specific cGMP-dependent protein kinase (PKG) [257] gene as a mediator of observed resistance to RL003 (**Table 3.4**). Specific complementation of wild-type parasites with a plasmid carrying PKG with the C524R mutation was sufficient to confer ~2.6X resistance to RL003, while this was not the case when an unmutated PKG allele was similarly complemented into the wild-type parasites (**Table 3.5**). This is an approximate recapitulation of the ~2.6X resistance observed in the F11 strain, and a slightly lower value than the ~3.5X resistance seen in the H11 strain (**Table 3.4**); together, the similarity of these values is supportive of a substantial role for this mutation in facilitating resistance to RL003.

Intriguingly, the most resistant clonal isolate, H11, contained an additional mutation (T683A) in a calcium-dependent protein kinase (CDPK) gene. CDPKs, as a general class, are known to act as downstream mediators of signaling events by PKG [265], as discussed more fully below; correspondingly, complementation of this mutation, while not recapitulating the observed resistance of either mutagenesis-generated strain, was still sufficient to confer a low level (1.5X) of significant resistance to RL003, which may indicate

that an additive effect of both the PKG C524R mutation and the CDPK T683A mutation plays a role in the variable levels of resistance across the F11 and H11 isolates, although this assertion requires additional evidence to confirm any potential additive effect.

The essentiality of PKG, particularly given its high conservation across *T. gondii* strains and low incidence of naturally-occurring SNPs [257], presents a level of technical difficulty in examining effects of gene knockouts, a classical method for confirmation of putative protein roles in given processes; to maintain viable parasites, PKG cannot be knocked out without a corresponding compensatory complement present at another locus, arguing in support of its indispensability [257]. However, to further assess the role of this gene in resistance to RL003, we evaluated compound activity against a strain containing at the 3' end of the endogenous PKG gene a tag for an auxin-inducible degron (PKG-mAID-3HA) created by Brown *et al*., which is targeted for proteasomal degradation upon the addition of 3-indoleacetic acid (IAA). Induction of a PKG knockdown in this manner resulted in a dramatic >500X resistance to RL003 relative to the uninduced strain (**Figure 3.3**); however, this drastic change may partially be a result of the evident hyper-sensitivity of PKG-mAID-tagged parasites to RL003, given that the IC_{50} of the uninduced strain was >30X lower that of the RH-dTom WT strain. Ostensibly, this may be a consequence of general fitness disadvantage resulting from altered regulation of PKG. However, even when compared to the IC_{50} of the RH-dTom WT strain, the conditional knockdown still demonstrated a significant ~17X increase in resistance, a substantial alteration that supports the comparatively-moderate resistance of single mutations in PKG to RL003 (**Figure 3.3**). Corroborating this finding, similar treatment of a strain containing a copy of PKG complemented into the *UPRT* locus (PKG-mAID-3HA/PKG-6Ty) led to

restoration of RL003 activity to levels similar to the PKG-mAID-3HA strain (**Figure 3.3**), indicating that specific reduction in PKG was responsible for the observed effects.

In *T. gondii* and other Apicomplexan parasites, PKG is an essential protein controlling a number of critical processes related to the parasite infection and lytic cycle, including attachment to the host cell, movement along the cell surface, invasion or entry into the host cell, and egress for eventual reinfection of other cells [266]. As described below, these processes stem primarily from the regulation of the parasite gliding motility, which is intimately connected to fluctuations in intracellular cAMP, cGMP, and calcium levels [267]. As the primary sensor of cGMP levels, PKG plays a critical role in propagating signals from this molecule [267]. Additionally, combined inhibition of PKG and the downstream effector

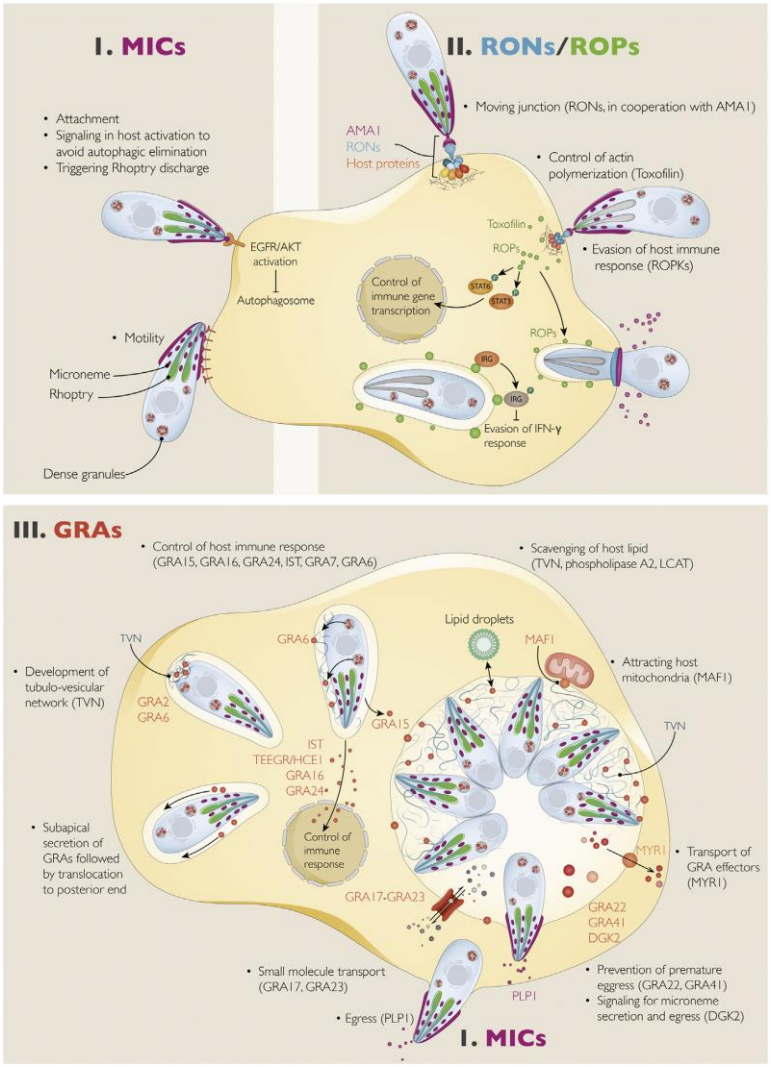

Figure 3.9. Motility, invasion, and egress in *T. gondii* are mediated by a variety of parasite and host factors contributing to successful parasite replication and dissemination. A summary of key steps in parasite invasion mediated by MICs and RONs/ROPs(I, II) as well as maturation by GRAs (III). Reprinted from *Toxoplasma gondii*, 3rd Ed.; Maryse Lebrun,Vern B. Carruthers,Marie-France Cesbron-Delauw; *Toxoplasma gondii:* "Chapter 14: Toxoplasma secretory proteins and their roles in parasite cell cycle and infection," p. 608, Copyright (2020), with permission from Elsevier.

CDPK1 at sublethal levels causes cyst-forming strains of *T. gondii* to differentiate into bradyzoites and subsequently form cysts in tissue culture, even in the absence of additional stressors, indicating that the PKG signaling pathway plays a role in stage conversion (possibly from responding to stress)[263]. The essentiality of PKG [257], combined with its specificity to *T. gondii* over mammalian cells [261], makes this a promising therapeutic target.

For many parasitic pathogens, gliding motility is a crucial motor process required for successful invasion, movement over the cell surface, and egress from host cells [268]; its success is critical to facilitating the intracellular lifestyle necessary for replication [269]. As shown in **Figure 3.9.I.** [298], gliding motility depends on secretion of micronemes, small, vesicle-like organelles located primarily along the apical end of the parasite that, upon response of an appropriate signal, release a series of transmembrane adhesins known as MIC proteins in order to bind components of the host cell membrane or the extracellular matrix [270]. The regulation of microneme secretion is tightly-controlled by both Ca^{2+} signals and cGMP levels, and perturbation of this pathway can cause marked defects in successful invasion and/or egress [265]. Existing data implicates PKG as the central regulator of microneme secretion in *T. gondii*, given that treatment with Ca^{2+}-elevating compounds is not sufficient to induce microneme secretion in the absence of PKG activation [265]. PKG regulation directs a number of downstream effectors responsible for phosphorylation leading to signal transduction and vesicular localization as well as transport to the parasite membrane (for timed release of micronemes) [270], though the most well-characterized are the calcium-dependent protein kinases (CDPKs) [271]. Together, these effectors orchestrate microneme secretion and, by extension, successful parasite infection [272].

Specific inhibition of PKG by chemical means—such as 4-[2-(4-fluorophenyl)-5-(1-methylpiperidine-4-yl)-1H-pyrrol-3-yl]pyridine, or “compound 1”—results in defects across invasion, motility, and egress [257]; therefore, we hypothesized that, if RL003 does indeed act through PKG in some manner, one or more of these central physiologic components would be negatively impacted. Corroborating this hypothesis, parasites treated with RL003 showed defects in invasion, reduced 2D motility across planar surfaces treated with adhesin-compatible charged residues, and reduced ability to egress following stimulation (**Figure 3.4**). That these components are intimately interconnected, as described above, and that these components are all regulated to a high degree by PKG, both strengthen our genetic and molecular data and further point to the importance of PKG in RL003 activity.

When examining parasites for potential morphological abnormalities resulting from ostensible changes to PKG function, ultrastructural analysis by SEM appeared to show some form of membrane blebbing, surprisingly; parasites exhibited apoptosis-like or autophagic-like vesicular structures that seemed to indicate a concerted, rather than non-specific, progression of cellular breakdown more compatible with progression of programmed cell death. Our RT-qPCR data supported this, with particularly strong upregulation of autophagy- and phagocytosis-associated proteins, which may well be in part responsible for the vesicular structures appearing in SEM (**Figure 3.8**); these same changes in expression were not observed after treatment with either pyrimethamine or atovaquone, though the known pro-apoptotic molecule miltefosine did show a similar, but not identical pattern (**Supplementary Figure 2**).

Interestingly, despite the apparent contradiction of a single-celled organism performing apoptosis-like programmed cell death, this process has previously been observed to occur in protozoa under certain conditions, including such organisms as *Plasmodium*

spp., *Leishmania spp., Trypanosoma spp.*, and, more recently, in *T. gondii* [273]. Though the precise pathway for programmed cell death in *T. gondii* remains elusive, treatment with chemical stimulators of mammalian apoptosis has allowed for the identification of several key features of this primitive process [264]. As in metazoan cells, progression of programmed cell death is characterized by fragmentation of parasite DNA, leading to TUNEL-positive staining such as that shown in **Figure 1.7** [264; 273]. Additionally, parasites show distinctive morphological changes, including membrane blebbing, deadhesion from the monolayer, and loss of the distinctive crescent moon cell shape. A number of genes resembling homologs of mammalian proteins, including those shown in **Figure 1.8**, have also been shown to be upregulated, including a number of autophagy-associated and phagocytosis-associated proteins in addition to a DNA endonuclease, calcium-dependent endopeptidases, and several predicted proteases [264]. Caspase-like proteolytic activity is also increased in parasites exposed to pro-apoptotic stimuli and abrogated by protease inhibitors, as would be expected in apoptosis-like cell death [264]. Further, the identification and characterization of a metacaspase—the functional equivalent of a mammalian caspase—called TgMCA1 showed that this protein participates in the orchestrated breakdown of parasite components during stimulation [273]. The support from our SEM and RT-qPCR data may indicate that such activities are occurring in RL003-treated *T. gondii* tachyzoites; due to the specific and potent role this process may play in parasite toxicity, the possible induction of programmed cell death by RL003 warrants further investigation.

RNA-seq data yielded interesting findings appearing to provide a tentative, though yet-unconfirmed, link between the apparent upregulation in programmed cell death-associated *T. gondii* genes (supported by the morphological changes sporting membrane blebbing visible in SEM images (**Figure 3.8**)) and the clear capacity for PKG mutations to

facilitate resistance to RL003 (**Table 3.5**, **Figure 3.3**). Processes indicative of downstream or parallel PKG effects appeared to be differentially expressed in RL003-treated populations; namely, genes falling into the GO Biological Processes of signaling, cell-cell communication, transport, phosphorylation events, and processing of nucleobases showed altered expression relative to the DMSO-treated populations, particularly in less-resistant isolates (**Figure 3.2**). More specifically, identification of the top 5 differentially-expressed genes in each parasite population showed particular genes known to interact with PKG or with downstream effectors of PKG, including calcium-dependent protein kinase (CDPK), cAMP-dependent protein kinase (PKA), and 3'5'-cyclic phosphodiesterase proteins (**Tables 3.6-3.7**); the upregulation of PKA in WT parasites at 8 hours post-addition of RL003 is particularly interesting, given that recent work has indicated a strong interplay between PKA and PKG [271].

Simultaneously, however, there were additional genes that appeared to align more closely with autophagic or apoptosis-like pathways. ULK kinases, DNA/RNA endonucleases, and various endopeptidases, in particular, seemed to be strongly differentially-expressed in both wild-type and RL003-resistant parasites (though the effect was most pronounced in wild-type parasites (**Tables 3.6-3.7**)). In other eukaryotes, ULK kinases are known to be responsible for the formation of the pre-autophagosome in response to phosphatidylinositol-3-kinase (PI3K) signaling [274], and endopeptidases as well as endonucleases are critical effector molecules for the degradation of cellular components [275]. Future work providing a more definitive relationship between PKG and programmed cell death in *T. gondii* would help to clarify this apparent association.

Taken in sum, these data point to an interesting potential sequence of events; mutations in PKG appear to affect compound activity in some manner, and the parasiticidal effect appears to be mediated by the primitive programmed cell death pathway present

(though arguably poorly-described) in *T. gondii*. This may indicate some level of involvement of PKG in the process of parasite programmed cell death, a previously unreported association that may result from either constitutive activation or catalytic inhibition of PKG. Supporting this possible association, mutants episomally expressing PKG carrying the RL003 resistance-conferring C524R mutation showed nearly an opposite effect as the wild-type when subjected to RT-qPCR, downregulating many of the pro-death proteins and upregulating a key anti-death protein (FASI inhibitor) (**Figure 3.6**). Even episomal expression of the wild-type PKG allele seemed to modify the expression of these genes, with far less alteration in expression of many of the PCD-associated genes compared to the DMSO control than was seen in the wild-type, perhaps as a consequence of altering intracellular cGMP levels (**Figure 3.7**).

Such a relationship between PKG and apoptosis in eukaryotic cells is not unprecedented; constitutive activation of PKG in mammalian cancer cell lines—such as colorectal, pancreatic, and smooth muscle cells [276]—is sufficient to induce apoptosis. Increases in levels of cGMP, leading to stronger activation of PKG, were associated with triggering apoptosis in these cells. It is therefore possible that RL003 acts in some manner through PKG and that, as a consequence, downstream events of this interaction favor programmed cell death over necrosis. This potential link certainly merits additional examination, as it would represent a novel and previously-unreported pathway for activation of apoptosis-like cell death in *T. gondii*.

Conclusion

Overall, these findings support a role of the parasite-specific cGMP-dependent protein kinase in facilitating the activity of, or resistance to, the potent pyrrolomycin derivative RL003. With support from genomic, transcriptional, and phenotypic data, these results point to an association between PKG-mediated events or downstream processes

and resistance to RL003. Both ultrastructure and transcriptomic analysis further suggested a likely activation of the primitive *T. gondii* apoptosis-like cell death pathway following treatment with RL003, which was not observed when resistant mutants were subjected to identical analyses. This may indicate some previously-unreported link between PKG and programmed cell death in *T. gondii* and provides a possible avenue for further exploration.

Methods

Cell Lines and Maintenance

Human foreskin fibroblasts (HFF) were obtained from ATCC (HFF-1: ATCC® SCRC-1041™) and maintained under serial passage at 37 ^{o}C and 5% CO_2. Type I *T. gondii* RH-strain parasites constitutively expressing fluorescent tdTomato protein (dTom) were used for a majority of the assays in this work; additional strains included RH-strain parasites expressing the TIR1 auxin receptor from *Oryza sativa* genetically modified to have mini-auxin inducible degron (mAID) tags at the 3' end of endogenous PKG (PKG-mAID-3HA) as well as the corresponding complement strain with PKG-6Ty complemented at the *UPRT* locus (PKG-mAID-3HA/PKG-6Ty), with both of these strains being a kind gift of Dr. Kevin Brown at the University of Oklahoma. All other strains were generated in this work as described below from the RH-dTom parental strain. Parasites were maintained by serial passage in HFF cells at 37 ^{o}C and 5% CO_2. All host cell and parasite lines were maintained in D10 media with the following composition: Dulbecco's Modified Eagle's Medium (DMEM) supplemented with 20% Medium-199, 10% heat-inactivated bovine calf serum, 2 mM L-alanyl-L-glutamine, 100 µg/mL penicillin/streptomycin, and 20 µg/mL gentamicin sulfate.

Preparasitic and Precellular Assays

Procedures for preparasitic and precellular assays follow largely from our work outlined in [151]. Preparasitic treatment was completed by treating extracellular RH-strain parasites constitutively expressing the dimerized Tomato fluorescent protein (RH-dTom) with RL003 at the IC_{90} or with a volume-matched DMSO solvent control for 7 hours (approximately 1 complete cell cycle), after which compound was removed and parasites were washed with D10 media. This was immediately followed by infection of triplicate wells of an untreated HFF cell monolayer in an optical-bottom 96-well plate at 2,000 parasites/well. Parasites were allowed to invade for 24 hours and fluorescent parasites (dTom-positive) representing viable tachyzoites were counted with the BioTek® Lionheart and compared to the DMSO control. The precellular assay was conducted similarly; however, in this case, HFF host cells were treated with RL003 at the parasite IC_{90} for 29 hours (approximately 1 complete cell cycle), washed with D10 media, and infected with 2,000 tachyzoites/well of untreated parasites for 24 hours prior to automated counting.

Random Chemical Mutagenesis

Random chemical mutagenesis was carried out as described in [259]. Two flasks (α and β) of wild-type RH-dTom tachyzoites were treated with 11 mM ethyl methanesulfonate (EMS) at 37 ^{o}C for 4 hours to induce random mutations in the genome at approximately 1 mutation/1 Mb, after which parasites were thoroughly washed three times with D10 media to remove residual EMS and subsequently used to reinfect 2 new flasks (corresponding to α or β). Mock treatment with DMSO alone was completed in a control flask and subjected to an identical procedure. Following 24 hours of recovery in D10 medium, each flask was treated with RL003 starting at 0.5X the IC_{50} for 2 full passages, with the concentration of RL003 being increased on surviving parasites until the mock-mutagenized control no longer had any viable parasites. Tachyzoites surviving from the

mutagenized flasks were clonally isolated by limiting dilution under maintained RL003 pressure, after which clones were grown up in T25 flasks before IC_{50} analysis as described below.

Whole-Genome Sequencing and SNV Analysis

Tachyzoites from each RL003-resistant strain F11, H11, and E12, in addition to the RH-dTom wild-type parental strain, were cultured to confluence in T75 flasks of HFF host cells, after which the monolayer was scraped, the cells were homogenized with a Dounce homogenizer, and the resulting suspension was filtered 3X through a 5 µm filter and 3X through a 3 µm filter to maximally remove host cell nuclei. Cells were washed twice by centrifugation at 900 *xg* for 12 minutes at room temperature, removal of the supernatant, and resuspension in 1X PBS to remove media contamination. Genomic DNA was then isolated with the Promega Wizard® Genomic DNA Purification Kit following manufacturer recommendations. Quality of the DNA was assessed by determination of the $A_{260/280}$ ratio obtained by a Thermo Scientific™ NanoDrop™ 2000 spectrophotometer; samples were retained only if this ratio was between 1.70 and 1.90. If samples passed this quality control, DNA was diluted in nuclease-free sterile water to 100 ng/µL, and 5 µg was submitted to the University of Nebraska Medical Center Genomics Core for library preparation and next-generation sequencing by Illumina paired-end reads. Raw reads for clonal isolates F11, H11, and E12 as well as the parental RH-dTom strain were deposited in the NCBI SRA repository under the following accessions, respectively: SRR14338357, SRR14338356, SRR14338355, SRR14338354.

Upon completion of the sequencing runs, we analyzed the paired-end ~150-160 bp short read data for SNVs utilizing our in-house script published previously [259] and available at https://github.com/matthew-martens/SNVVerificationPipeline. This analysis included trimming of reads for quality using PRINSEQ Lite v0.20.4 [277] to remove low-

confidence base calls from the reads, alignment to the RH-parental GT1 reference genome (https://toxodb.org/toxo/app/record/dataset/DS_ac2a27fcc5) with Bowtie2 v2.2.9 [278] followed by post-processing indexing and sorting with SAMTools v1.2 [279]. Identification of single nucleotide changes was completed by FreeBayes v1.1.0 (which provides genomic location, type of mutation (e.g., insertion, deletion, transversion), and confidence of mutation site)[280], and annotation of single nucleotide transversions was performed with SNPEff v4.1 (including ID of affected gene; amino acid change, if applicable; notation of whether the mutation occurs in a protein-coding, regulatory, or splice site region; and predicted impact of mutation)[281]. SNVs that were present in both the RH-dTom strain and the mutant strains were subsequently removed by manual filtering, with only those present exclusively in one or more mutant strains being retained.

Due to the large number of acquired mutations predicted by this analysis, SNVs were prioritized to emphasize those that were (1) present in multiple RL003-resistant strains; (2) located at higher proximity to a coding region, splice site, transcriptional start/end site, or regulatory sequence (where possible to determine); (3) predicted to have an impact of “moderate” or higher by SNPEff; and (4) present in literature-described genes essential for parasite survival, invasion, or replication. Mutations of interest were subsequently confirmed by Sanger sequencing with 2 distinct primer sets to confirm presence in the predicted mutant strain(s) and absence of the SNV in the RH-dTom parental strain.

RNA-seq of Tachyzoites

To perform RNA-seq, wild-type RH-dTom, mutated F11, and mutated H11 strains were each grown to 50% confluence in a T75 flask of HFF host cells, after which either RL003 at the IC_{90} or a volume-matched DMSO control was added. Flasks were incubated for 8 hours or 24 hours and high-quality RNA was isolated as follows: Flasks containing parasites were chilled on ice for 5 minutes and then washed with cold 1X PBS. Monolayers

were then scraped, homogenized with a chilled Dounce homogenizer, and filtered 3X through 3 µm filters to remove as much host cell contamination as possible. RNA was isolated following the Qiagen RNEasy® Mini Kit instructions following the manufacturer recommendations for tissue culture cells to obtain RNA. After validating that the RNA was of sufficient quality ($A_{260/280}$ between 1.9 and 2.2), samples were diluted to 200 ng/µL and 3 µg of each sample was submitted to the University of Nebraska Medical Center Genomics Core for library preparation and next-generation sequencing as above. Raw sequencing reads for each strain and condition were deposited in the NCBI SRA repository in BioProject PRJNA725560 under accessions SRR14342021-SRR14342032.

Upon completion of the sequencing runs, reads were trimmed for quality as above and aligned to the annotated *T. gondii* GT1 transcriptome (https://toxodb.org/toxo/app/record/dataset/DS_ef984802b1) using Bowtie2 v2.2.9 as before and processed with SAMTools v1.2 to convert the output to a BAM file. Processed reads were quantified for relative transcript abundance using Salmon v1.4.0 [282]. Differential expression of RL003-treated samples at 8 hours and 24 hours relative to the corresponding DMSO control for each strain at the same time point was then determined using DESeq2 v1.30. [283]. Results were filtered to include only differentially-expressed genes representing a p-value < 0.05 and a log2FC (log2 fold-change) ≤-2.5 or ≥2.5 (to examine only the highest-upregulated and highest-downregulated genes). These genes were then annotated for computed gene ontology (GO) functions through the use of the annotation tool of ToxoDB release 50 (https://toxodb.org/) [284].

Fitness Assay

Determination of strain fitness for F11 and H11 was completed through determination of doubling time. Tachyzoites of each strain, or the corresponding RH-dTom parental wild-type (WT) strain, were used to infect confluent HFF monolayers in a 96-well plate

at 2,000 tachyzoites/well. Fluorescence was measured every 24 hours for 5 days. The point at which fluorescence had doubled relative to the starting point (subtracting the minor autofluorescence of host cells) was calculated as the doubling time and compared to the WT control.

IC_{50} Analyses

The 50% inhibitory concentrations (IC_{50}s) were determined essentially as described in [151]. Parasites were plated at 2,000 tachyzoites/well in confluent HFF monolayers in a 96-well plate and allowed to invade for 24 hours prior to the addition of increasing concentrations of each compound to be tested, including a volume-matched DMSO control. Each concentration was completed in triplicate to ensure sufficient n-values for calculating significance. Plates were incubated for 5 days, after which fluorescence readings for dTom, correlating to parasite viability, were obtained at 530/25 (excitation) and 590/35 (emission) using a BioTek® Synergy™ multi-mode plate reader. The IC_{50} for each compound was calculated as the concentration of compound at which fluorescence was 50% that of the solvent control.

Cloning by Gibson Assembly

Gibson assembly for the insertion of PKG and CDPK alleles into the M2M3 pyrimethamine selection cassette [285] was completed through the use of the New England Biolabs® NEBuilder® HiFi DNA Assembly Kit following manufacturer recommendations, with a molar ratio of 1:3 backbone: insert. Once the constructs were completed, each product was run at 100V for 1 hour at room temperature on a 0.9% agarose gel that was subsequently stained with GelRed® nucleic acid stain to identify bands present. The band representing a product of the anticipated size was excised and DNA was isolated using the QIAquick® Gel Extraction Kit following manufacturer recommendations for products >10 kb. Isolated DNA was transformed into NEB 10-β chemically competent *E. coli* by

heat shock at 42 ^{o}C for 30 seconds, following the recommended protocol, and colonies carrying the plasmid were selected from LB agar plates containing 100 µg/mL ampicillin.

Following amplification by maxiprep with a Promega PureYield™ Maxiprep Kit, Sanger sequencing was used to confirm that each construct carried the mutation of interest, and that no extraneous mutations had been introduced. Ethanol precipitation was then used to concentrate and sterilize plasmids before transfecting by electroporation 50 µg of each plasmid into wild-type RH-dTom parasites using the method described in [285] and below. Surviving parasites were clonally isolated by limiting dilution. To confirm that the selected clone(s) carried the plasmid and mutation of interest, validation by Sanger sequencing was conducted, including additional Sanger sequencing of wild-type RH-dTom to ensure that no mutation was present in this wild-type strain.

Transfection of *T. gondii* tachyzoites

Transfection of wild-type RH-dTom parasites with the plasmids of interest was completed largely following the recommended protocol from [285], implemented previously in [259]. Briefly, plasmid DNA was concentrated by ethanol precipitation and 50 µg was resuspended in cytomix buffer (120 mM KCl, 25 mM HEPES, 8.66 mM K_2HPO_4, 5 mM MgCl2, 2 mM EDTA, 1.36 KH_2PO_4, 0.15 mM $CaCl_2$, pH-adjusted to 7.6)[285]. The resuspended plasmid was added to 3.7 x 10^7 RH-dTom tachyzoites in cytomix buffer in a 2-mm-gap electroporation cuvette and placed on ice for 10 minutes. Electroporation was conducted as a single pulse at1.5 kV, 50 Ω, and 50 µF with a Gene Pulser Xcell, after which parasites were returned to ice for 10 minutes and subsequently used to infect fresh T25 flasks for 12 hours. After this recovery period, 1 µM pyrimethamine was added to each flask and selection was maintained for 7 days.

Confirmation of Construct Expression by RT-qPCR

To confirm expression of the insert, RNA was isolated from a confluent T25 flask of each Sanger-confirmed strain as described above Confirmation of expression of each transfected construct was completed by reverse-transcriptase quantitative polymerase reaction (RT-qPCR) using the PowerSYBR® Green RNA-to-CT™ 1-Step Kit with primers specific to the corresponding gene of interest. Genes were examined in technical triplicate and compared to the RH-dTom vector-only control by the $2^{-\Delta\Delta Ct}$ method, using alpha-tubulin TUBA (TGGT1_316400A) as a housekeeping gene. All transfected strains had appropriately-increased RNA expression for the indicated gene relative to the vector control, confirming, in conjunction with the maintained pyrimethamine resistance, that the inserts for these strains were being expressed (**Supplementary Table 2**).

RT-qPCR Analysis of T. gondii Programmed Cell Death

Parasites were treated in T25 flasks with RL003 at the IC_{90} or with a volume-matched DMSO control for 48 hours before isolation of RNA as described above. Based on previous studies showing the association of several key genes with apoptosis-like cell death in *T. gondii* [264; 273], primers targeting the genes of interest described in the "Results" section and **Appendix B** were generated and confirmed for appropriate product size in RH-strain parasites, given that previous studies utilized the ME49 reference strain for design. For those primers that showed the proper product size, RT-qPCR was completed as before using the PowerSYBR® Green RNA-to-CT™ 1-Step Kit in technical triplicate. Additionally, three separate housekeeping genes—histone 2B (TGME49_009910), ribosomal protein L33 (TGME49_108930), and DEAD-DEAH-box helicase (TGME49_056900)—were used for normalization across sample sets, completed in technical triplicate. Non-template controls were included for each primer set to confirm lack of unexpected expression from reagent contamination. Expression was examined as fold-change (FC) relative to the DMSO control by the $2^{-\Delta\Delta Ct}$ method.

Invasion and Motility Assays

To quantify invasion, tachyzoites were treated with RL003 at the IC_{90} (or a volume-matched solvent control) in T25 flasks for 1, 3, or 5 days. At each time point, surviving parasites were resuspended in high-potassium Endo buffer (106 mM sucrose, 20 mM Tris–H_2SO_4, 10 mM $MgSO_4$, 5 mM glucose, 4.7 mM K_2SO_4, 3.5 mg/ml BSA, pH-adjusted to 8.2; [286]) for synchronization of invasion. HFF cells in a 96-well plate were infected with these parasites at an MOI of 10 in triplicate for each time point to be tested. Plates were centrifuged at 250 *xg* for 5 minutes to facilitate parasite interaction with the host cells. Attachment was allowed for 20 minutes at 37 ^{o}C, after which the Endo buffer was carefully removed and replaced with D10 media to allow for invasion, which was allowed to proceed for 15 minutes before fixation of the wells with 4% PFA for 15 minutes, followed by blocking of the fixed cells with 3% BSA/PBS for 1 hour at room temperature. Extracellular parasites present in blocked wells were stained with 1:500 murine monoclonal α-SAG1 primary antibodies for 1 hour at room temperature in 3% BSA/PBS, after which they were washed with PBS and stained with 1:1,000 Alexa-488-conjugated goat-α mouse IgG secondary antibodies for 1 hour at room temperature. Subsequently, secondary antibodies were removed, the wash step was repeated, and 1:500 murine monoclonal α-SAG1 antibodies were added, this time in PBT buffer (3% BSA and 0.1% Triton-X in PBS) in order to permeabilize cells and allow staining of intracellular parasites. Secondary Alexa-594-conjugated goat-α mouse IgG antibodies were added at 1:1,000 in PBT buffer and wells were incubated for 1 hour at room temperature. Parasites were counted with a BioTek Lionheart, with Alexa-488+ (green) parasites being counted as extracellular and Alexa-594+ (red) parasites being counted as intracellular parasites. Percent invasion was calculated as the number of Alexa-488+ parasites/the total number of parasites (Alexa 488+ and Alexa 594+).

The motility assay was conducted in a similar manner. RL003-treated or DMSO-treated parasites were isolated from host cells and resuspended in Ringer's solution (115 mM NaCl, 10 mM glucose, 10 mM HEPES, 3 mM NaH_2PO_4, 3 mM KCl, 2 mM $CaCl_2$, 1 mM $MgCl_2$, pH-adjusted to 7.2) with 1% FBS [287]. This suspension was placed on poly-L-lysine-coated glass coverslips contained within a 12-well plate, with each sample performed in technical triplicate. Parasites were permitted to glide on the coverslips for 1 hour at 37 ^oC and were then fixed as above prior to staining with 1:500 murine monoclonal α-SAG1 primary antibodies and 1:1,000 Alexa-488 secondary antibodies for 1 hour each at room temperature. Parasites with SAG1+/Alexa-488+ trails were counted and compared to the total number of parasites, which was evaluated as a percentage relative to the corresponding DMSO control.

Egress Assay

Egress in parasites was evaluated using the general host cell nuclei staining technique described in [288], in which egress is quantified in 2D by the extent to which a nuclear stain or marker is able to label host cells as they are increasingly permeabilized during the process of egress. To evaluate effects of RL003 on tachyzoite egress, 10,000 parasites/well in a 96-well plate were treated with RL003 at the IC_{90} for 1, 3, or 5 days or with DMSO as a solvent control, with 6 wells for each condition. At each indicated time point, triplicate wells were treated with 500 µM zaprinast or with volume-matched DMSO control, and incubated for 15 minutes at 37 ^oC. Wells were then treated with CellToxGreen to identify permeabilized host cells, correlating to relative egress. Cells showing positive CellToxGreen fluorescence were counted with a BioTek® Lionheart automated microscope, adjusting for size to exclude tachyzoites (2-5 µm). Cells were then completely permeabilized with 0.1% Triton-X and re-counted to identify the total number of cells in the

well. The percentage of host cells permeabilized prior to the addition of Triton-X was used as the metric for egress.

SEM of RL003-Treated Parasites

Methodology for SEM analysis was based largely on work described in [289] and [290]. Briefly, confluent HFF cells in T25 flasks were infected with RH-dTom tachyzoites at an MOI of 10 and incubated for 12 hours to allow for invasion. Flasks were then treated with either RL003 at the IC_{90} or with a volume-matched quantity of DMSO for an additional 24 hours, after which surviving parasites were isolated by scraping the monolayer, homogenization with a Dounce homogenizer, and filtering 1X through a 5 µm filter and 2X through a 3 µm filter to limit host cell debris. Isolated parasites were centrifuged at 400 *xg* for 12 minutes and the supernatant was removed. The pellet was resuspended in 1 mL 1X PBS and centrifuged as before. Supernatant was removed and replaced with 1 mL of 0.1 M sodium cacodylate buffer containing 2.5% glutaraldehyde and 2% PFA at a pH of 7.4. Fixed tachyzoites were submitted to the Electron Microscopy Core Facility (EMCF) at the University of Nebraska Medical Center for imaging.

DISCUSSION

Parasitic and bacterial infections remain a serious global health burden today, with the rise of antibiotic resistance rendering many patients vulnerable to serious treatment-refractory systemic infections [188-234]. A number of these infections represent difficult-to-treat ailments for which existing therapies are either limited or ineffective [188-234]. The protozoan parasite *T. gondii*, the focus of the majority of this work, falls into the former category, with its high worldwide prevalence and distribution in conjunction with few existing treatment options for the acute infection rendering it a topic of continued research [61]. Though a combinatorial pyrimethamine and sulfadiazine treatment has become the standard of care, implemented successfully in the clinic due to the synergistic effect of this combination, the lack of specificity to the parasite compound targets (dihydrofolate reductase and dihydropteroate synthase) has presented a serious issue: patient side effects from this intervention can be severe, particularly due to the high dosages and extended time period of treatment [11]. To make matters more challenging, there are no FDA-approved therapeutic options known to effectively clear cyst burden, rendering this infection lifelong and posing a threat for patients who become immunocompromised later in life [11, 61].

Summary of Key Findings

To address the issues of poor potency and notable cross-reactivity with human proteins in anti-*Toxoplasma* treatments, we sought to examine a series of molecules derived from the potent anti-staphylococcal marine natural product marinopyrrole A for their activity against *T. gondii* tachyzoites and cysts *in vitro* (**Chapter 1**). Compilation of the data showed that RL002, RL003, and RL125 had significantly greater potency than pyrimethamine against RH-dTom tachyzoites (3.6-6.8X lower IC_{50} values), with RL003 showing the most potent activity (**Figure 1.4**). Unlike RL002 or the parent compound, marinopyrrole A, RL003 had limited susceptibility to serum *in vitro*, with a 5X increase in IC_{50} in the presence of 1%-50% bovine calf serum (**Table 1.2**). Surprisingly, evaluation of efficacy against *in vitro*-generated tissue cysts demonstrated that RL003 is a potent inhibitor of bradyzoites even when encapsulated by the cyst wall, with an IC_{50} <0.5 μM (**Figure 1.5**). Promisingly, determination of expanded cell viability against a broad panel of host cell lines indicated ≥20X selectivity for RH-dTom tachyzoites over any tested cell line, and >40X selectivity over any susceptible immortalized cell line (**Figure 1.6**), given that the primary cells for which toxicity was observed (PBMCs) were hypersensitive to pyrimethamine compared to HFF (**Supplementary Figure 1**). Toxicity against non-tumorigenic cell lines was even lower, at >140X higher IC_{50} values compared to those of RH-dTom. These data support that RL003 is a potent and selective inhibitor of *T. gondii* tachyzoites and bradyzoites *in vitro*.

The potency of compound RL003 against both stages of the asexual reproductive cycle, as well as the known activity of many marinopyrroles and pyrrolomycins against gram-positive bacteria, led us to hypothesize that RL003 may show potency against a number of other pathogens apart from *T. gondii* (**Chapter 2**). To test this, we treated a panel of gram-variable bacteria and selected eukaryotic parasites with RL003 and found that, surprisingly, a number of these were susceptible to RL003. Gram-positive pathogens

susceptible to RL003 included *S. aureus* USA300, *B. anthracis* Ames35, and *S. pneumoniae*, all of which had MIC_{50} values <1 µM (**Figure 2.1**). Fewer of the gram-positive pathogens were susceptible, though *V. cholerae* and *L. pneumophila* showed potent inhibition by RL003 at <1 µM (**Figure 2.1**). Additionally, the *M. tuberculosis* surrogate *M. bovis* BCG had an MIC_{50} of <0.5 µM against RL003 (**Figure 2.1**), which may indicate that RL003 has anti-tuberculosis properties and, given that *M. tuberculosis* is known to infect macrophages and given the observed low IC_{50} of RL003 against THP-1 derived macrophages, shows possible therapeutic applicability for this compound in tuberculosis. In addition to the prokaryotes described above, RL003 potently inhibited the pathogenic free-living amoebae *A. castellanii* and *N. fowleri*, both known for causing amebic meningoencephalitis with poor prognosis, at <0.5 µM (**Table 2.1**); with mortality rates as high as 97% in the case of primary amebic meningoencephalitis [214-216], this lead warrants further investigation for addressing such devastating infections. RL003, therefore, appears to show broad inhibition of disparate pathogenic organisms *in vitro* along with its low host cell toxicity.

To determine a genetic basis for RL003 activity by identification of parasite target(s) or resistance-conferring gene(s) (**Chapter 3**), we proceeded to perform whole-genome sequencing of significantly resistant *T. gondii* mutants and molecular complementation of putative resistance-conferring alleles. These genetic analyses implicated the *T. gondii* cGMP-dependent protein kinase (PKG) as a mediator of resistance to RL003, as expression of a C524R mutation in this gene was sufficient to confer >2.5X resistance to wild-type parasites (**Table 3.5**). Conditional knockdown of PKG further enhanced this effect, with PKG-reduced parasites having >500X resistance to RL003. Corresponding phenotypic analyses confirmed deficiencies in the PKG-associated processes of invasion, motility, and egress following treatment of wild-type parasites with RL003 (**Figure 3.3**).

Supporting this, RNA-seq analysis showed differential expression in pathways related to cell signaling, signal transduction, cyclic nucleotide metabolism, catabolism of nucleic acids, and oxidation-reduction processes at 8-24 hours post-RL003 treatment (**Figure 3.2**). Interestingly, both ultrastructure analysis by SEM (**Figure 3.8**) and targeted RT-qPCR at 48 hours post-treatment (**Figure 3.6**) showed upregulation in programmed cell death components, both in morphological changes and in upregulation of genes associated with miltefosine-induced apoptosis-like cell death in *T. gondii*, suggesting a potential role of programmed cell death in RL003-mediated parasite toxicity.

Discussion of Aggregated Results

This unexpectedly high cross-susceptibility of such disparate organisms to RL003 may suggest further mechanistic insight when considered in conjunction with our *in vitro* mutagenesis and complementation results. While *M. bovis* and similar *Mycobacterium* strains do have a known PKG homolog, PknG [291], the remaining bacterial pathogens do not; superficial local alignments yield no significant results when the *T. gondii* PKG sequence is considered. Additionally, the presence and activity of PKG in either amoeba species is unclear; while high cGMP levels appear to play an inhibitory role in the fusion of phagolysosomes in *A. castellanii* [292], which would suggest that this molecule in important in regulation of phagocytosis in these organisms, the signaling cascades resulting from this are currently unknown. It is therefore possible that yet-unreported homologs of PKG are present across these very different species; this may explain the broad activity, given the importance of cGMP in a variety of cellular and enzymatic processes [293].

However, it is also possible—and perhaps more likely, given the strong differences in prokaryotic and eukaryotic cGMP signaling pathways [294]—that RL003 has more than one target. This would hardly be unprecedented for marinopyrroles; indeed, marinopyrrole A is expected to have at least 2 targets that have been proposed: actin (elucidated by acyl

dye transfer) [126] and Mcl-1 (elucidated by *in vitro* cell toxicity assays and molecular modelling) [118]. Further, more recent data suggests that marinopyrrole A may be less selective for Mcl-1-dependent cell lines than first thought, which may indicate alternate targets [125]. That a derivative of this compound may exhibit more than one target would, therefore, be entirely feasible. This may also explain the selective toxicity of RL003 to certain host cell lines, primarily tumorigenic immortalized lines, over others. It may even be the case that in *T. gondii* PKG is simply an upstream mediator of an additional process affected by RL003, and that our results point to a resistance-conferring role for PKG rather than a primary target.

It is, additionally, feasible that RL003 and other pyrrolomycin derivatives may—in addition to protein targets—affect the components of cell membranes, such as membrane potential, particularly of the mitochondria in eukaryotes. Recent work in [295] indicates that the pyrrolomycins C and D are native protonophores capable of depolarizing the bacterial membrane, resulting in loss of proton motive force (PMF) and uncoupling of oxidative phosphorylation; this was demonstrated to occur with regard to both the prokaryotic membrane (particularly in gram-positive bacteria) and in isolated rat mitochondria. This may partially explain the seemingly-unpredictable susceptibilities seen in the above organisms. However, while the authors suggest that this decoupling activity may represent a mechanism of toxicity for both pyrrolomycins and marinopyrroles against human cell lines [295], it is insufficient to suggest that this is the exclusive mechanism of action against pathogens or host cells, particularly given the known protein targets for marinopyrrole A [118; 126]. This explanation alone also fails to address the susceptibility of some, but not all, human cell lines to these molecules [110], in addition to the findings of the present work that demonstrate a clear genetic basis for resistance to RL003 by a (non-transporter) gene product. In light of the uncoupling capacities of pyrrolomycins, the impact of treatment on

host cell and parasite mitochondrial membrane potential, as well as on the membrane potential of prokaryotic species, would aid in further clarifying a potential mechanism of action.

Apart from the particular molecular target(s) of RL003 and related marinopyrrole derivatives, our findings indicate an intriguing parallel between susceptible HEK-293 cells and *T. gondii* parasites: in both cases, treatment with RL003 appears to induce programmed cell death processes. In HEK-293 cells, this was demonstrated by appearance of TUNEL-positive staining and a strong increase in CAS9 expression (**Figures 1.7**-**1.8**), while in *T. gondii* this was demonstrated by increased expression of an autophagy-associated protein, a phagocytosis-associated protein, and a DNA endonuclease in addition to apparent blebbing visible by SEM (**Figures 3.6**-**3.8**). The upregulation of DNA endonuclease in *T. gondii* also aligns with the DNA fragmentation observed in the HEK TUNEL assay. Whether this points to a shared target or a common pathway response to insult by RL003 is, at present, unclear, given that parasite and human programmed cell death differ substantially. Notably, in colon cancer cell lines, constitutive activation of PKG has previously been shown to be sufficient to induce apoptosis [276], and so initial interpretation of these results may suggest cross-reactivity of RL003 between the human and *T. gondii* PKG isoforms; this may also provide a link between activity of PKG and programmed cell death in RL003-treated *T. gondii* tachyzoites. However, in apparent contrast to this possibility, parasitic PKG is known to be very specific to *T. gondii* over humans [296], with key structural differences in the catalytic domain and the presence of an additional allosteric domain making this protein substantially different than any animal PKG isoform [261]. This may, then, support the presence of multiple targets in RL003-mediated toxicity, as discussed above.

Alternatively, if RL003 is indeed playing a role as a protonophore, it would seem possible that the uncoupling of mitochondrial respiration could induce programmed cell death even in the absence of a shared target. This sequence—mitochondrial uncoupling leading to initiation of programmed cell death—has not yet been demonstrated in *T. gondii*, and so definitive statements on this possibility are premature. Not only so, but mitochondrial uncoupling alone can induce *or* inhibit apoptotic events in human cells, depending upon the cell line, presence of other signaling molecules, and metabolic state of the cell [297], which would indicate that uncoupling, even if present in RL003-treated cells, is insufficient to induce the observed effects. Elucidation of the precise means by which apoptosis is triggered in susceptible host cells, and by which the apoptosis-like programmed cell death is induced in *T. gondii*, would therefore shed additional light onto the activity of RL003.

Future Directions

While much of our data presents encouraging insight into the potent marinopyrrole A analog RL003, further investigation is needed to establish therapeutic feasibility and to distinguish the multiple possibilities described above in an effort to determine the precise mechanism of action for this compound. Regarding the former, *in vivo* evaluation of RL003 will be a crucial next step, both in evaluating toxicity and in identifying efficacy against a number of these susceptible pathogens on an organism-wide level. This holds true not only for the acute infections by these pathogens, but also for the chronic stage of *T. gondii*; while the *in vitro* potency is promising, the ability of RL003 to cross the blood-brain barrier and to reliably reduce cyst burden in the brain will provide key insight into the applicability of RL003 for chronic toxoplasmosis. Further, determination of recrudescence following cessation of RL003 treatment, such as by artificially ablating the immune system with

immunosuppressants, would allow for complementary confirmation of parasite clearance from brain and muscle tissue.

In addition to the *in vivo* data, further exploration of the role of PKG RL003 activity against *T. gondii* will be necessary to unambiguously suggest a likely mechanism of action. A number of biochemical assays would function for this purpose. First, regarding the PKG protein itself, enzyme inhibition assays with purified PKG from resistant parasites, susceptible parasites, and human cells would validate the genetic findings implicating PKG as a resistance gene and may further differentiate whether RL003 primarily targets this protein. Complementarily, *in silico* molecular docking studies of RL003 and PKG would aid in identifying a specific binding site for this molecule and would allow for further examination of the impact of the C524R mutation on compound binding. Additionally, as performed in [126], tagging of RL003 with a transferable acyl dye would allow for subsequent immunoprecipitation of proteins with which this compound interacts, facilitating further verification of not only the interaction of RL003 with PKG, but also of the hypothesis that RL003 may have more than one putative target.

The role of programmed cell death in the activity of RL003 and its possible link to PKG would further clarify the means of compound-mediated toxicity in *T. gondii*, amoebae, and human cells. Repetition of the TUNEL assay performed on HFF and HEK-293 cells using RL003-treated *T. gondii*, amoebae, and other human cell lines would provide broader quantitative data regarding potential apoptosis-like activity across broad organisms (which may provide a link to common pathways affected by RL003). Validation of apoptotic or autophagic events could be provided by the addition of known autophagy and apoptosis inhibitors to impacted cell lines in the presence of RL003, with a partial or full rescue effect expected if either (or both) events are indeed occurring. Similarly, the purported decoupling activity of pyrrolomycins, and the potential relation to programmed cell

death, could be further explored by relative comparison of changes in mitochondrial membrane potential by potentiometric dyes across RL003-treated parasite lines and/or isolated mitochondria. This may also be useful for determining whether prokaryotic pathogens experience loss of PMF in the presence of RL003. Finally, stronger evidence supporting a link between PKG expression and programmed cell death in *T. gondii* may be accomplished by RNA-seq, RT-qPCR, and/or proteomic analysis of programmed cell death-associated genes in episomal PKG mutants (PKG^{C524R}, PKG^{WT}) and the conditional knockdown/complement strains (PKG-mAID-3HA, PKG-mAID-3HA/PKG^{6Ty}) may provide key insight illuminating the regulation of apoptotic/autophagic events in *T. gondii*, facilitating further study of this therapeutically-relevant process.

FINAL CONCLUSIONS

The human parasite *T. gondii* presents a serious issue for human health as a result of the relatively low potency and poor specificity of existing therapeutic interventions, along with the inability of these interventions to satisfactorily clear cyst burden [11; 61]. We showed in this work that the novel pyrrolomycin molecule RL003 is a potent inhibitor of both tachyzoites and encysted bradyzoites *in vitro* with high selectivity for parasites over human cells, and that this potency even extends to the high-mortality amebic pathogens *A. castellanii* and *N. fowleri*. Further, we showed that several gram-positive gram-negative bacterial pathogens, as well as the *M. tuberculosis* surrogate *M. bovis* BCG, are also susceptible to RL003, showing that perhaps this compound may aid in combating the continued rise in antimicrobial resistance. Genetic and transcriptomic data indicated that mutation or knockdown of the parasite-specific PKG gene is sufficient to confer resistance to RL003 in *T. gondii*, and that a number of programmed cell death-associated genes are upregulated as a consequence of compound treatment. Taken as a whole, these data provide key insight into a novel and potent antiparasitic compound and thereby may pave

the way for further improvement to therapeutic small-molecule inhibitors acting against both prokaryotic and eukaryotic human pathogens.

BIBLIOGRAPHY

1. Halonen, S. K., & Weiss, L. M. (2013). Toxoplasmosis. *Handbook of clinical neurology*, *114*, 125–145. https://doi.org/10.1016/B978-0-444-53490-3.00008-X.

2. Bai, M. J., Wang, J. L., Elsheikha, H. M., Liang, Q. L., Chen, K., Nie, L. B., & Zhu, X. Q. (2018). Functional Characterization of Dense Granule Proteins in *Toxoplasma gondii* RH Strain Using CRISPR-Cas9 System. *Frontiers in cellular and infection microbiology*, *8*, 300. https://doi.org/10.3389/fcimb.2018.00300.

3. Jones, J. L., & Dubey, J. P. (2012). Foodborne toxoplasmosis. *Clinical infectious diseases : an official publication of the Infectious Diseases Society of America*, *55*(6), 845–851. https://doi.org/10.1093/cid/cis508.

4. Dubey J. P. (2009). History of the discovery of the life cycle of Toxoplasma gondii. *International journal for parasitology*, *39*(8), 877–882. https://doi.org/10.1016/j.ijpara.2009.01.005.

5. Montoya, J. G., & Liesenfeld, O. (2004). Toxoplasmosis. *Lancet (London, England)*, *363*(9425), 1965–1976. https://doi.org/10.1016/S0140-6736(04)16412-X.

6. Robert-Gangneux, F., & Belaz, S. (2016). Molecular diagnosis of toxoplasmosis in immunocompromised patients. *Current opinion in infectious diseases*, *29*(4), 330–339. https://doi.org/10.1097/QCO.0000000000000275.

7. Sonneville, R., Magalhaes, E., & Meyfroidt, G. (2017). Central nervous system infections in immunocompromised patients. *Current opinion in critical care*, *23*(2), 128–133. https://doi.org/10.1097/MCC.0000000000000397.

8. Biswas, A., French, T., Düsedau, H. P., Mueller, N., Riek-Burchardt, M., Dudeck, A., Bank, U., Schüler, T., & Dunay, I. R. (2017). Behavior of Neutrophil Granulocytes during *Toxoplasma gondii* Infection in the Central Nervous System. *Frontiers in cellular and infection microbiology*, *7*, 259. https://doi.org/10.3389/fcimb.2017.00259.

9. Kieffer, F., & Wallon, M. (2013). Congenital toxoplasmosis. *Handbook of clinical neurology*, *112*, 1099–1101. https://doi.org/10.1016/B978-0-444-52910-7.00028-3.

10. Hampton M. M. (2015). Congenital Toxoplasmosis: A Review. *Neonatal network : NN*, *34*(5), 274–278. https://doi.org/10.1891/0730-0832.34.5.274.

11. Neville, A. J., Zach, S. J., Wang, X., Larson, J. J., Judge, A. K., Davis, L. A., Vennerstrom, J. L., & Davis, P. H. (2015). Clinically Available Medicines Demonstrating Anti-Toxoplasma Activity. *Antimicrobial agents and chemotherapy*, *59*(12), 7161–7169. https://doi.org/10.1128/AAC.02009-15.

12. Tenter, A. M., Heckeroth, A. R., & Weiss, L. M. (2000). Toxoplasma gondii: from animals to humans. *International journal for parasitology*, *30*(12-13), 1217–1258. https://doi.org/10.1016/s0020-7519(00)00124-7.

13. Donaldson, T. M., Cassera, M. B., Ho, M. C., Zhan, C., Merino, E. F., Evans, G. B., Tyler, P. C., Almo, S. C., Schramm, V. L., & Kim, K. (2014). Inhibition and structure of Toxoplasma gondii purine nucleoside phosphorylase. *Eukaryotic cell*, *13*(5), 572–579. https://doi.org/10.1128/EC.00308-13.

14. Marino, N. D., & Boothroyd, J. C. (2017). Toxoplasma growth in vitro is dependent on exogenous tyrosine and is independent of AAH2 even in tyrosine-limiting conditions. *Experimental parasitology*, *176*, 52–58. https://doi.org/10.1016/j.exppara.2017.02.018.

15. Silver, D. M., & Lane, D. P. (1975). Dominant nonresponsiveness in the induction of autoimmunity to liver-specific F antigen. *The Journal of experimental medicine*, *142*(6), 1455–1461. https://doi.org/10.1084/jem.142.6.1455.

16. Mendez, O. A., & Koshy, A. A. (2017). Toxoplasma gondii: Entry, association, and physiological influence on the central nervous system. *PLoS pathogens*, *13*(7), e1006351. https://doi.org/10.1371/journal.ppat.1006351.

17. Portes, J., Barrias, E., Travassos, R., Attias, M., & de Souza, W. (2020). *Toxoplasma gondii* Mechanisms of Entry Into Host Cells. *Frontiers in cellular and infection microbiology*, *10*, 294. https://doi.org/10.3389/fcimb.2020.00294.

18. Blume, M., & Seeber, F. (2018). Metabolic interactions between *Toxoplasma gondii* and its host. *F1000Research*, *7*, F1000 Faculty Rev-1719. https://doi.org/10.12688/f1000research.16021.1.

19. Harker, K. S., Ueno, N., & Lodoen, M. B. (2015). Toxoplasma gondii dissemination: a parasite's journey through the infected host. *Parasite immunology*, *37*(3), 141–149. https://doi.org/10.1111/pim.12163.

20. Muflikhah, N. D., Supargiyono, & Artama, W. T. (2018). SEROPREVALENCE AND RISK FACTOR OF TOXOPLASMOSIS IN SCHIZOPHRENIA PATIENTS REFERRED TO GRHASIA PSYCHIATRIC HOSPITAL, YOGYAKARTA, INDONESIA. *African journal of infectious diseases*, *12*(1 Suppl), 76–82. https://doi.org/10.2101/Ajid.12v1S.11.

21. Jeffers, V., Tampaki, Z., Kim, K., & Sullivan, W. J., Jr (2018). A latent ability to persist: differentiation in Toxoplasma gondii. *Cellular and molecular life sciences : CMLS*, *75*(13), 2355–2373. https://doi.org/10.1007/s00018-018-2808-x.

22. Garfoot, A. L., Wilson, G. M., Coon, J. J., & Knoll, L. J. (2019). Proteomic and transcriptomic analyses of early and late-chronic Toxoplasma gondii infection shows novel and stage specific transcripts. *BMC genomics*, *20*(1), 859. https://doi.org/10.1186/s12864-019-6213-0.

23. Delgado Betancourt, E., Hamid, B., Fabian, B. T., Klotz, C., Hartmann, S., & Seeber, F. (2019). From Entry to Early Dissemination-*Toxoplasma gondii's* Initial Encounter With Its Host. *Frontiers in cellular and infection microbiology*, *9*, 46. https://doi.org/10.3389/fcimb.2019.00046.

24. Luu, L., Johnston, L. J., Derricott, H., Armstrong, S. D., Randle, N., Hartley, C. S., Duckworth, C. A., Campbell, B. J., Wastling, J. M., & Coombes, J. L. (2019). An Open-Format Enteroid Culture System for Interrogation of Interactions Between *Toxoplasma gondii* and the Intestinal Epithelium. *Frontiers in cellular and infection microbiology*, *9*, 300. https://doi.org/10.3389/fcimb.2019.00300.

25. Barragan, A., & Sibley, L. D. (2003). Migration of Toxoplasma gondii across biological barriers. *Trends in microbiology*, *11*(9), 426–430. https://doi.org/10.1016/s0966-842x(03)00205-1.

26. Unno, A., Suzuki, K., Xuan, X., Nishikawa, Y., Kitoh, K., & Takashima, Y. (2008). Dissemination of extracellular and intracellular Toxoplasma gondii tachyzoites in the blood flow. *Parasitology international*, *57*(4), 515–518. https://doi.org/10.1016/j.parint.2008.06.004.

27. Drewry, L. L., Jones, N. G., Wang, Q., Onken, M. D., Miller, M. J., & Sibley, L. D. (2019). The secreted kinase ROP17 promotes Toxoplasma gondii dissemination by hijacking monocyte tissue migration. *Nature microbiology*, *4*(11), 1951–1963. https://doi.org/10.1038/s41564-019-0504-8.

28. Park, J., & Hunter, C. A. (2020). The role of macrophages in protective and pathological responses to Toxoplasma gondii. *Parasite immunology*, *42*(7), e12712. https://doi.org/10.1111/pim.12712.

29. Ueno, N., & Lodoen, M. B. (2015). From the blood to the brain: avenues of eukaryotic pathogen dissemination to the central nervous system. *Current opinion in microbiology*, *26*, 53–59. https://doi.org/10.1016/j.mib.2015.05.006.

30. Konradt, C., Ueno, N., Christian, D. A., Delong, J. H., Pritchard, G. H., Herz, J., Bzik, D. J., Koshy, A. A., McGavern, D. B., Lodoen, M. B., & Hunter, C. A. (2016). Endothelial cells are a replicative niche for entry of Toxoplasma gondii to the central nervous system. *Nature microbiology*, *1*, 16001. https://doi.org/10.1038/nmicrobiol.2016.1.

31. Mayoral, J., Di Cristina, M., Carruthers, V. B., & Weiss, L. M. (2020). Toxoplasma gondii: Bradyzoite Differentiation In Vitro and In Vivo. *Methods in molecular biology (Clifton, N.J.)*, *2071*, 269–282. https://doi.org/10.1007/978-1-4939-9857-9_15.

32. Huang, S., Holmes, M. J., Radke, J. B., Hong, D. P., Liu, T. K., White, M. W., & Sullivan, W. J., Jr (2017). *Toxoplasma gondii* AP2IX-4 Regulates Gene

Expression during Bradyzoite Development. *mSphere*, *2*(2), e00054-17. https://doi.org/10.1128/mSphere.00054-17.

33. Ferreira da Silva, M., Barbosa, H. S., Gross, U., & Lüder, C. G. (2008). Stress-related and spontaneous stage differentiation of Toxoplasma gondii. *Molecular bioSystems*, *4*(8), 824–834. https://doi.org/10.1039/b800520f.

34. Tomavo, S., & Boothroyd, J. C. (1995). Interconnection between organellar functions, development and drug resistance in the protozoan parasite, Toxoplasma gondii. *International journal for parasitology*, *25*(11), 1293–1299. https://doi.org/10.1016/0020-7519(95)00066-b.

35. Soête, M., Camus, D., & Dubremetz, J. F. (1994). Experimental induction of bradyzoite-specific antigen expression and cyst formation by the RH strain of Toxoplasma gondii in vitro. *Experimental parasitology*, *78*(4), 361–370. https://doi.org/10.1006/expr.1994.1039.

36. Dupont, C. D., Christian, D. A., & Hunter, C. A. (2012). Immune response and immunopathology during toxoplasmosis. *Seminars in immunopathology*, *34*(6), 793–813. https://doi.org/10.1007/s00281-012-0339-3.

37. Zhao, X. Y., & Ewald, S. E. (2020). The molecular biology and immune control of chronic Toxoplasma gondii infection. *The Journal of clinical investigation*, *130*(7), 3370–3380. https://doi.org/10.1172/JCI136226.

38. Weiss, L. M., & Dubey, J. P. (2009). Toxoplasmosis: A history of clinical observations. *International journal for parasitology*, *39*(8), 895–901. https://doi.org/10.1016/j.ijpara.2009.02.004.

39. Lourido S. (2019). Toxoplasma gondii. *Trends in parasitology*, *35*(11), 944–945. https://doi.org/10.1016/j.pt.2019.07.001.

40. Rajapakse, S., Weeratunga, P., Rodrigo, C., de Silva, N. L., & Fernando, S. D. (2017). Prophylaxis of human toxoplasmosis: a systematic review. *Pathogens and global health*, *111*(7), 333–342. https://doi.org/10.1080/20477724.2017.1370528.

41. El-Sayed, N. M., Ismail, K. A., Badawy, A. F., & Elhasanein, K. F. (2016). In vivo effect of anti-TNF agent (etanercept) in reactivation of latent toxoplasmosis. *Journal of parasitic diseases : official organ of the Indian Society for Parasitology*, *40*(4), 1459–1465. https://doi.org/10.1007/s12639-015-0712-y.

42. Castaño-Amores, C., & Nieto-Gómez, P. (2021). Cerebral toxoplasmosis associated with treatment with rituximab, azathioprine and prednisone for dermatomyositis. *British journal of clinical pharmacology*, *87*(3), 1525–1528. https://doi.org/10.1111/bcp.14445.

43. Berk, S. L., & Verghese, A. (1988). Parasitic pneumonia. *Seminars in respiratory infections*, *3*(2), 172–178..

44. Marra C. M. (2018). Central nervous system infection with Toxoplasma gondii. *Handbook of clinical neurology*, *152*, 117–122. https://doi.org/10.1016/B978-0-444-63849-6.00009-8.

45. Bowen, L. N., Smith, B., Reich, D., Quezado, M., & Nath, A. (2016). HIV-associated opportunistic CNS infections: pathophysiology, diagnosis and treatment. *Nature reviews. Neurology*, *12*(11), 662–674. https://doi.org/10.1038/nrneurol.2016.149.

46. Vidal J. E. (2019). HIV-Related Cerebral Toxoplasmosis Revisited: Current Concepts and Controversies of an Old Disease. *Journal of the International Association of Providers of AIDS Care*, *18*, 2325958219867315. https://doi.org/10.1177/2325958219867315.

47. Butler, N. J., Furtado, J. M., Winthrop, K. L., & Smith, J. R. (2013). Ocular toxoplasmosis II: clinical features, pathology and management. *Clinical & experimental ophthalmology*, *41*(1), 95–108. https://doi.org/10.1111/j.1442-9071.2012.02838.x.

48. Garweg J. G. (2016). Ocular Toxoplasmosis: an Update. Aktuelles zur okulären Toxoplasmose. *Klinische Monatsblatter fur Augenheilkunde*, *233*(4), 534–539. https://doi.org/10.1055/s-0041-111821.

49. Mariuz, P., Bosler, E. M., & Luft, B. J. (1997). Toxoplasma pneumonia. *Seminars in respiratory infections*, *12*(1), 40–43.

50. Oksenhendler, E., Cadranel, J., Sarfati, C., Katlama, C., Datry, A., Marche, C., Wolf, M., Roux, P., Derouin, F., & Clauvel, J. P. (1990). Toxoplasma gondii pneumonia in patients with the acquired immunodeficiency syndrome. *The American journal of medicine*, *88*(5N), 18N–21N.

51. Sumi, M., Norose, K., Hikosaka, K., Kaiume, H., Takeda, W., Kirihara, T., Kurihara, T., Sato, K., Ueki, T., Hiroshima, Y., Kuraishi, H., Watanabe, M., & Kobayashi, H. (2016). Clinical characteristics and computed tomography findings of pulmonary toxoplasmosis after hematopoietic stem cell transplantation. *International journal of hematology*, *104*(6), 729–740. https://doi.org/10.1007/s12185-016-2077-0.

52. Petersen, E., Edvinsson, B., Lundgren, B., Benfield, T., & Evengård, B. (2006). Diagnosis of pulmonary infection with Toxoplasma gondii in immunocompromised HIV-positive patients by real-time PCR. *European journal of clinical microbiology & infectious diseases : official publication of the European Society of Clinical Microbiology*, *25*(6), 401–404. https://doi.org/10.1007/s10096-006-0156-5.

53. Dunay, I. R., Gajurel, K., Dhakal, R., Liesenfeld, O., & Montoya, J. G. (2018). Treatment of Toxoplasmosis: Historical Perspective, Animal Models, and Current

Clinical Practice. *Clinical microbiology reviews*, *31*(4), e00057-17. https://doi.org/10.1128/CMR.00057-17.

54. Piao, L. X., Cheng, J. H., Aosai, F., Zhao, X. D., Norose, K., & Jin, X. J. (2018). Cellular immunopathogenesis in primary Toxoplasma gondii infection during pregnancy. *Parasite immunology*, *40*(9), e12570. https://doi.org/10.1111/pim.12570.

55. Jones, J., Lopez, A., & Wilson, M. (2003). Congenital toxoplasmosis. *American family physician*, *67*(10), 2131–2138.

56. Dellacasa-Lindberg, I., Hitziger, N., & Barragan, A. (2007). Localized recrudescence of Toxoplasma infections in the central nervous system of immunocompromised mice assessed by in vivo bioluminescence imaging. *Microbes and infection*, *9*(11), 1291–1298. https://doi.org/10.1016/j.micinf.2007.06.003

57. Brandão, G. P., Melo, M. N., Caetano, B. C., Carneiro, C. M., Silva, L. A., & Vitor, R. W. (2011). Susceptibility to re-infection in C57BL/6 mice with recombinant strains of Toxoplasma gondii. *Experimental parasitology*, *128*(4), 433–437. https://doi.org/10.1016/j.exppara.2011.05.015.

58. Dubey, J. P., & Frenkel, J. K. (1998). Toxoplasmosis of rats: a review, with considerations of their value as an animal model and their possible role in epidemiology. *Veterinary parasitology*, *77*(1), 1–32. https://doi.org/10.1016/s0304-4017(97)00227-6.

59. Silva, R. C., Silva, A. V., & Langoni, H. (2010). Recrudescence of Toxoplasma gondii infection in chronically infected rats (Rattus norvegicus). *Experimental parasitology*, *125*(4), 409–412. https://doi.org/10.1016/j.exppara.2010.04.003.

60. Ramanan, P., Scherger, S., Benamu, E., Bajrovic, V., Jackson, W., Hage, C. A., Hakki, M., Baddley, J. W., & Abidi, M. Z. (2020). Toxoplasmosis in non-cardiac

solid organ transplant recipients: A case series and review of literature. *Transplant infectious disease : an official journal of the Transplantation Society*, *22*(1), e13218. https://doi.org/10.1111/tid.13218.

61. McFarland, M. M., Zach, S. J., Wang, X., Potluri, L. P., Neville, A. J., Vennerstrom, J. L., & Davis, P. H. (2016). Review of Experimental Compounds Demonstrating Anti-Toxoplasma Activity. *Antimicrobial agents and chemotherapy*, *60*(12), 7017–7034. https://doi.org/10.1128/AAC.01176-16.

62. Chaudhary, K., Darling, J. A., Fohl, L. M., Sullivan, W. J., Jr, Donald, R. G., Pfefferkorn, E. R., Ullman, B., & Roos, D. S. (2004). Purine salvage pathways in the apicomplexan parasite Toxoplasma gondii. *The Journal of biological chemistry*, *279*(30), 31221–31227. https://doi.org/10.1074/jbc.M404232200.

63. Reynolds, M. G., Oh, J., & Roos, D. S. (2001). In vitro generation of novel pyrimethamine resistance mutations in the Toxoplasma gondii dihydrofolate reductase. *Antimicrobial agents and chemotherapy*, *45*(4), 1271–1277. https://doi.org/10.1128/AAC.45.4.1271-1277.2001.

64. Fohl, L. M., & Roos, D. S. (2003). Fitness effects of DHFR-TS mutations associated with pyrimethamine resistance in apicomplexan parasites. *Molecular microbiology*, *50*(4), 1319–1327. https://doi.org/10.1046/j.1365-2958.2003.03756.x.

65. Hopper, A. T., Brockman, A., Wise, A., Gould, J., Barks, J., Radke, J. B., Sibley, L. D., Zou, Y., & Thomas, S. (2019). Discovery of Selective Toxoplasma gondii Dihydrofolate Reductase Inhibitors for the Treatment of Toxoplasmosis. *Journal of medicinal chemistry*, *62*(3), 1562–1576. https://doi.org/10.1021/acs.jmedchem.8b01754.

66. Tawari, N. R., Bag, S., & Degani, M. S. (2011). A review of molecular modelling studies of dihydrofolate reductase inhibitors against opportunistic microorganisms and comprehensive evaluation of new models. *Current pharmaceutical design*, *17*(7), 712–751. https://doi.org/10.2174/138161211795428966.

67. Silva, L. A., Reis-Cunha, J. L., Bartholomeu, D. C., & Vítor, R. W. (2017). Genetic Polymorphisms and Phenotypic Profiles of Sulfadiazine-Resistant and Sensitive Toxoplasma gondii Isolates Obtained from Newborns with Congenital Toxoplasmosis in Minas Gerais, Brazil. *PloS one*, *12*(1), e0170689. https://doi.org/10.1371/journal.pone.0170689.

68. Allegra, C. J., Boarman, D., Kovacs, J. A., Morrison, P., Beaver, J., Chabner, B. A., & Masur, H. (1990). Interaction of sulfonamide and sulfone compounds with Toxoplasma gondii dihydropteroate synthase. *The Journal of clinical investigation*, *85*(2), 371–379. https://doi.org/10.1172/JCI114448.

69. Mack, D. G., & McLeod, R. (1984). New micromethod to study the effect of antimicrobial agents on Toxoplasma gondii: comparison of sulfadoxine and sulfadiazine individually and in combination with pyrimethamine and study of clindamycin, metronidazole, and cyclosporin A. *Antimicrobial agents and chemotherapy*, *26*(1), 26–30. https://doi.org/10.1128/aac.26.1.26.

70. Derouin, F., Almadany, R., Chau, F., Rouveix, B., & Pocidalo, J. J. (1992). Synergistic activity of azithromycin and pyrimethamine or sulfadiazine in acute experimental toxoplasmosis. *Antimicrobial agents and chemotherapy*, *36*(5), 997–1001. https://doi.org/10.1128/aac.36.5.997.

71. Meneceur, P., Bouldouyre, M. A., Aubert, D., Villena, I., Menotti, J., Sauvage, V., Garin, J. F., & Derouin, F. (2008). In vitro susceptibility of various genotypic strains

of Toxoplasma gondii to pyrimethamine, sulfadiazine, and atovaquone. *Antimicrobial agents and chemotherapy*, *52*(4), 1269–1277. https://doi.org/10.1128/AAC.01203-07.

72. Alder, J., Hutch, T., Meulbroek, J. A., & Clement, J. C. (1994). Treatment of experimental Toxoplasma gondii infection by clarithromycin-based combination therapy with minocycline or pyrimethamine. *Journal of acquired immune deficiency syndromes*, *7*(11), 1141–1148.

73. Piketty, C., Derouin, F., Rouveix, B., & Pocidalo, J. J. (1990). In vivo assessment of antimicrobial agents against Toxoplasma gondii by quantification of parasites in the blood, lungs, and brain of infected mice. *Antimicrobial agents and chemotherapy*, *34*(8), 1467–1472. https://doi.org/10.1128/aac.34.8.1467.

74. Ben-Harari, R. R., Goodwin, E., & Casoy, J. (2017). Adverse Event Profile of Pyrimethamine-Based Therapy in Toxoplasmosis: A Systematic Review. *Drugs in R&D*, *17*(4), 523–544. https://doi.org/10.1007/s40268-017-0206-8.

75. Van Delden, C., & Hirschel, B. (1996). Folinic acid supplements to pyrimethamine-sulfadiazine for Toxoplasma encephalitis are associated with better outcome. *The Journal of infectious diseases*, *173*(5), 1294–1295. https://doi.org/10.1093/infdis/173.5.1294.

76. Hiraoka, M., & Kagawa, Y. (2017). Genetic polymorphisms and folate status. *Congenital anomalies*, *57*(5), 142–149. https://doi.org/10.1111/cga.12232.

77. Bertacine Dias, M. V., Santos, J. C., Libreros-Zúñiga, G. A., Ribeiro, J. A., & Chavez-Pacheco, S. M. (2018). Folate biosynthesis pathway: mechanisms and insights into drug design for infectious diseases. *Future medicinal chemistry*, *10*(8), 935–959. https://doi.org/10.4155/fmc-2017-0168.

78. Grossman, P. L., & Remington, J. S. (1979). The effect of trimethoprim and sulfamethoxazole on Toxoplasma gondii in vitro and in vivo. *The American journal of tropical medicine and hygiene*, *28*(3), 445–455. https://doi.org/10.4269/ajtmh.1979.28.445.

79. Dumas, J. L., Pizzolato, G., & Pechère, J. C. (1999). Evaluation of trimethoprim and sulphamethoxazole as monotherapy or in combination in the management of toxoplasmosis in murine models. *International journal of antimicrobial agents*, *13*(1), 35–39. https://doi.org/10.1016/s0924-8579(99)00073-4.

80. Ribera, E., Fernandez-Sola, A., Juste, C., Rovira, A., Romero, F. J., Armadans-Gil, L., Ruiz, I., Ocaña, I., & Pahissa, A. (1999). Comparison of high and low doses of trimethoprim-sulfamethoxazole for primary prevention of toxoplasmic encephalitis in human immunodeficiency virus-infected patients. *Clinical infectious diseases : an official publication of the Infectious Diseases Society of America*, *29*(6), 1461–1466. https://doi.org/10.1086/313515.

81. Derouin, F., Piketty, C., Chastang, C., Chau, F., Rouveix, B., & Pocidalo, J. J. (1991). Anti-Toxoplasma effects of dapsone alone and combined with pyrimethamine. *Antimicrobial agents and chemotherapy*, *35*(2), 252–255. https://doi.org/10.1128/aac.35.2.252.

82. Hernández-Díaz, S., Werler, M. M., Walker, A. M., & Mitchell, A. A. (2000). Folic acid antagonists during pregnancy and the risk of birth defects. *The New England journal of medicine*, *343*(22), 1608–1614. https://doi.org/10.1056/NEJM200011303432204.

83. Low, L. M., Stanisic, D. I., & Good, M. F. (2018). Exploiting the apicoplast: apicoplast-targeting drugs and malaria vaccine development. *Microbes and infection*, *20*(9-10), 477–483. https://doi.org/10.1016/j.micinf.2017.12.005.

84. Wiesner, J., Reichenberg, A., Heinrich, S., Schlitzer, M., & Jomaa, H. (2008). The plastid-like organelle of apicomplexan parasites as drug target. *Current pharmaceutical design*, *14*(9), 855–871. https://doi.org/10.2174/138161208784041105.

85. Camps, M., Arrizabalaga, G., & Boothroyd, J. (2002). An rRNA mutation identifies the apicoplast as the target for clindamycin in Toxoplasma gondii. *Molecular microbiology*, *43*(5), 1309–1318. https://doi.org/10.1046/j.1365-2958.2002.02825.x.

86. Chang, H. R., Comte, R., & Pechère, J. C. (1990). In vitro and in vivo effects of doxycycline on Toxoplasma gondii. *Antimicrobial agents and chemotherapy*, *34*(5), 775–780. https://doi.org/10.1128/aac.34.5.775.

87. Lago, K., Telu, K., Tribble, D., Ganesan, A., Kunz, A., Geist, C., Fraser, J., Mitra, I., Lalani, T., Yun, H., & For The Infectious Disease Clinical Research Program TravMil Study Group (2020). Impact of Doxycycline as Malaria Prophylaxis on Risk of Influenza-Like Illness among International Travelers. *The American journal of tropical medicine and hygiene*, *102*(4), 821–826. https://doi.org/10.4269/ajtmh.19-0648.

88. Hagberg, L., Palmertz, B., & Lindberg, J. (1993). Doxycycline and pyrimethamine for toxoplasmic encephalitis. *Scandinavian journal of infectious diseases*, *25*(1), 157–160. https://doi.org/10.1080/00365549309169687.

89. Brisson-Noël, A., Trieu-Cuot, P., & Courvalin, P. (1988). Mechanism of action of spiramycin and other macrolides. *The Journal of antimicrobial chemotherapy*, *22 Suppl B*, 13–23. https://doi.org/10.1093/jac/22.supplement_b.13.

90. Vázquez-Laslop, N., & Mankin, A. S. (2018). How Macrolide Antibiotics Work. *Trends in biochemical sciences*, *43*(9), 668–684. https://doi.org/10.1016/j.tibs.2018.06.011.

91. Beckers, C. J., Roos, D. S., Donald, R. G., Luft, B. J., Schwab, J. C., Cao, Y., & Joiner, K. A. (1995). Inhibition of cytoplasmic and organellar protein synthesis in Toxoplasma gondii. Implications for the target of macrolide antibiotics. *The Journal of clinical investigation*, *95*(1), 367–376. https://doi.org/10.1172/JCI117665.

92. Gratzl, R., Sodeck, G., Platzer, P., Jäger, W., Graf, J., Pollak, A., & Thalhammer, T. (2002). Treatment of toxoplasmosis in pregnancy: concentrations of spiramycin and neospiramycin in maternal serum and amniotic fluid. *European journal of clinical microbiology & infectious diseases : official publication of the European Society of Clinical Microbiology*, *21*(1), 12–16. https://doi.org/10.1007/s10096-001-0644-6.

93. Chamberland, S., Kirst, H. A., & Current, W. L. (1991). Comparative activity of macrolides against Toxoplasma gondii demonstrating utility of an in vitro microassay. *Antimicrobial agents and chemotherapy*, *35*(5), 903–909. https://doi.org/10.1128/aac.35.5.903.

94. Araujo, F. G., Shepard, R. M., & Remington, J. S. (1991). In vivo activity of the macrolide antibiotics azithromycin, roxithromycin and spiramycin against Toxoplasma gondii. *European journal of clinical microbiology & infectious diseases : official publication of the European Society of Clinical Microbiology*, *10*(6), 519–524. https://doi.org/10.1007/BF01963942.

95. Olliaro, P., Gorini, G., Jabes, D., Regazzetti, A., Rossi, R., Marchetti, A., Tinelli, C., & Della Bruna, C. (1994). In-vitro and in-vivo activity of rifabutin against

Toxoplasma gondii. *The Journal of antimicrobial chemotherapy*, *34*(5), 649–657. https://doi.org/10.1093/jac/34.5.649.

96. Araujo, F. G., Prokocimer, P., Lin, T., & Remington, J. S. (1992). Activity of clarithromycin alone or in combination with other drugs for treatment of murine toxoplasmosis. *Antimicrobial agents and chemotherapy*, *36*(11), 2454–2457. https://doi.org/10.1128/aac.36.11.2454.

97. Saba, J., Morlat, P., Raffi, F., Hazebroucq, V., Joly, V., Leport, C., & Vildé, J. L. (1993). Pyrimethamine plus azithromycin for treatment of acute toxoplasmic encephalitis in patients with AIDS. *European journal of clinical microbiology & infectious diseases : official publication of the European Society of Clinical Microbiology*, *12*(11), 853–856. https://doi.org/10.1007/BF02000407.

98. Fernandez-Martin, J., Leport, C., Morlat, P., Meyohas, M. C., Chauvin, J. P., & Vilde, J. L. (1991). Pyrimethamine-clarithromycin combination for therapy of acute Toxoplasma encephalitis in patients with AIDS. *Antimicrobial agents and chemotherapy*, *35*(10), 2049–2052. https://doi.org/10.1128/aac.35.10.2049.

99. Pfefferkorn, E. R., Nothnagel, R. F., & Borotz, S. E. (1992). Parasiticidal effect of clindamycin on Toxoplasma gondii grown in cultured cells and selection of a drug-resistant mutant. *Antimicrobial agents and chemotherapy*, *36*(5), 1091–1096. https://doi.org/10.1128/aac.36.5.1091.

100. Salin, N. H., Noordin, R., Al-Najjar, B. O., Kamarulzaman, E. E., Yunus, M. H., Karim, I., Nasim, N., Zakaria, I. I., & Wahab, H. A. (2020). Identification of potential dual -targets anti- toxoplasma gondii compounds through structure-based virtual screening and in-vitro studies. *PloS one*, *15*(5), e0225232. https://doi.org/10.1371/journal.pone.0225232.

101. Djurković-Djaković, O., Nikolić, T., Robert-Gangneux, F., Bobić, B., & Nikolić, A. (1999). Synergistic effect of clindamycin and atovaquone in acute murine toxoplasmosis. *Antimicrobial agents and chemotherapy*, *43*(9), 2240–2244. https://doi.org/10.1128/AAC.43.9.2240.

102. Vuković, D., Djurković-Djaković, O., Kovacević, S., Bobić, B., Nikolić, A., Todorović, V., V, & Babić, D. (1997). Effect of clindamycin in a model of acute murine toxoplasmosis. *Clinical microbiology and infection : the official publication of the European Society of Clinical Microbiology and Infectious Diseases*, *3*(1), 89–94. https://doi.org/10.1111/j.1469-0691.1997.tb00256.x.

103. Konstantinovic, N., Guegan, H., Stäjner, T., Belaz, S., & Robert-Gangneux, F. (2019). Treatment of toxoplasmosis: Current options and future perspectives. *Food and waterborne parasitology*, *15*, e00036. https://doi.org/10.1016/j.fawpar.2019.e00036.

104. Wei, H. X., Wei, S. S., Lindsay, D. S., & Peng, H. J. (2015). A Systematic Review and Meta-Analysis of the Efficacy of Anti-Toxoplasma gondii Medicines in Humans. *PloS one*, *10*(9), e0138204. https://doi.org/10.1371/journal.pone.0138204.

105. Kremsner, P. G., Looareesuwan, S., & Chulay, J. D. (1999). Atovaquone and proguanil hydrochloride for treatment of malaria. *Journal of travel medicine*, *6 Suppl 1*, S18–S20.

106. Baggish, A. L., & Hill, D. R. (2002). Antiparasitic agent atovaquone. *Antimicrobial agents and chemotherapy*, *46*(5), 1163–1173. https://doi.org/10.1128/aac.46.5.1163-1173.2002.

107. Doggett, J. S., Nilsen, A., Forquer, I., Wegmann, K. W., Jones-Brando, L., Yolken, R. H., Bordón, C., Charman, S. A., Katneni, K., Schultz, T., Burrows, J. N., Hinrichs, D. J., Meunier, B., Carruthers, V. B., & Riscoe, M. K. (2012). Endochin-like quinolones are highly efficacious against acute and latent experimental toxoplasmosis. *Proceedings of the National Academy of Sciences of the United States of America*, *109*(39), 15936–15941. https://doi.org/10.1073/pnas.1208069109.

108. McFadden, D. C., Tomavo, S., Berry, E. A., & Boothroyd, J. C. (2000). Characterization of cytochrome b from Toxoplasma gondii and Q(o) domain mutations as a mechanism of atovaquone-resistance. *Molecular and biochemical parasitology*, *108*(1), 1–12. https://doi.org/10.1016/s0166-6851(00)00184-5.

109. Montazeri, M., Sharif, M., Sarvi, S., Mehrzadi, S., Ahmadpour, E., & Daryani, A. (2017). A Systematic Review of *In vitro* and *In vivo* Activities of Anti-*Toxoplasma* Drugs and Compounds (2006-2016). *Frontiers in microbiology*, *8*, 25. https://doi.org/10.3389/fmicb.2017.00025.

110. Li R. (2016). Marinopyrroles: Unique Drug Discoveries Based on Marine Natural Products. *Medicinal research reviews*, *36*(1), 169–189. https://doi.org/10.1002/med.21359.

111. Pimentel-Elardo, S. M., Kozytska, S., Bugni, T. S., Ireland, C. M., Moll, H., & Hentschel, U. (2010). Anti-parasitic compounds from Streptomyces sp. strains isolated from Mediterranean sponges. *Marine drugs*, *8*(2), 373–380. https://doi.org/10.3390/md8020373.

112. Subramani, R., & Aalbersberg, W. (2012). Marine actinomycetes: an ongoing source of novel bioactive metabolites. *Microbiological research*, *167*(10), 571–580. https://doi.org/10.1016/j.micres.2012.06.005.

113. Hughes, C. C., Prieto-Davo, A., Jensen, P. R., & Fenical, W. (2008). The marinopyrroles, antibiotics of an unprecedented structure class from a marine Streptomyces sp. *Organic letters*, *10*(4), 629–631. https://doi.org/10.1021/ol702952n.

114. Hughes, C. C., Kauffman, C. A., Jensen, P. R., & Fenical, W. (2010). Structures, reactivities, and antibiotic properties of the marinopyrroles A-F. *The Journal of organic chemistry*, *75*(10), 3240–3250. https://doi.org/10.1021/jo1002054.

115. Sancak, B., Yagci, S., Gür, D., Gülay, Z., Ogunc, D., Söyletir, G., Yalcin, A. N., Dündar, D. O., Topçu, A. W., Aksit, F., Usluer, G., Ozakin, C., Akalin, H., Hayran, M., & Korten, V. (2013). Vancomycin and daptomycin minimum inhibitory concentration distribution and occurrence of heteroresistance among methicillin-resistant Staphylococcus aureus blood isolates in Turkey. *BMC infectious diseases*, *13*, 583. https://doi.org/10.1186/1471-2334-13-583.

116. Nunes, S. F., Bexiga, R., Cavaco, L. M., & Vilela, C. L. (2007). Technical note: Antimicrobial susceptibility of Portuguese isolates of Staphylococcus aureus and Staphylococcus epidermidis in subclinical bovine mastitis. *Journal of dairy science*, *90*(7), 3242–3246. https://doi.org/10.3168/jds.2006-739.

117. Haste, N. M., Hughes, C. C., Tran, D. N., Fenical, W., Jensen, P. R., Nizet, V., & Hensler, M. E. (2011). Pharmacological properties of the marine natural product marinopyrrole A against methicillin-resistant Staphylococcus aureus. *Antimicrobial agents and chemotherapy*, *55*(7), 3305–3312. https://doi.org/10.1128/AAC.01211-10.

118. Doi, K., Li, R., Sung, S. S., Wu, H., Liu, Y., Manieri, W., Krishnegowda, G., Awwad, A., Dewey, A., Liu, X., Amin, S., Cheng, C., Qin, Y., Schonbrunn, E.,

Daughdrill, G., Loughran, T. P., Jr, Sebti, S., & Wang, H. G. (2012). Discovery of marinopyrrole A (maritoclax) as a selective Mcl-1 antagonist that overcomes ABT-737 resistance by binding to and targeting Mcl-1 for proteasomal degradation. *The Journal of biological chemistry*, *287*(13), 10224–10235. https://doi.org/10.1074/jbc.M111.334532.

119. Doi, K., Liu, Q., Gowda, K., Barth, B. M., Claxton, D., Amin, S., Loughran, T. P., Jr, & Wang, H. G. (2014). Maritoclax induces apoptosis in acute myeloid leukemia cells with elevated Mcl-1 expression. *Cancer biology & therapy*, *15*(8), 1077–1086. https://doi.org/10.4161/cbt.29186.

120. Jeon, M. Y., Min, K. J., Woo, S. M., Seo, S. U., Choi, Y. H., Kim, S. H., Kim, D. E., Lee, T. J., Kim, S., Park, J. W., & Kwon, T. K. (2018). Maritoclax Enhances TRAIL-Induced Apoptosis via CHOP-Mediated Upregulation of DR5 and miR-708-Mediated Downregulation of cFLIP. *Molecules (Basel, Switzerland)*, *23*(11), 3030. https://doi.org/10.3390/molecules23113030.

121. Doi, K., Gowda, K., Liu, Q., Lin, J. M., Sung, S. S., Dower, C., Claxton, D., Loughran, T. P., Jr, Amin, S., & Wang, H. G. (2014). Pyoluteorin derivatives induce Mcl-1 degradation and apoptosis in hematological cancer cells. *Cancer biology & therapy*, *15*(12), 1688–1699. https://doi.org/10.4161/15384047.2014.972799.

122. Gomez-Bougie, P., Dousset, C., Descamps, G., Schnitzler, A., Audiger, L., Tessier, A., Dubreuil, D., Lebreton, J., Pellat-Deceunynck, C., & Amiot, M. (2018). The selectivity of Marinopyrrole A to induce apoptosis in $MCL1^{high}$ $BCL2^{low}$ expressing myeloma cells is related to its ability to impair protein translation. *British journal of haematology*, *180*(1), 157–159. https://doi.org/10.1111/bjh.14293.

123. Brunner, D., Frank, J., Appl, H., Schöffl, H., Pfaller, W., & Gstraunthaler, G. (2010). Serum-free cell culture: the serum-free media interactive online database. *ALTEX*, *27*(1), 53–62. https://doi.org/10.14573/altex.2010.1.53.

124. van der Valk, J., Brunner, D., De Smet, K., Fex Svenningsen, A., Honegger, P., Knudsen, L. E., Lindl, T., Noraberg, J., Price, A., Scarino, M. L., & Gstraunthaler, G. (2010). Optimization of chemically defined cell culture media--replacing fetal bovine serum in mammalian in vitro methods. *Toxicology in vitro : an international journal published in association with BIBRA*, *24*(4), 1053–1063. https://doi.org/10.1016/j.tiv.2010.03.016.

125. Eichhorn, J. M., Alford, S. E., Hughes, C. C., Fenical, W., & Chambers, T. C. (2013). Purported Mcl-1 inhibitor marinopyrrole A fails to show selective cytotoxicity for Mcl-1-dependent cell lines. *Cell death & disease*, *4*(10), e880. https://doi.org/10.1038/cddis.2013.411.

126. Hughes, C. C., Yang, Y. L., Liu, W. T., Dorrestein, P. C., La Clair, J. J., & Fenical, W. (2009). Marinopyrrole A target elucidation by acyl dye transfer. *Journal of the American Chemical Society*, *131*(34), 12094–12096. https://doi.org/10.1021/ja903149u.

127. Nicolaou, K. C., Simmons, N. L., Chen, J. S., Haste, N. M., & Nizet, V. (2011). Total synthesis and biological evaluation of marinopyrrole A and analogues. *Tetrahedron letters*, *52*(17), 2041–2043. https://doi.org/10.1016/j.tetlet.2010.09.059.

128. Liu, Y., Haste, N. M., Thienphrapa, W., Nizet, V., Hensler, M., & Li, R. (2012). Marinopyrrole derivatives as potential antibiotic agents against methicillin-

resistant Staphylococcus aureus (I). *Marine drugs*, *10*(4), 953–962. https://doi.org/10.3390/md10040953.

129. Liu, Y., Haste, N. M., Thienphrapa, W., Li, J., Nizet, V., Hensler, M., & Li, R. (2014). Marinopyrrole derivatives as potential antibiotic agents against methicillin-resistant Staphylococcus aureus (III). *Marine drugs*, *12*(5), 2458–2470. https://doi.org/10.3390/md12052458.

130. Cheng, C., Liu, Y., Song, H., Pan, L., Li, J., Qin, Y., & Li, R. (2013). Marinopyrrole derivatives as potential antibiotic agents against methicillin-resistant Staphylococcus aureus (II). *Marine drugs*, *11*(8), 2927–2948. https://doi.org/10.3390/md11082927.

131. Yang, Z., Liu, Y., Ahn, J., Qiao, Z., Endres, J. L., Gautam, N., Huang, Y., Li, J., Zheng, J., Alnouti, Y., Bayles, K. W., & Li, R. (2016). Novel fluorinated pyrrolomycins as potent anti-staphylococcal biofilm agents: Design, synthesis, pharmacokinetics and antibacterial activities. *European journal of medicinal chemistry*, *124*, 129–137. https://doi.org/10.1016/j.ejmech.2016.08.017.

132. Frattini, A., Fabbri, M., Valli, R., De Paoli, E., Montalbano, G., Gribaldo, L., Pasquali, F., & Maserati, E. (2015). High variability of genomic instability and gene expression profiling in different HeLa clones. *Scientific reports*, *5*, 15377. https://doi.org/10.1038/srep15377.

133. Mirabelli, P., Coppola, L., & Salvatore, M. (2019). Cancer Cell Lines Are Useful Model Systems for Medical Research. *Cancers*, *11*(8), 1098. https://doi.org/10.3390/cancers11081098.

134. Gillet, J. P., Varma, S., & Gottesman, M. M. (2013). The clinical relevance of cancer cell lines. *Journal of the National Cancer Institute*, *105*(7), 452–458. https://doi.org/10.1093/jnci/djt007.

135. Li, J., Zhao, W., Akbani, R., Liu, W., Ju, Z., Ling, S., Vellano, C. P., Roebuck, P., Yu, Q., Eterovic, A. K., Byers, L. A., Davies, M. A., Deng, W., Gopal, Y. N., Chen, G., von Euw, E. M., Slamon, D., Conklin, D., Heymach, J. V., Gazdar, A. F., … Liang, H. (2017). Characterization of Human Cancer Cell Lines by Reverse-phase Protein Arrays. *Cancer cell*, *31*(2), 225–239. https://doi.org/10.1016/j.ccell.2017.01.005.

136. Maqsood, M. I., Matin, M. M., Bahrami, A. R., & Ghasroldasht, M. M. (2013). Immortality of cell lines: challenges and advantages of establishment. *Cell biology international*, *37*(10), 1038–1045. https://doi.org/10.1002/cbin.10137.

137. Gamboa, J. M., & Leong, K. W. (2013). In vitro and in vivo models for the study of oral delivery of nanoparticles. *Advanced drug delivery reviews*, *65*(6), 800–810. https://doi.org/10.1016/j.addr.2013.01.003.

138. Mechanism matters. (2010). *Nature medicine*, *16*(4), 347. https://doi.org/10.1038/nm0410-347.

139. Rossiter, S. E., Fletcher, M. H., & Wuest, W. M. (2017). Natural Products as Platforms To Overcome Antibiotic Resistance. *Chemical reviews*, *117*(19), 12415–12474. https://doi.org/10.1021/acs.chemrev.7b00283.

140. Hill, D., & Dubey, J. P. (2002). Toxoplasma gondii: transmission, diagnosis and prevention. *Clinical microbiology and infection : the official publication of the European Society of Clinical Microbiology and Infectious Diseases*, *8*(10), 634–640. https://doi.org/10.1046/j.1469-0691.2002.00485.x.

141. Hill, D. E., & Dubey, J. P. (2013). Toxoplasma gondii prevalence in farm animals in the United States. *International Journal for Parasitology*, *43*(2), 107–113. https://doi.org/10.1016/j.ijpara.2012.09.012.

142. Shaapan R. M. (2016). The common zoonotic protozoal diseases causing abortion. *Journal of parasitic diseases: official organ of the Indian Society for Parasitology*, 40(4), 1116–1129. https://doi.org/10.1007/s12639-015-0661-5

143. Avelino, M. M., Amaral, W. N., Rodrigues, I. M., Rassi, A. R., Gomes, M. B., Costa, T. L., & Castro, A. M. (2014). Congenital toxoplasmosis and prenatal care state programs. *BMC infectious diseases*, *14*, 33. https://doi.org/10.1186/1471-2334-14-33.

144. Loveridge-Easther, C., Yardley, A. M., & Breidenstein, B. (2018). Use of polymerase chain reaction (PCR) in the diagnosis of congenital toxoplasmosis. *Journal of AAPOS : the official publication of the American Association for Pediatric Ophthalmology and Strabismus*, *22*(3), 239–240. https://doi.org/10.1016/j.jaapos.2017.12.013.

145. Zhang, Y., Lin, X., & Lu, F. (2018). Current treatment of ocular toxoplasmosis in immunocompetent patients: a network meta-analysis. *Acta tropica*, *185*, 52–62. https://doi.org/10.1016/j.actatropica.2018.04.026.

146. Ben-Harari, R. R., Goodwin, E., & Casoy, J. (2017). Adverse Event Profile of Pyrimethamine-Based Therapy in Toxoplasmosis: A Systematic Review. *Drugs in R&D*, *17*(4), 523–544. https://doi.org/10.1007/s40268-017-0206-8.

147. Cohn, J. A., McMeeking, A., Cohen, W., Jacobs, J., & Holzman, R. S. (1989). Evaluation of the policy of empiric treatment of suspected Toxoplasma encephalitis in patients with the acquired immunodeficiency syndrome. *The*

American journal of medicine, *86*(5), 521–527. https://doi.org/10.1016/0002-9343(89)90378-1.

148. Dalimi, A., & Abdoli, A. (2012). Latent toxoplasmosis and human. *Iranian journal of parasitology*, *7*(1), 1–17.

149. Cheng, C., Pan, L., Chen, Y., Song, H., Qin, Y., & Li, R. (2010). Total synthesis of (+/-)-marinopyrrole A and its library as potential antibiotic and anticancer agents. *Journal of combinatorial chemistry*, *12*(4), 541–547. https://doi.org/10.1021/cc100052j.

150. Liu, Y., Haste, N. M., Thienphrapa, W., Nizet, V., Hensler, M., & Li, R. (2012). Marinopyrrole derivatives as potential antibiotic agents against methicillin-resistant Staphylococcus aureus (I). *Marine drugs*, *10*(4), 953–962. https://doi.org/10.3390/md10040953.

151. Sanford, A. G., Schulze, T. T., Potluri, L. P., Hemsley, R. M., Larson, J. J., Judge, A. K., Zach, S. J., Wang, X., Charman, S. A., Vennerstrom, J. L., & Davis, P. H. (2018). Novel Toxoplasma gondii inhibitor chemotypes. *Parasitology international*, *67*(2), 107–111. https://doi.org/10.1016/j.parint.2017.10.010.

152. Khan, A., & Grigg, M. E. (2017). Toxoplasma gondii: Laboratory Maintenance and Growth. *Current protocols in microbiology*, *44*, 20C.1.1–20C.1.17. https://doi.org/10.1002/cpmc.26

153. Li, R.; Sebtie, S.; Liu, Y.; Qin, Y.; Song, H.; Cheng, C. Marinopyrrole Derivatives and Methods of Making and Using Same, U.S. Patent No. 9,868,747 (2018).

154. Li, R.; Sebtie, S. Liu, Y. Marinopyrrole Derivatives as Anticancer Agents. U.S. Patent No. 9,340,501 (2016).

155. Bernatchez, J. A., Yang, Z., Coste, M., Li, J., Beck, S., Liu, Y., Clark, A. E., Zhu, Z., Luna, L. A., Sohl, C. D., Purse, B. W., Li, R., & Siqueira-Neto, J. L. (2018). Development and Validation of a Phenotypic High-Content Imaging Assay for Assessing the Antiviral Activity of Small-Molecule Inhibitors Targeting Zika Virus. Antimicrobial agents and chemotherapy, 62(10), e00725-18. https://doi.org/10.1128/AAC.00725-18.

156. McGuire, T. R., Coulter, D. W., Bai, D., Sughroue, J. A., Li, J., Yang, Z., Qiao, Z., Liu, Y., Murry, D. J., Chhonker, Y. S., McIntyre, E. M., Alexander, G., Sharp, J. G., & Li, R. (2019). Effects of novel pyrrolomycin MP1 in MYCN amplified chemoresistant neuroblastoma cell lines alone and combined with temsirolimus. *BMC cancer*, *19*(1), 837. https://doi.org/10.1186/s12885-019-6033-2.

157. Li, R. Pyrrolomycin Derivative Compositions and Methods of Use. U.S. Serial No. 62,052,583 (2014)

158. Li, R.; Liu, Y. Pyrrolomycins and Methods of Using the Same. U.S. Serial No. 62,193,192 (2014)

159. Li, R.; Liu, Y. Pyrrolomycins and Methods of Using the Same. U.S. Serial No. 62,193,192 (2015).

160. Li, R.; Liu, Y. Pyrrolomycins and Methods of Using the Same. U.S. Serial No. 62,219,289 (2015).

161. Li, R.; Liu, Y. Pyrrolomycins and Methods of Using the Same. U.S. Serial No. 62,309,685 (2016).

162. Li, R.; Liu, Y. Pyrrolomycins and Methods of Using the Same. U.S. Serial No. 62,299,588 (2016).

163. Li, R.; Liu, Y. Synthesis of pyrrolomycins as antibiofilm agents. Patent Co-operation Treaty International Application WO 2016-US42423 (2016).

164. Li, R.; Liu, Y.; Bayles, K.W. Pyrrolomycins and methods of using the same. Patent Cooperation Treaty International Application WO2017011725 (2017).

165. Li, R.; Liu, Y.; Bayles, K.W. Pyrrolomycins and methods of using the same. U.S. Patent US20180194725A1 (2018).

166. Bayles, K.W.; Li, R.; Liu, Y. Pyrrolomycins and methods of using the same. U.S. Patent No. 10,414,725 (2019).

167. Bayles, K.W.; Li, R.; Liu, Y. Pyrrolomycins and methods of using the same. U.S. continuation parent application, international publication number US2019/0330147A1 (2019).

168. Zhang, Y., Lai, B. S., Juhas, M., & Zhang, Y. (2019). Toxoplasma gondii secretory proteins and their role in invasion and pathogenesis. *Microbiological research*, *227*, 126293. https://doi.org/10.1016/j.micres.2019.06.003.

169. Rondon-Villarreal, P., & Pinzon-Reyes, E. (2018). Computer Aided Design of Non-toxic Antibacterial Peptides. *Current topics in medicinal chemistry*, *18*(13), 1044–1052. https://doi.org/10.2174/1568026618666180719163251.

170. Präbst, K., Engelhardt, H., Ringgeler, S., & Hübner, H. (2017). Basic Colorimetric Proliferation Assays: MTT, WST, and Resazurin. *Methods in molecular biology (Clifton, N.J.)*, *1601*, 1–17. https://doi.org/10.1007/978-1-4939-6960-9_1.

171. Kyrylkova, K., Kyryachenko, S., Leid, M., & Kioussi, C. (2012). Detection of apoptosis by TUNEL assay. *Methods in molecular biology (Clifton, N.J.)*, *887*, 41–47. https://doi.org/10.1007/978-1-61779-860-3_5.

172. Degterev, A., Lugovskoy, A., Cardone, M., Mulley, B., Wagner, G., Mitchison, T., & Yuan, J. (2001). Identification of small-molecule inhibitors of interaction between the BH3 domain and Bcl-xL. *Nature cell biology*, *3*(2), 173–182. https://doi.org/10.1038/35055085.

173. Rao, X., Huang, X., Zhou, Z., & Lin, X. (2013). An improvement of the 2ˆ(-delta delta CT) method for quantitative real-time polymerase chain reaction data analysis. *Biostatistics, bioinformatics and biomathematics*, *3*(3), 71–85.

174. Li, R., Cheng, C., Balasis, M. E., Liu, Y., Garner, T. P., Daniel, K. G., Li, J., Qin, Y., Gavathiotis, E., & Sebti, S. M. (2015). Design, synthesis and evaluation of marinopyrrole derivatives as selective inhibitors of Mcl-1 binding to pro-apoptotic Bim and dual Mcl-1/Bcl-xL inhibitors. *European journal of medicinal chemistry*, *90*, 315–331. https://doi.org/10.1016/j.ejmech.2014.11.035.

175. McGuire, T. R., Coulter, D. W., Bai, D., Sughroue, J. A., Li, J., Yang, Z., Qiao, Z., Liu, Y., Murry, D. J., Chhonker, Y. S., McIntyre, E. M., Alexander, G., Sharp, J. G., & Li, R. (2019). Effects of novel pyrrolomycin MP1 in MYCN amplified chemoresistant neuroblastoma cell lines alone and combined with temsirolimus. *BMC cancer*, *19*(1), 837. https://doi.org/10.1186/s12885-019-6033-2.

176. Shen, C., Gu, M., Song, C., Miao, L., Hu, L., Liang, D., & Zheng, C. (2008). The tumorigenicity diversification in human embryonic kidney 293 cell line cultured in vitro. *Biologicals : journal of the International Association of Biological Standardization*, *36*(4), 263–268. https://doi.org/10.1016/j.biologicals.2008.02.002.

177. Tang, Q. L., Liang, Y., Xie, X. B., Yin, J. Q., Zou, C. Y., Zhao, Z. Q., Shen, J. N., & Wang, J. (2011). Enrichment of osteosarcoma stem cells by

chemotherapy. *Chinese journal of cancer*, *30*(6), 426–432. https://doi.org/10.5732/cjc.011.10127.

178. Sturman, L. S., & Takemoto, K. K. (1972). Enhanced growth of a murine coronavirus in transformed mouse cells. *Infection and immunity*, *6*(4), 501–507. https://doi.org/10.1128/IAI.6.4.501-507.1972.

179. Qiu, G. H., Xie, X., Xu, F., Shi, X., Wang, Y., & Deng, L. (2015). Distinctive pharmacological differences between liver cancer cell lines HepG2 and Hep3B. *Cytotechnology*, *67*(1), 1–12. https://doi.org/10.1007/s10616-014-9761-9.

180. Schildberger, A., Rossmanith, E., Eichhorn, T., Strassl, K., & Weber, V. (2013). Monocytes, peripheral blood mononuclear cells, and THP-1 cells exhibit different cytokine expression patterns following stimulation with lipopolysaccharide. *Mediators of inflammation*, *2013*, 697972. https://doi.org/10.1155/2013/697972.

181. Carneiro, B. A., & El-Deiry, W. S. (2020). Targeting apoptosis in cancer therapy. *Nature reviews. Clinical oncology*, *17*(7), 395–417. https://doi.org/10.1038/s41571-020-0341-y.

182. Crowley, L. C., & Waterhouse, N. J. (2016). Detecting Cleaved Caspase-3 in Apoptotic Cells by Flow Cytometry. *Cold Spring Harbor protocols*, *2016*(11), 10.1101/pdb.prot087312. https://doi.org/10.1101/pdb.prot087312

183. Gubbels, M. J., Li, C., & Striepen, B. (2003). High-throughput growth assay for Toxoplasma gondii using yellow fluorescent protein. *Antimicrobial agents and chemotherapy*, *47*(1), 309–316. https://doi.org/10.1128/aac.47.1.309-316.2003.

184. Huynh, M. H., Rabenau, K. E., Harper, J. M., Beatty, W. L., Sibley, L. D., & Carruthers, V. B. (2003). Rapid invasion of host cells by Toxoplasma requires

secretion of the MIC2-M2AP adhesive protein complex. *The EMBO journal*, *22*(9), 2082–2090. https://doi.org/10.1093/emboj/cdg217.

185. Fox, B. A., Falla, A., Rommereim, L. M., Tomita, T., Gigley, J. P., Mercier, C., Cesbron-Delauw, M. F., Weiss, L. M., & Bzik, D. J. (2011). Type II Toxoplasma gondii KU80 knockout strains enable functional analysis of genes required for cyst development and latent infection. *Eukaryotic cell*, *10*(9), 1193–1206. https://doi.org/10.1128/EC.00297-10.

186. Waldman, B. S., Schwarz, D., Wadsworth, M. H., 2nd, Saeij, J. P., Shalek, A. K., & Lourido, S. (2020). Identification of a Master Regulator of Differentiation in Toxoplasma. *Cell*, *180*(2), 359–372.e16. https://doi.org/10.1016/j.cell.2019.12.013.

187. Oltersdorf, T., Elmore, S. W., Shoemaker, A. R., Armstrong, R. C., Augeri, D. J., Belli, B. A., Bruncko, M., Deckwerth, T. L., Dinges, J., Hajduk, P. J., Joseph, M. K., Kitada, S., Korsmeyer, S. J., Kunzer, A. R., Letai, A., Li, C., Mitten, M. J., Nettesheim, D. G., Ng, S., Nimmer, P. M., … Rosenberg, S. H. (2005). An inhibitor of Bcl-2 family proteins induces regression of solid tumours. *Nature*, *435*(7042), 677–681. https://doi.org/10.1038/nature03579.

188. Kennedy P. G. (2013). Clinical features, diagnosis, and treatment of human African trypanosomiasis (sleeping sickness). *The Lancet. Neurology*, *12*(2), 186–194. https://doi.org/10.1016/S1474-4422(12)70296-X.

189. Stanley S. L., Jr (2003). Amoebiasis. *Lancet (London, England)*, *361*(9362), 1025–1034. https://doi.org/10.1016/S0140-6736(03)12830-9.

190. Reguera, R. M., Morán, M., Pérez-Pertejo, Y., García-Estrada, C., & Balaña-Fouce, R. (2016). Current status on prevention and treatment of canine

leishmaniasis. *Veterinary parasitology*, *227*, 98–114. https://doi.org/10.1016/j.vetpar.2016.07.011.

191. Tiberi, S., du Plessis, N., Walzl, G., Vjecha, M. J., Rao, M., Ntoumi, F., Mfinanga, S., Kapata, N., Mwaba, P., McHugh, T. D., Ippolito, G., Migliori, G. B., Maeurer, M. J., & Zumla, A. (2018). Tuberculosis: progress and advances in development of new drugs, treatment regimens, and host-directed therapies. *The Lancet. Infectious diseases*, *18*(7), e183–e198. https://doi.org/10.1016/S1473-3099(18)30110-5.

192. Zollner-Schwetz, I., & Krause, R. (2015). Therapy of acute gastroenteritis: role of antibiotics. *Clinical microbiology and infection : the official publication of the European Society of Clinical Microbiology and Infectious Diseases*, *21*(8), 744–749. https://doi.org/10.1016/j.cmi.2015.03.002.

193. Holden, M. T., Feil, E. J., Lindsay, J. A., Peacock, S. J., Day, N. P., Enright, M. C., Foster, T. J., Moore, C. E., Hurst, L., Atkin, R., Barron, A., Bason, N., Bentley, S. D., Chillingworth, C., Chillingworth, T., Churcher, C., Clark, L., Corton, C., Cronin, A., Doggett, J., … Parkhill, J. (2004). Complete genomes of two clinical Staphylococcus aureus strains: evidence for the rapid evolution of virulence and drug resistance. *Proceedings of the National Academy of Sciences of the United States of America*, *101*(26), 9786–9791. https://doi.org/10.1073/pnas.0402521101.

194. Appelbaum P. C. (2002). Resistance among Streptococcus pneumoniae: Implications for drug selection. *Clinical infectious diseases : an official publication of the Infectious Diseases Society of America*, *34*(12), 1613–1620. https://doi.org/10.1086/340400.

195. Jia, X., Ren, H., Nie, X., Li, Y., Li, J., & Qin, T. (2019). Antibiotic Resistance and Azithromycin Resistance Mechanism of Legionella pneumophila Serogroup 1 in China. *Antimicrobial agents and chemotherapy*, *63*(10), e00768-19. https://doi.org/10.1128/AAC.00768-19.

196. Furin, J., Cox, H., & Pai, M. (2019). Tuberculosis. *Lancet (London, England)*, *393*(10181), 1642–1656. https://doi.org/10.1016/S0140-6736(19)30308-3.

197. Pontes, D. S., de Araujo, R., Dantas, N., Scotti, L., Scotti, M. T., de Moura, R. O., & Mendonca-Junior, F. (2018). Genetic Mechanisms of Antibiotic Resistance and the Role of Antibiotic Adjuvants. *Current topics in medicinal chemistry*, *18*(1), 42–74. https://doi.org/10.2174/1568026618666180206095224.

198. Davies, J., & Davies, D. (2010). Origins and evolution of antibiotic resistance. *Microbiology and molecular biology reviews : MMBR*, *74*(3), 417–433. https://doi.org/10.1128/MMBR.00016-10.

199. Azam, M. W., Kumar, A., & Khan, A. U. (2020). ACD: Antimicrobial chemotherapeutics database. *PloS one*, *15*(6), e0235193. https://doi.org/10.1371/journal.pone.0235193.

200. Haenni, M., Lupo, A., & Madec, J. Y. (2018). Antimicrobial Resistance in *Streptococcus* spp. *Microbiology spectrum*, *6*(2), 10.1128/microbiolspec.ARBA-0008-2017. https://doi.org/10.1128/microbiolspec.ARBA-0008-2017.

201. Domenech, A., Brochado, A. R., Sender, V., Hentrich, K., Henriques-Normark, B., Typas, A., & Veening, J. W. (2020). Proton Motive Force Disruptors Block Bacterial Competence and Horizontal Gene Transfer. *Cell host & microbe*, *27*(4), 544–555.e3. https://doi.org/10.1016/j.chom.2020.02.002.

202. Passalacqua, K. D., & Bergman, N. H. (2006). Bacillus anthracis: interactions with the host and establishment of inhalational anthrax. *Future microbiology*, *1*(4), 397–415. https://doi.org/10.2217/17460913.1.4.397.

203. Ashley, R. E., Lindsey, R. H., Jr, McPherson, S. A., Turnbough, C. L., Jr, Kerns, R. J., & Osheroff, N. (2017). Interactions between Quinolones and Bacillus anthracis Gyrase and the Basis of Drug Resistance. *Biochemistry*, *56*(32), 4191–4200. https://doi.org/10.1021/acs.biochem.7b00203.

204. Bassetti, M., & Shorr, A. F. (2018). Update on epidemiology and appropriate treatment of life-threatening gram-negative infections. *Current opinion in infectious diseases*, *31*(6), 553–554. https://doi.org/10.1097/QCO.0000000000000501.

205. Agyepong, N., Govinden, U., Owusu-Ofori, A., & Essack, S. Y. (2018). Multidrug-resistant gram-negative bacterial infections in a teaching hospital in Ghana. *Antimicrobial resistance and infection control*, *7*, 37. https://doi.org/10.1186/s13756-018-0324-2.

206. Pappa, O., Chochlakis, D., Sandalakis, V., Dioli, C., Psaroulaki, A., & Mavridou, A. (2020). Antibiotic Resistance of *Legionella pneumophila* in Clinical and Water Isolates-A Systematic Review. *International journal of environmental research and public health*, *17*(16), 5809. https://doi.org/10.3390/ijerph17165809.

207. Liu, X., & Shin, S. (2019). Viewing Legionella pneumophila Pathogenesis through an Immunological Lens. *Journal of molecular biology*, *431*(21), 4321–4344. https://doi.org/10.1016/j.jmb.2019.07.028.

208. Fu, L. M., & Fu-Liu, C. S. (2002). Is Mycobacterium tuberculosis a closer relative to Gram-positive or Gram-negative bacterial pathogens?. *Tuberculosis (Edinburgh, Scotland)*, *82*(2-3), 85–90. https://doi.org/10.1054/tube.2002.0328.

209. Cole, S. T., Brosch, R., Parkhill, J., Garnier, T., Churcher, C., Harris, D., Gordon, S. V., Eiglmeier, K., Gas, S., Barry, C. E., 3rd, Tekaia, F., Badcock, K., Basham, D., Brown, D., Chillingworth, T., Connor, R., Davies, R., Devlin, K., Feltwell, T., Gentles, S., … Barrell, B. G. (1998). Deciphering the biology of Mycobacterium tuberculosis from the complete genome sequence. *Nature*, *393*(6685), 537–544. https://doi.org/10.1038/31159.

210. Momčilović, S., Cantacessi, C., Arsić-Arsenijević, V., Otranto, D., & Tasić-Otašević, S. (2019). Rapid diagnosis of parasitic diseases: current scenario and future needs. *Clinical microbiology and infection : the official publication of the European Society of Clinical Microbiology and Infectious Diseases*, *25*(3), 290–309. https://doi.org/10.1016/j.cmi.2018.04.028.

211. Pomari, E., Piubelli, C., Perandin, F., & Bisoffi, Z. (2019). Digital PCR: a new technology for diagnosis of parasitic infections. *Clinical microbiology and infection : the official publication of the European Society of Clinical Microbiology and Infectious Diseases*, *25*(12), 1510–1516. https://doi.org/10.1016/j.cmi.2019.06.009.

212. Li, J., Wang, Z., Karim, M. R., & Zhang, L. (2020). Detection of human intestinal protozoan parasites in vegetables and fruits: a review. *Parasites & vectors*, *13*(1), 380. https://doi.org/10.1186/s13071-020-04255-3.

213. Reed S. L. (1992). Amebiasis: an update. *Clinical infectious diseases : an official publication of the Infectious Diseases Society of America*, *14*(2), 385–393. https://doi.org/10.1093/clinids/14.2.385.

214. Grace, E., Asbill, S., & Virga, K. (2015). Naegleria fowleri: pathogenesis, diagnosis, and treatment options. *Antimicrobial agents and chemotherapy*, *59*(11), 6677–6681. https://doi.org/10.1128/AAC.01293-15.

215. Siddiqui, R., & Khan, N. A. (2014). Primary amoebic meningoencephalitis caused by Naegleria fowleri: an old enemy presenting new challenges. *PLoS neglected tropical diseases*, *8*(8), e3017. https://doi.org/10.1371/journal.pntd.0003017.

216. Bellini, N. K., Santos, T. M., da Silva, M., & Thiemann, O. H. (2018). The therapeutic strategies against Naegleria fowleri. *Experimental parasitology*, *187*, 1–11. https://doi.org/10.1016/j.exppara.2018.02.010.

217. Kalra, S. K., Sharma, P., Shyam, K., Tejan, N., & Ghoshal, U. (2020). Acanthamoeba and its pathogenic role in granulomatous amebic encephalitis. *Experimental parasitology*, *208*, 107788. https://doi.org/10.1016/j.exppara.2019.107788.

218. Lorenzo-Morales, J., Khan, N. A., & Walochnik, J. (2015). An update on Acanthamoeba keratitis: diagnosis, pathogenesis and treatment. *Parasite (Paris, France)*, *22*, 10. https://doi.org/10.1051/parasite/2015010.

219. Jahangeer, M., Mahmood, Z., Munir, N., Waraich, U. E., Tahir, I. M., Akram, M., Ali Shah, S. M., Zulfqar, A., & Zainab, R. (2020). Naegleria fowleri: Sources of infection, pathophysiology, diagnosis, and management; a review. *Clinical and experimental pharmacology & physiology*, *47*(2), 199–212. https://doi.org/10.1111/1440-1681.13192.

220. Sakkas, H., Gartzonika, C., & Levidiotou, S. (2016). Laboratory diagnosis of human visceral leishmaniasis. *Journal of vector borne diseases*, *53*(1), 8–16..

221. Duthie, M. S., Goto, Y., Ghosh, P., & Mondal, D. (2019). Impact of sequelae of visceral leishmaniasis and their contribution to ongoing transmission of Leishmania donovani. *Pathogens and disease*, *77*(6), ftz057. https://doi.org/10.1093/femspd/ftz057.

222. Chappuis, F., Sundar, S., Hailu, A., Ghalib, H., Rijal, S., Peeling, R. W., Alvar, J., & Boelaert, M. (2007). Visceral leishmaniasis: what are the needs for diagnosis, treatment and control?. *Nature reviews. Microbiology*, *5*(11), 873–882. https://doi.org/10.1038/nrmicro1748.

223. Hommel M. (1999). Visceral leishmaniasis: biology of the parasite. *The Journal of infection*, *39*(2), 101–111. https://doi.org/10.1016/s0163-4453(99)90000-2.

224. Oliveira-Sena, I. V., & Werneck, G. L. (2020). Risk factors for in-hospital mortality from visceral leishmaniasis: A case-control study. *Journal of infection and public health*, *13*(4), 538–543. https://doi.org/10.1016/j.jiph.2019.10.003.

225. Kumar, A., Pandey, S. C., & Samant, M. (2020). A spotlight on the diagnostic methods of a fatal disease Visceral Leishmaniasis. *Parasite immunology*, *42*(10), e12727. https://doi.org/10.1111/pim.12727.

226. Voak, A. A., Standing, J. F., Sepúlveda, N., Harris, A., Croft, S. L., & Seifert, K. (2018). Pharmacodynamics and cellular accumulation of amphotericin B and miltefosine in Leishmania donovani-infected primary macrophages. *The Journal of antimicrobial chemotherapy*, *73*(5), 1314–1323. https://doi.org/10.1093/jac/dky014.

227. Paila, Y. D., Saha, B., & Chattopadhyay, A. (2010). Amphotericin B inhibits entry of Leishmania donovani into primary macrophages. *Biochemical and*

biophysical research communications, *399*(3), 429–433. https://doi.org/10.1016/j.bbrc.2010.07.099.

228. Adler-Moore, J. P., Gangneux, J. P., & Pappas, P. G. (2016). Comparison between liposomal formulations of amphotericin B. *Medical mycology*, *54*(3), 223–231. https://doi.org/10.1093/mmy/myv111.

229. Pinto-Martinez, A. K., Rodriguez-Durán, J., Serrano-Martin, X., Hernandez-Rodriguez, V., & Benaim, G. (2017). Mechanism of Action of Miltefosine on Leishmania donovani Involves the Impairment of Acidocalcisome Function and the Activation of the Sphingosine-Dependent Plasma Membrane Ca^{2+} Channel. *Antimicrobial agents and chemotherapy*, *62*(1), e01614-17. https://doi.org/10.1128/AAC.01614-17.

230. Eberhardt, E., Bulté, D., Van Bockstal, L., Van den Kerkhof, M., Cos, P., Delputte, P., Hendrickx, S., Maes, L., & Caljon, G. (2019). Miltefosine enhances the fitness of a non-virulent drug-resistant Leishmania infantum strain. *The Journal of antimicrobial chemotherapy*, *74*(2), 395–406. https://doi.org/10.1093/jac/dky450.

231. Ware, J. M., O'Connell, E. M., Brown, T., Wetzler, L., Talaat, K. R., Nutman, T. B., & Nash, T. E. (2020). Efficacy and Tolerability of Miltefosine in the Treatment of Cutaneous Leishmaniasis. *Clinical infectious diseases : an official publication of the Infectious Diseases Society of America*, ciaa1238. Advance online publication. https://doi.org/10.1093/cid/ciaa1238.

232. Ponte-Sucre, A., Gamarro, F., Dujardin, J. C., Barrett, M. P., López-Vélez, R., García-Hernández, R., Pountain, A. W., Mwenechanya, R., & Papadopoulou, B. (2017). Drug resistance and treatment failure in leishmaniasis: A 21st century

challenge. *PLoS neglected tropical diseases*, *11*(12), e0006052. https://doi.org/10.1371/journal.pntd.0006052.

233. Das, M., Saudagar, P., Sundar, S., & Dubey, V. K. (2013). Miltefosine-unresponsive Leishmania donovani has a greater ability than miltefosine-responsive L. donovani to resist reactive oxygen species. *The FEBS journal*, *280*(19), 4807–4815. https://doi.org/10.1111/febs.12449.

234. Bansal, R., Sen, S. S., Muthuswami, R., & Madhubala, R. (2020). Stigmasterol as a potential biomarker for amphotericin B resistance in Leishmania donovani. *The Journal of antimicrobial chemotherapy*, *75*(4), 942–950. https://doi.org/10.1093/jac/dkz515.

235. Varadarajan, S., Poornima, P., Milani, M., Gowda, K., Amin, S., Wang, H. G., & Cohen, G. M. (2015). Maritoclax and dinaciclib inhibit MCL-1 activity and induce apoptosis in both a MCL-1-dependent and -independent manner. *Oncotarget*, *6*(14), 12668–12681. https://doi.org/10.18632/oncotarget.3706.

236. Siebert, C., Lindgren, H., Ferré, S., Villers, C., Boisset, S., Perard, J., Sjöstedt, A., Maurin, M., Brochier-Armanet, C., Couté, Y., & Renesto, P. (2019). *Francisella tularensis*: FupA mutation contributes to fluoroquinolone resistance by increasing vesicle secretion and biofilm formation. *Emerging microbes & infections*, *8*(1), 808–822. https://doi.org/10.1080/22221751.2019.1615848.

237. Wilson, R. E., Hill, R., Chalker, V. J., Mentasti, M., & Ready, D. (2018). Antibiotic susceptibility of Legionella pneumophila strains isolated in England and Wales 2007-17. *The Journal of antimicrobial chemotherapy*, *73*(10), 2757–2761. https://doi.org/10.1093/jac/dky253.

238. Lepuschitz, S., Huhulescu, S., Hyden, P., Springer, B., Rattei, T., Allerberger, F., Mach, R. L., & Ruppitsch, W. (2018). Characterization of a community-acquired-MRSA USA300 isolate from a river sample in Austria and whole genome sequence based comparison to a diverse collection of USA300 isolates. *Scientific reports*, *8*(1), 9467. https://doi.org/10.1038/s41598-018-27781-8.

239. Sahm, D. F., Peterson, D. E., Critchley, I. A., & Thornsberry, C. (2000). Analysis of ciprofloxacin activity against Streptococcus pneumoniae after 10 years of use in the United States. *Antimicrobial agents and chemotherapy*, *44*(9), 2521–2524. https://doi.org/10.1128/aac.44.9.2521-2524.2000.

240. Takiff, H. E., Salazar, L., Guerrero, C., Philipp, W., Huang, W. M., Kreiswirth, B., Cole, S. T., Jacobs, W. R., Jr, & Telenti, A. (1994). Cloning and nucleotide sequence of Mycobacterium tuberculosis gyrA and gyrB genes and detection of quinolone resistance mutations. *Antimicrobial agents and chemotherapy*, *38*(4), 773–780. https://doi.org/10.1128/aac.38.4.773.

241. Taravaud, A., Loiseau, P. M., & Pomel, S. (2017). In vitro evaluation of antimicrobial agents on Acanthamoeba sp. and evidence of a natural resilience to amphotericin B. *International journal for parasitology. Drugs and drug resistance*, *7*(3), 328–336. https://doi.org/10.1016/j.ijpddr.2017.09.002.

242. Parnham, M. J., Erakovic Haber, V., Giamarellos-Bourboulis, E. J., Perletti, G., Verleden, G. M., & Vos, R. (2014). Azithromycin: mechanisms of action and their relevance for clinical applications. *Pharmacology & therapeutics*, *143*(2), 225–245. https://doi.org/10.1016/j.pharmthera.2014.03.003.

243. McMullan, B. J., & Mostaghim, M. (2015). Prescribing azithromycin. *Australian prescriber*, *38*(3), 87–89. https://doi.org/10.18773/austprescr.2015.030.

244. Maurin, M., Bryskier, A., & Raoult, D. (2002). Antibiotic susceptibilities of Parachlamydia acanthamoeba in amoebae. *Antimicrobial agents and chemotherapy*, *46*(9), 3065–3067. https://doi.org/10.1128/aac.46.9.3065-3067.2002.

245. Pang, Y., Lu, J., Wang, Y., Song, Y., Wang, S., & Zhao, Y. (2013). Study of the rifampin monoresistance mechanism in Mycobacterium tuberculosis. *Antimicrobial agents and chemotherapy*, *57*(2), 893–900. https://doi.org/10.1128/AAC.01024-12.

246. Thornsberry, C., Hill, B. C., Swenson, J. M., & McDougal, L. K. (1983). Rifampin: spectrum of antibacterial activity. *Reviews of infectious diseases*, *5 Suppl 3*, S412–S417. https://doi.org/10.1093/clinids/5.supplement_3.s412.

247. Ondarza, R. N., Iturbe, A., & Hernández, E. (2006). In vitro antiproliferative effects of neuroleptics, antimycotics and antibiotics on the human pathogens Acanthamoeba polyphaga and Naegleria fowleri. *Archives of medical research*, *37*(6), 723–729. https://doi.org/10.1016/j.arcmed.2006.02.007.

248. Jenkins, C. L., & Bean, H. D. (2020). Dependence of the Staphylococcal Volatilome Composition on Microbial Nutrition. *Metabolites*, *10*(9), 347. https://doi.org/10.3390/metabo10090347.

249. Müller, A., Salmen, A., Aebi, S., de Gouveia, L., von Gottberg, A., & Hathaway, L. J. (2020). Pneumococcal serotype determines growth and capsule size in human cerebrospinal fluid. *BMC microbiology*, *20*(1), 16. https://doi.org/10.1186/s12866-020-1700-7.

250. O'Malley, K. J., Bowling, J. D., Barry, E. M., Hazlett, K., & Reed, D. S. (2019). Development, Characterization, and Standardization of a Nose-Only Inhalation Exposure System for Exposure of Rabbits to Small-Particle Aerosols

Containing Francisella tularensis. *Infection and immunity*, *87*(8), e00198-19. https://doi.org/10.1128/IAI.00198-19.

251. Chatfield, C. H., & Cianciotto, N. P. (2013). Culturing, media, and handling of legionella. *Methods in molecular biology (Clifton, N.J.)*, *954*, 151–162. https://doi.org/10.1007/978-1-62703-161-5_7.

252. Meyers, P. R., Bourn, W. R., Steyn, L. M., van Helden, P. D., Beyers, A. D., & Brown, G. D. (1998). Novel method for rapid measurement of growth of mycobacteria in detergent-free media. *Journal of clinical microbiology*, *36*(9), 2752–2754. https://doi.org/10.1128/JCM.36.9.2752-2754.1998.

253. Goyard, S., Segawa, H., Gordon, J., Showalter, M., Duncan, R., Turco, S. J., & Beverley, S. M. (2003). An in vitro system for developmental and genetic studies of Leishmania donovani phosphoglycans. *Molecular and biochemical parasitology*, *130*(1), 31–42. https://doi.org/10.1016/s0166-6851(03)00142-7.

254. Zaongo, S. D., Shaio, M. F., & Ji, D. D. (2018). Effects of Culture Media On Naegleria fowleri Growth At Different Temperatures. *The Journal of parasitology*, *104*(5), 451–456. https://doi.org/10.1645/18-6.

255. Zhang, N., Prasad, S., Huyghues Despointes, C. E., Young, J., & Kima, P. E. (2018). Leishmania parasitophorous vacuole membranes display phosphoinositides that create conditions for continuous Akt activation and a target for miltefosine in Leishmania infections. *Cellular microbiology*, *20*(11), e12889. https://doi.org/10.1111/cmi.12889.

256. Martins-Duarte, É. S., Carias, M., Vommaro, R., Surolia, N., & de Souza, W. (2016). Apicoplast fatty acid synthesis is essential for pellicle formation at the

end of cytokinesis in Toxoplasma gondii. *Journal of cell science*, *129*(17), 3320–3331. https://doi.org/10.1242/jcs.185223.

257. Donald, R. G., Zhong, T., Wiersma, H., Nare, B., Yao, D., Lee, A., Allocco, J., & Liberator, P. A. (2006). Anticoccidial kinase inhibitors: identification of protein kinase targets secondary to cGMP-dependent protein kinase. *Molecular and biochemical parasitology*, *149*(1), 86–98. https://doi.org/10.1016/j.molbiopara.2006.05.003.

258. Barna, F., Debache, K., Vock, C. A., Küster, T., & Hemphill, A. (2013). In vitro effects of novel ruthenium complexes in Neospora caninum and Toxoplasma gondii tachyzoites. *Antimicrobial agents and chemotherapy*, *57*(11), 5747–5754. https://doi.org/10.1128/AAC.02446-12.

259. Martens, M. C., Won, M. M., Won, H. I., Schulze, T. T., Judge, A. K., Neville, A. J., Vennerstrom, J. L., & Davis, P. H. (2021). *In Vitro* Selection Implicates ROP1 as a Resistance Gene for an Experimental Therapeutic Benzoquinone Acyl Hydrazone in Toxoplasma gondii. *Antimicrobial agents and chemotherapy*, *65*(3), e01040-20. https://doi.org/10.1128/AAC.01040-20.

260. Uboldi, A. D., Wilde, M. L., McRae, E. A., Stewart, R. J., Dagley, L. F., Yang, L., Katris, N. J., Hapuarachchi, S. V., Coffey, M. J., Lehane, A. M., Botte, C. Y., Waller, R. F., Webb, A. I., McConville, M. J., & Tonkin, C. J. (2018). Protein kinase A negatively regulates Ca2+ signalling in Toxoplasma gondii. *PLoS biology*, *16*(9), e2005642. https://doi.org/10.1371/journal.pbio.2005642.

261. Donald, R. G., Allocco, J., Singh, S. B., Nare, B., Salowe, S. P., Wiltsie, J., & Liberator, P. A. (2002). Toxoplasma gondii cyclic GMP-dependent kinase:

chemotherapeutic targeting of an essential parasite protein kinase. *Eukaryotic cell*, *1*(3), 317–328. https://doi.org/10.1128/ec.1.3.317-328.2002.

262. Kim K. (2017). AID-ing Signaling in *Toxoplasma gondii*. *mBio*, *8*(4), e01076-17. https://doi.org/10.1128/mBio.01076-17.

263. Brown, K. M., Long, S., & Sibley, L. D. (2017). Plasma Membrane Association by N-Acylation Governs PKG Function in *Toxoplasma gondii*. *mBio*, *8*(3), e00375-17. https://doi.org/10.1128/mBio.00375-17.

264. Ni Nyoman, A. D., & Lüder, C. G. (2013). Apoptosis-like cell death pathways in the unicellular parasite Toxoplasma gondii following treatment with apoptosis inducers and chemotherapeutic agents: a proof-of-concept study. *Apoptosis : an international journal on programmed cell death*, *18*(6), 664–680. https://doi.org/10.1007/s10495-013-0832-8.

265. Brown, K. M., Lourido, S., & Sibley, L. D. (2016). Serum Albumin Stimulates Protein Kinase G-dependent Microneme Secretion in Toxoplasma gondii. *The Journal of biological chemistry*, *291*(18), 9554–9565. https://doi.org/10.1074/jbc.M115.700518.

266. Wiersma, H. I., Galuska, S. E., Tomley, F. M., Sibley, L. D., Liberator, P. A., & Donald, R. G. (2004). A role for coccidian cGMP-dependent protein kinase in motility and invasion. *International journal for parasitology*, *34*(3), 369–380. https://doi.org/10.1016/j.ijpara.2003.11.019.

267. Howard, B. L., Harvey, K. L., Stewart, R. J., Azevedo, M. F., Crabb, B. S., Jennings, I. G., Sanders, P. R., Manallack, D. T., Thompson, P. E., Tonkin, C. J., & Gilson, P. R. (2015). Identification of potent phosphodiesterase inhibitors that demonstrate cyclic nucleotide-dependent functions in apicomplexan

parasites. *ACS chemical biology*, *10*(4), 1145–1154. https://doi.org/10.1021/cb501004q.

268. Frénal, K., Dubremetz, J. F., Lebrun, M., & Soldati-Favre, D. (2017). Gliding motility powers invasion and egress in Apicomplexa. *Nature reviews. Microbiology*, *15*(11), 645–660. https://doi.org/10.1038/nrmicro.2017.86.

269. Alexander, D. L., Mital, J., Ward, G. E., Bradley, P., & Boothroyd, J. C. (2005). Identification of the moving junction complex of Toxoplasma gondii: a collaboration between distinct secretory organelles. *PLoS pathogens*, *1*(2), e17. https://doi.org/10.1371/journal.ppat.0010017.

270. Dubois, D. J., & Soldati-Favre, D. (2019). Biogenesis and secretion of micronemes in Toxoplasma gondii. *Cellular microbiology*, *21*(5), e13018. https://doi.org/10.1111/cmi.13018.

271. Jia, Y., Marq, J. B., Bisio, H., Jacot, D., Mueller, C., Yu, L., Choudhary, J., Brochet, M., & Soldati-Favre, D. (2017). Crosstalk between PKA and PKG controls pH-dependent host cell egress of *Toxoplasma gondii*. *The EMBO journal*, *36*(21), 3250–3267. https://doi.org/10.15252/embj.201796794.

272. Soldati, D., Dubremetz, J. F., & Lebrun, M. (2001). Microneme proteins: structural and functional requirements to promote adhesion and invasion by the apicomplexan parasite Toxoplasma gondii. *International journal for parasitology*, *31*(12), 1293–1302. https://doi.org/10.1016/s0020-7519(01)00257-0.

273. Li, M., Wang, H., Liu, J., Hao, P., Ma, L., & Liu, Q. (2016). The Apoptotic Role of Metacaspase in Toxoplasma gondii. *Frontiers in microbiology*, *6*, 1560. https://doi.org/10.3389/fmicb.2015.01560.

274. Kim, J., Kundu, M., Viollet, B., & Guan, K. L. (2011). AMPK and mTOR regulate autophagy through direct phosphorylation of Ulk1. *Nature cell biology*, *13*(2), 132–141. https://doi.org/10.1038/ncb2152.

275. Glick, D., Barth, S., & Macleod, K. F. (2010). Autophagy: cellular and molecular mechanisms. *The Journal of pathology*, *221*(1), 3–12. https://doi.org/10.1002/path.2697.

276. Deguchi, A., Thompson, W. J., & Weinstein, I. B. (2004). Activation of protein kinase G is sufficient to induce apoptosis and inhibit cell migration in colon cancer cells. *Cancer research*, *64*(11), 3966–3973. https://doi.org/10.1158/0008-5472.CAN-03-3740.

277. Schmieder, R., & Edwards, R. (2011). Quality control and preprocessing of metagenomic datasets. *Bioinformatics (Oxford, England)*, *27*(6), 863–864. https://doi.org/10.1093/bioinformatics/btr026.

278. Langmead, B., & Salzberg, S. L. (2012). Fast gapped-read alignment with Bowtie 2. *Nature methods*, *9*(4), 357–359. https://doi.org/10.1038/nmeth.1923.

279. Li, H., Handsaker, B., Wysoker, A., Fennell, T., Ruan, J., Homer, N., Marth, G., Abecasis, G., Durbin, R., & 1000 Genome Project Data Processing Subgroup (2009). The Sequence Alignment/Map format and SAMtools. *Bioinformatics (Oxford, England)*, *25*(16), 2078–2079. https://doi.org/10.1093/bioinformatics/btp352.

280. Garrison E, Marth G. 2012. Haplotype-based variant detection from short-read sequencing. arXiv 1207.3907 [q-bio.GN]. https://arxiv.org/abs/1207.3907.

281. Cingolani, P., Platts, A., Wang, l., Coon, M., Nguyen, T., Wang, L., Land, S. J., Lu, X., & Ruden, D. M. (2012). A program for annotating and predicting the effects of single nucleotide polymorphisms, SnpEff: SNPs in the genome of

Drosophila melanogaster strain w1118; iso-2; iso-3. *Fly*, *6*(2), 80–92. https://doi.org/10.4161/fly.19695.

282. Patro, R., Duggal, G., Love, M. I., Irizarry, R. A., & Kingsford, C. (2017). Salmon provides fast and bias-aware quantification of transcript expression. *Nature methods*, *14*(4), 417–419. https://doi.org/10.1038/nmeth.4197.

283. Love, M. I., Huber, W., & Anders, S. (2014). Moderated estimation of fold change and dispersion for RNA-seq data with DESeq2. *Genome biology*, *15*(12), 550. https://doi.org/10.1186/s13059-014-0550-8.

284. Harb, O. S., & Roos, D. S. (2020). ToxoDB: Functional Genomics Resource for Toxoplasma and Related Organisms. *Methods in molecular biology (Clifton, N.J.)*, *2071*, 27–47. https://doi.org/10.1007/978-1-4939-9857-9_2.

285. Soldati, D., & Boothroyd, J. C. (1993). Transient transfection and expression in the obligate intracellular parasite Toxoplasma gondii. *Science (New York, N.Y.)*, *260*(5106), 349–352. https://doi.org/10.1126/science.8469986.

286. Kafsack, B. F., Beckers, C., & Carruthers, V. B. (2004). Synchronous invasion of host cells by Toxoplasma gondii. *Molecular and biochemical parasitology*, *136*(2), 309–311. https://doi.org/10.1016/j.molbiopara.2004.04.004.

287. Sidik, S. M., Hortua Triana, M. A., Paul, A. S., El Bakkouri, M., Hackett, C. G., Tran, F., Westwood, N. J., Hui, R., Zuercher, W. J., Duraisingh, M. T., Moreno, S. N., & Lourido, S. (2016). Using a Genetically Encoded Sensor to Identify Inhibitors of Toxoplasma gondii Ca2+ Signaling. *The Journal of biological chemistry*, *291*(18), 9566–9580. https://doi.org/10.1074/jbc.M115.703546.

288. Shortt, E., & Lourido, S. (2020). Plate-Based Quantification of Stimulated Toxoplasma Egress. *Methods in molecular biology (Clifton, N.J.)*, *2071*, 171–186. https://doi.org/10.1007/978-1-4939-9857-9_10.

289. Khosravi, M., Mohammad Rahimi, H., Doroud, D., Mirsamadi, E. S., Mirjalali, H., & Zali, M. R. (2020). *In vitro* Evaluation of Mannosylated Paromomycin-Loaded Solid Lipid Nanoparticles on Acute Toxoplasmosis. *Frontiers in cellular and infection microbiology*, *10*, 33. https://doi.org/10.3389/fcimb.2020.00033.

290. Farahat Allam, A., Shehab, A. Y., Fawzy Hussein Mogahed, N. M., Farag, H. F., Elsayed, Y., & Abd El-Latif, N. F. (2020). Effect of nitazoxanide and spiramycin metronidazole combination in acute experimental toxoplasmosis. *Heliyon*, *6*(4), e03661. https://doi.org/10.1016/j.heliyon.2020.e03661.

291. Walburger, A., Koul, A., Ferrari, G., Nguyen, L., Prescianotto-Baschong, C., Huygen, K., Klebl, B., Thompson, C., Bacher, G., & Pieters, J. (2004). Protein kinase G from pathogenic mycobacteria promotes survival within macrophages. *Science (New York, N.Y.)*, *304*(5678), 1800–1804. https://doi.org/10.1126/science.1099384.

292. Oates, P. J., & Touster, O. (1980). In vitro fusion of Acanthamoeba phagolysosomes. III. Evidence that cyclic nucleotides and vacuole subpopulations respectively control the rate and the extent of vacuole fusion in Acanthamoeba homogenates. *The Journal of cell biology*, *85*(3), 804–810. https://doi.org/10.1083/jcb.85.3.804.

293. Maurice, D. H., Ke, H., Ahmad, F., Wang, Y., Chung, J., & Manganiello, V. C. (2014). Advances in targeting cyclic nucleotide phosphodiesterases. *Nature reviews. Drug discovery*, *13*(4), 290–314. https://doi.org/10.1038/nrd4228.

294. Jenal, U., Reinders, A., & Lori, C. (2017). Cyclic di-GMP: second messenger extraordinaire. *Nature reviews. Microbiology*, *15*(5), 271–284. https://doi.org/10.1038/nrmicro.2016.190.

295. Valderrama, K., Pradel, E., Firsov, A. M., Drobecq, H., Bauderlique-le Roy, H., Villemagne, B., Antonenko, Y. N., & Hartkoorn, R. C. (2019). Pyrrolomycins Are Potent Natural Protonophores. *Antimicrobial agents and chemotherapy*, *63*(10), e01450-19. https://doi.org/10.1128/AAC.01450-19.

296. Donald, R. G., & Liberator, P. A. (2002). Molecular characterization of a coccidian parasite cGMP dependent protein kinase. *Molecular and biochemical parasitology*, *120*(2), 165–175. https://doi.org/10.1016/s0166-6851(01)00451-0.

297. Demine, S., Renard, P., & Arnould, T. (2019). Mitochondrial Uncoupling: A Key Controller of Biological Processes in Physiology and Diseases. *Cells*, *8*(8), 795. https://doi.org/10.3390/cells8080795.

298. Lebrun, M., Carruthers, V., & Cesbron-Delauw, M. “Chapter 14: Toxoplasma secretory proteins and their roles in parasite cell cycle and infection”. In *Toxoplasma gondii*, 3rd Ed.; p. 608. https://doi.org/10.1016/B978-0-12-815041-2.00014-1.

299. Selseleh, M., Modarressi, M., Shojaee, S., Mohebali, M., Eshraghian, M., Selseleh, M., & Keshavarz, H. (2013). Brain Tissue Cysts in Infected Mice with RH-Strain of Toxoplasma gondii and Evaluation of BAG1 and SAG1 Genes Expression. *Iranian journal of parasitology*, *8*(1), 40–46.

APPENDIX A: SUPPLEMENTARY FIGURES AND TABLES

Cell Line	Pyrimethamine IC_{50} (μM)	IC_{50} Relative to HFF
PBMC	1.87	<0.19
HFF	>10	-

Supplementary Table 1. Comparison of HFF and PBMC susceptibility to common antiparasitic compound pyrimethamine shows that PBMCs are more susceptible to this compound than is HFF, indicating potential hypersensitivity to treatment in cell culture. To determine whether primary PBMCs are hypersensitive to compound treatment in culture, these cells or immortalized HFF cells were treated with the antiparasitic drug pyrimethamine, which our laboratory has previously shown to have low toxicity to human cell lines [151], and subjected to the resazurin assay described in the text. Results showed that PBMCs were >5X more susceptible to pyrimethamine than was HFF, suggesting that these cells may be hypersensitive to compound treatment *in vitro*

Gene of Interest	Fold Change Relative to Vector Control
PKG^{SNV}	1.7*
PKG^{WT}	2.9*
$CDPK^{WT}$	1.3*
$CDPK^{SNV}$	3.2*

Supplementary Table 2. RT-qPCR confirms the expression of relevant genes of interest. To confirm that transfected parasites were expressing the gene of interest, RT-qPCR was completed as described in the text using primers listed in **Appendix B**. Results demonstrated that, in all cases, episomal mutants were expressing higher levels of the gene of interest than was the vector control, further confirming (along with resistance to pyrimethamine) that parasites were expressing the transfected constructs. *$p < 0.01$ by Student's paired *t*-test assuming unequal variance.

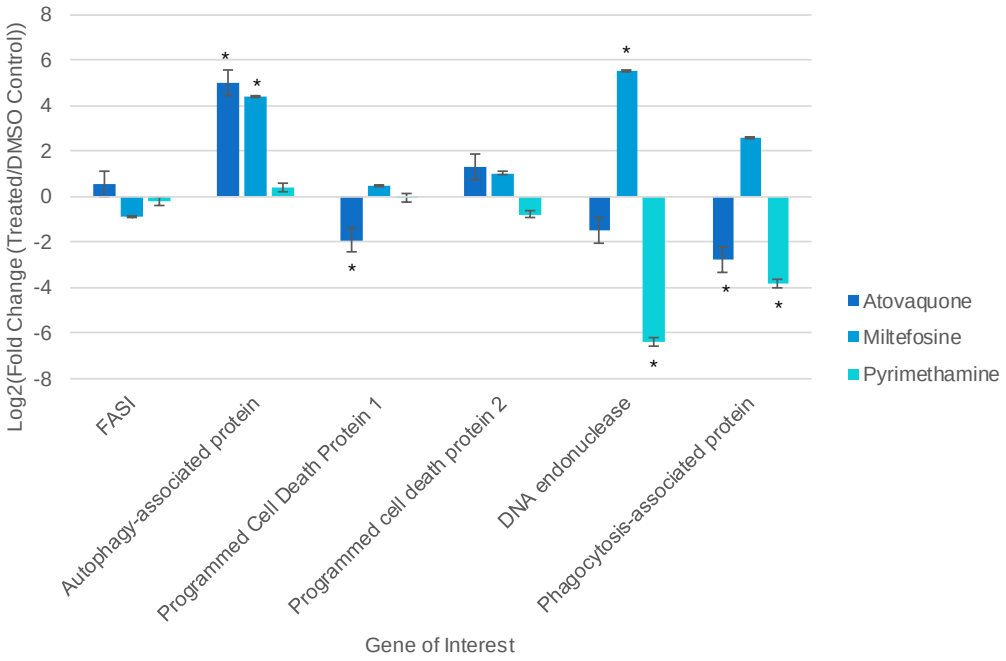

Supplementary Figure 1. Treatment of wild-type RH-dTom tachyzoites with atovaquone, pyrimethamine, and miltefosine yields differential expression of programmed cell death-associated genes, and this expression differs from the pattern seen with RL003 treatment. To determine whether the observed changes to programmed cell death (PCD)-associated genes are shared between multiple anti-*Toxoplasma* compounds, we repeated the RT-qPCR analysis from **Figure 3.6** with three different antiparasitic compounds. Pyrimethamine and atovaquone are not expected to elicit a programmed cell death response based on their known modes of action [63; 64; 105], while miltefosine has been observed to cause upregulation of these genes [264]. Results showed that the FASI and programmed cell death protein 2 genes had no significant change in expression compared to the DMSO control across any of the compounds tested. Pyrimethamine treatment led to no significant change in expression of the autophagy-associated protein at programmed cell death protein 1, and strong downregulation of the DNA endonuclease ($Log_2FC = -6.4$) and phagocytosis-associated protein ($Log_2FC = -3.8$). Atovaquone showed no significant change in DNA endonuclease expression, but had strong upregulation in the autophagy-associated protein ($Log_2FC = 5.0$), as would be expected from the mitochondrial damage induced by its association with the cytochrome b_1 complex [105], and a significant downregulation in expression of the phagocytosis-associated protein ($Log_2FC = -2.7$). In contrast, following previous findings in literature, miltefosine showed significant increase in expression for the autophagy-associated protein ($Log_2FC = 4.4$), DNA endonuclease ($Log_2FC = 5.5$), and phagocytosis-associated protein ($Log_2FC = 2.6$). Together, these findings support that the change in expression of key PCD genes is not a general consequence of treatment with anti-*Toxoplasma* compounds, and that the activity of RL003 more closely resembles that of the known PCD inducer miltefosine. Error bars represent standard error from the mean. *$p < 0.001$ by Student's paired t-test assuming unequal variance.

APPENDIX B: PRIMERS USED IN THIS WORK

Primer Name	Sequence	Gene Amplified	External Source (if applicable)	Use Case
TgFASInh_FWD	GCCATTGTTCCACGTCTTTT	TGGT1_249770	PMID: 23468121	qRT-PCR of Programmed Cell Death in *T. gon*
TgFASInh_REV	GAAGGGGAAGGAAGGAGATG	TGGT1_249770	PMID: 23468121	qRT-PCR of Programmed Cell Death in *T. gon*
TgPrgDth_FWD	AGAGAGGAGGGAGACGAAGG	TGGT1_294420	PMID: 23468121	qRT-PCR of Programmed Cell Death in *T. gon*
TgPrgDth_REV	CAGCGAACTGTGTTCGTCAT	TGGT1_294420	PMID: 23468121	qRT-PCR of Programmed Cell Death in *T. gon*
TgPrgDth2_FWD	TCTTGCCAGCGTGAATACTG	TGGT1_305490	PMID: 23468121	qRT-PCR of Programmed Cell Death in *T. gon*
TgPrgDth2_REV	GCGCTGATAGTCACTCCACA	TGGT1_305490	PMID: 23468121	qRT-PCR of Programmed Cell Death in *T. gon*
TgEndonuc_FWD	AGGCAGCGAAACACAGAAAG	TGGT1_208710	PMID: 23468121	qRT-PCR of Programmed Cell Death in *T. gon*
TgEndonuc_REV	ACATGCAGGGAAGCTCCA	TGGT1_208710	PMID: 23468121	qRT-PCR of Programmed Cell Death in *T. gon*
TgPhago_FWD	AAGGCGAGAGGAATGGATTT	TGGT1_253000	PMID: 23468121	qRT-PCR of Programmed Cell Death in *T. gon*
TgPhago_REV	CGTCGTAAAATTGCAGCAGA	TGGT1_253000	PMID: 23468121	qRT-PCR of Programmed Cell Death in *T. gon*
TgAuto_FWD	CTTCGTCAGCGGGAATATGT	TGGT1_221360	PMID: 23468121	qRT-PCR of Programmed Cell Death in *T. gon*
TgAuto_REV	GCCGATAGTGAGTTGGGTGT	TGGT1_221360	PMID: 23468121	qRT-PCR of Programmed Cell Death in *T. gon*
TgMCA2_FWD	ACATCTTACCGCAGTGCTCC	TGGT1_206490		qRT-PCR of Programmed Cell Death in *T. gon*
TgMCA2_REV	CACCCGGAGAACATCTGGAC	TGGT1_206490		qRT-PCR of Programmed Cell Death in *T. gon*
F583.m00589c_riboL33	AGAATTTCCGCATCGCTCTCCGAA	TGME49_108930		qRT-PCR Housekeeping Gene
R583.m00589c_riboL33	TTCCTGTCCAGCGAATGTACCGTT	TGME49_108930		qRT-PCR Housekeeping Gene
F25.m00008c_his2b	GCTTGGCTGATGAAGCAGTTCGTT	TGME49_009910		qRT-PCR Housekeeping Gene
R25.m00008c_his2b	AGTCGTGTACTTGGTCACTGCCTT	TGME49_009910		qRT-PCR Housekeeping Gene
F55.m04658c_helic	AGGTCGTCTACGTTGCCTTTCCTT	TGME49_056900		qRT-PCR Housekeeping Gene
R55.m04658c_helic	AATGGGCAGCAAACGATTCGACAG	TGME49_056900		qRT-PCR Housekeeping Gene
CakGib_InsFWD	catttccccgaaaagtgcGCTTCGTCTTCTCATGTACAGTG	TGGT1_240390		Gibson Assembly Cloning
CaKGib_InsREV	tacagggcgcgtcaggtgATTAGGCAAAAGTAGAAAGAAACAGAGG	TGGT1_240390		Gibson Assembly Cloning
CakGib_VecFWD	CCTCTGTTTCTTTCTACTTTTGCCTAATCACCTGACGCGCCCTGTA	M2M3 vector		Gibson Assembly Cloning
CakGib_VecREV	CACTGTACATGAGAAGACGAAGCGCACTTTTCGGGGAAATG	M2M3 vector		Gibson Assembly Cloning
PKGGib_InsFWD	catttccccgaaaagtgcGCGCGCTCTCTGACTGG	TGGT1_311360		Gibson Assembly Cloning
PKGGib_InsREV	tacagggcgcgtcaggtgCGTTTCGTCATGCAGGAAGT	TGGT1_311360		Gibson Assembly Cloning
PKGGib_VecFWD	ACTTCCTGCATGACGAAACGCACCTGACGCGCCCTGTA	M2M3 vector		Gibson Assembly Cloning
PKGGib_VecREV	CCAGTCAGAGAGCGCGCGCACTTTTCGGGGAAATG	M2M3 vector		Gibson Assembly Cloning
HsMcl1_FWD	TTTTGGCTACGGAGAAGGAGG	NM_182763.2		qRT-PCR of Human Apoptosis
HsMcl1_REV	AGGTTGCTAGGGTGCAACTC	NM_182763.2		qRT-PCR of Human Apoptosis
HsCAS9_FWD	TTTGGTGATGTCGAGCAGAAA	AB020979.1		qRT-PCR of Human Apoptosis
HsCAS9_REV	GACCCTAAGCAGGAGGGACT	AB020979.1		qRT-PCR of Human Apoptosis
HsCAS3_FWD	ATTTGGAACCAAAGATCATACATGG	NM_004346.4		qRT-PCR of Human Apoptosis
HsCAS3_REV	TTCCCTGAGGTTTGCTGCAT	NM_004346.4		qRT-PCR of Human Apoptosis
HsBad1_FWD	TCCCAGAGTTTGAGCCGAGT	AF031523.1		qRT-PCR of Human Apoptosis
HsBad1_REV	CTCTTCGGGCGAGGAAGTC	AF031523.1		qRT-PCR of Human Apoptosis
HsBcl2_FWD	GAACTGGGGGAGGATTGTGG	NM_000633.3		qRT-PCR of Human Apoptosis
HsBcl2_REV	ACTTCACTTGTGGCCCAGAT	NM_000633.3		qRT-PCR of Human Apoptosis
RabG1_FWD	TGGCAAATACACCAGCGACT	TGGT1_283530		Confirmation of RNA-seq Data
RabG1_REV	CATCGCCACATTCCTCCGTA	TGGT1_283530		Confirmation of RNA-seq Data
RiboL2_FWD	CTTGTAGAGCTAAAGGTGGGGG	TGGT1_300621B		Confirmation of RNA-seq Data
RiboL2_REV	CAGCATTCATTGCAGCTCCTC	TGGT1_300621B		Confirmation of RNA-seq Data
PKA_FWD	GATACTGCGGGTGAACCTGT	TGGT1_356400		Confirmation of RNA-seq Data
PKA_REV	TCTGTCCCACTAGGGATGGG	TGGT1_356400		Confirmation of RNA-seq Data
FHyd_FWD	AGAGAATGCCACGCAGTTGA	TGGT1_411100		Confirmation of RNA-seq Data
FHyd_REV	CGTAGACACGAGCATCCCTC	TGGT1_411100		Confirmation of RNA-seq Data
SulfOx_FWD	GTCGCGTATCGACATGGAGT	TGGT1_295720		Confirmation of RNA-seq Data
SulfOx_REV	CTGTTGTTGCCAGTGTGAGC	TGGT1_295720		Confirmation of RNA-seq Data
MicroGTP_FWD	TTCGCAAACTTCAAGCGTGG	TGGT1_231400A		Confirmation of RNA-seq Data
MicroGTP_REV	GTCGAAAGAGTGGTGGCTGA	TGGT1_231400A		Confirmation of RNA-seq Data
AcylDH_FWD	TCAACACGAGGGTTTCTCCG	TGGT1_231900		Confirmation of RNA-seq Data
AcylDH_REV	CCATCATATGCGGCTTCCCT	TGGT1_231900		Confirmation of RNA-seq Data
3_5_cyc1_FWD	TTACACTCTGGTGCTGCTGG	TGGT1_220420		Confirmation of RNA-seq Data
3_5_cyc1_REV	AGACGTCGCACCGTAAAGTT	TGGT1_220420		Confirmation of RNA-seq Data
efTU_GTP_FWD	GGCTGCCTCCTTTCCAGATT	TGGT1_320150		Confirmation of RNA-seq Data
efTU_GTP_REV	GGTACTCGGCGTACTGGATG	TGGT1_320150		Confirmation of RNA-seq Data
GMPCyc_FWD	CGAAACAAGCGGCACTCAAA	TGGT1_216280		Confirmation of RNA-seq Data
GMPCyc_REV	TCGACGACCACCGATGTTTT	TGGT1_216280		Confirmation of RNA-seq Data
MIC17C_FWD	TCAATCTCCAGGGCTCCGAAA	TGGT1_200230		Confirmation of RNA-seq Data
MIC17C_REV	CGTGCAGCCATCATTGTTGA	TGGT1_200230		Confirmation of RNA-seq Data
MyoK_FWD	GGAGACCGATACAAGGTCGTT	TGGT1_322000		Confirmation of RNA-seq Data
MyoK_REV	AACGATCCCCACCAAAGCAA	TGGT1_322000		Confirmation of RNA-seq Data
Sub9_FWD	CTGCGCTGGTCTAATAGGGG	TGGT1_231060		Confirmation of RNA-seq Data
Sub9_REV	CCTCAAAAGGGAGGGACACC	TGGT1_231060		Confirmation of RNA-seq Data
3_5_cyc2_FWD	GTGGACAGTGACACAGGAGG	TGGT1_257945		Confirmation of RNA-seq Data
3_5_cyc2_REV	GTTTGGCAGTTTGTGGCGAT	TGGT1_257945		Confirmation of RNA-seq Data
AGCKin_FWD	AATTCACCGCCAAAAGTCGC	TGGT1_272200		Confirmation of RNA-seq Data
AGCKin_REV	GCTCTTCAGTGGCAAAAGGC	TGGT1_272200		Confirmation of RNA-seq Data
ULK_FWD	ACTCGAGTTGTGCAGTGGAG	TGGT1_255710		Confirmation of RNA-seq Data
ULK_REV	CTCGGACTGCCGCAGATAAT	TGGT1_255710		Confirmation of RNA-seq Data
RabG2_FWD	TGGCAAATACACCAGCGACT	TGGT1_283530		Confirmation of RNA-seq Data
RabG2_REV	CATCGCCACATTCCTCCGTA	TGGT1_283530		Confirmation of RNA-seq Data
Fas1_FWD	CTCATGCAAGATTGCGGAGC	TGGT1_223830		Confirmation of RNA-seq Data
Fas1_REV	ATCGGTTGTTGGCGTTGTTG	TGGT1_223830		Confirmation of RNA-seq Data

Primers used for cloning and transcriptional analyses. This table shows the sequences and names of primers for the various components of this work, with specific use described in “use case”. Unless otherwise noted, all primers were developed in-house using the Geneious® Prime software (https://www.geneious.com/prime/) and NCBI Primer-Blast (https://www.ncbi.nlm.nih.gov/tools/primer-blast/). In the case of Gibson assembly cloning primers, lowercase characters indicate regions of overlap between the insert and vector sequences.